

**Characterization of  
interactions and trafficking of the  
Neuronal Ceroid Lipofuscinosis protein  
CLN3**

Dissertation  
Zur Erlangung des akademischen Grades  
des Doktors der Naturwissenschaften

des Fachbereichs Biologie,  
der Fakultät für Mathematik, Informatik und Naturwissenschaften  
der Universität Hamburg

vorgelegt von  
Sandra Kerstin Oetjen  
Aus Rotenburg (Wümme)

Hamburg, 2014

Erstgutachter: PD Dr. Guido Hermey  
Zentrum für Molekulare Neurobiologie Hamburg (ZMNH)

Zweitgutachter: Prof. Dr. Christian Lohr  
Universität Hamburg

Die Arbeit wurde im Zeitraum von Juni 2011 bis August 2014 im Zentrum für Molekulare Neurobiologie Hamburg (ZMNH) unter der Anleitung von PD Dr. Guido Hermey angefertigt.

Tag der Disputation: 31.10.2014

### **EIDESSTATTLICHE VERSICHERUNG**

Hiermit erkläre ich an Eides statt, dass ich die vorliegende Dissertationsschrift selbst verfasst und keine anderen als die angegebenen Quellen und Hilfsmittel benutzt habe.

Hamburg, den 21.08.2014



\_\_\_\_\_  
Unterschrift





# Inhaltsverzeichnis

<b>Zusammenfassung</b> .....	<b>1</b>
<b>Summary</b> .....	<b>2</b>
<b>1 Introduction</b> .....	<b>7</b>
1.1 Lysosomal storage disorders .....	7
1.2 Neuronal Ceroid Lipofuscinosis .....	7
1.2.1 Juvenile Neuronal Ceroid Lipofuscinosis .....	9
1.2.2 CLN3 – Ceroid Lipofuscinosis, neuronal 3.....	12
1.2.2.1 Described cellular functional implications of CLN3 .....	13
1.2.2.2 Described interaction partners for CLN3 .....	14
1.3 Intracellular compartmentalization and trafficking processes .....	14
1.3.1 General principles.....	14
1.3.2 Defining vesicular identities.....	15
1.4 The Lysosome.....	18
1.4.1 The active protein content of the lysosome .....	19
1.4.2 Autophagy – the route to lysosomal degradation.....	20
1.5 Aim of this study .....	22
<b>2 Materials</b> .....	<b>23</b>
2.1 Solutions and buffers .....	23
2.2 Antibodies .....	25
2.3 Technical laboratory equipment.....	26
2.4 Microscopes .....	26
2.5 Software .....	27
<b>3 Methods</b> .....	<b>29</b>
3.1 Molecular biology .....	29
3.1.1 Amplification of DNA-fragments by polymerase chain reaction (PCR) .....	29
3.1.2 Agarose-gelelectrophoresis.....	30
3.1.3 Restriction digestion.....	30
3.1.4 Gelextraction and purification of PCR reactions.....	30
3.1.5 Ligation of DNA-fragments .....	30
3.1.6 Transformation of chemically competent E. coli bacteria .....	31
3.1.7 DNA-preparation .....	31
3.1.8 DNA-concentration assessment.....	31
3.1.9 DNA-sequencing.....	32
3.1.10 Gateway cloning .....	32
3.1.11 Cloning of shRNAs.....	32
3.2 Biochemistry.....	33



3.2.1	Immunoprecipitation with anti-GFP-coupled beads .....	33
3.2.2	Separation of proteins and their detection.....	34
3.2.2.1	SDS-polyacrylamide-gel electrophoresis (SDS-PAGE).....	34
3.2.2.2	Western Blot .....	34
3.3	Cell culture.....	35
3.3.1	Cultivation of secondary cell lines.....	35
3.3.2	Cultivation of primary hippocampal mouse neurons.....	36
3.3.3	Transfection-methods.....	36
3.3.3.1	Transfection of secondary cell lines .....	36
3.3.3.2	Transfection of primary hippocampal mouse neurons .....	37
3.3.4	Immunocytochemistry.....	37
3.4	Luciferase-assays.....	38
3.4.1	Test of shRNAs .....	38
3.4.2	$\gamma$ -Secretase-assay .....	38
3.5	In situ hybridization .....	40
3.6	Statistics .....	41
<b>4</b>	<b>Results .....</b>	<b>43</b>
4.1	Identification of new interaction partners .....	43
4.2	Expression-pattern of CLN3-mRNA .....	46
4.2.1	Expression of CLN3-mRNA during embryonic development .....	46
4.2.2	Expression of CLN3-mRNA in the developing and adult brain .....	47
4.2.3	Activity-regulation of CLN3-mRNA levels.....	47
4.3	Subcellular localization of CLN3 .....	48
4.3.1	Localization of CLN3 in comparison to organelle markers in HeLa cells.....	48
4.3.2	Global localization of CLN3 in primary hippocampal neurons .....	51
4.3.3	Localization of CLN3 in comparison to organelle markers in primary hippocampal neurons.....	53
4.4	Trafficking of CLN3.....	57
4.4.1	Trafficking of CLN3 in HeLa-cells.....	57
4.4.2	Trafficking of CLN3 in neurons .....	58
4.4.2.1	Cotrafficking of CLN3 with organelle markers in primary hippocampal neurons.....	60
4.5	CLN3 and the putative interaction partner SorCS1 .....	62
4.5.1	Expression patterns of CLN3 and SorCS1 in mouse embryos .....	62
4.5.2	Co-localization of CLN3 and SorCS1 .....	63
4.5.3	Co-immunoprecipitation of CLN3 and SorCS1 .....	66
4.5.4	CLN3 and other members of the Vps10p-Domain receptor family .....	67
4.6	CLN3 and the putative interaction partner Pen2 .....	68
4.6.1	mRNA expression patterns of CLN3 and Pen2 in mouse embryos.....	69
4.6.2	Co-localization of CLN3 and Pen2.....	70
4.6.2.1	Co-localization of CLN3 and Pen2 in specific endosomal structures....	71



4.6.3	CLN3 and other $\gamma$ -secretase-associated proteins .....	72
4.6.4	Co-immunoprecipitation of CLN3 and Pen2 .....	73
4.6.5	Co-trafficking of CLN3 and Pen2 .....	75
4.6.5.1	Co-trafficking of CLN3 and Pen2 in HeLa cells .....	75
4.6.5.2	Co-trafficking of CLN3 and Pen2 in primary hippocampal neurons ....	77
4.6.6	CLN3 and $\gamma$ -secretase-activity .....	78
4.6.6.1	Development of the $\gamma$ -secretase-activity-assay.....	79
4.6.6.2	CLN3 and Pen2 specific shRNAs for the $\gamma$ -secretase-activity-assay.....	81
4.6.6.3	Assessment of CLN3-influence on $\gamma$ -secretase-cleavage activity on Notch .....	82
<b>5</b>	<b>Discussion .....</b>	<b>87</b>
5.1	Global and subcellular localization of CLN3.....	87
5.1.1	CLN3 mRNA shows highest expression in the gastrointestinal tract .....	87
5.1.2	CLN3 localizes to late endosomes and lysosomes .....	88
5.1.3	CLN3 localizes primarily to the somatodendritic region of neurons .....	89
5.1.4	Trafficking of CLN3-positive endosomes .....	91
5.2	Identification of new interaction partners for CLN3.....	92
5.2.1	CLN3 does co-localize with members of the Vps10p protein family but SorCS1 was not confirmed as an interaction partner.....	92
5.2.2	Pen2 is a new interaction partner for CLN3 .....	93
5.2.2.1	CLN3 – a new link between defects in NCL and Alzheimer’s disease?	98
<b>6</b>	<b>Appendix .....</b>	<b>103</b>
6.1	References .....	103
6.2	Publication.....	121
6.3	Acknowledgement.....	123



## Summary

Juvenile Neuronal Ceroid Lipofuscinoses (JNCL) is the most common neurodegenerative disease affecting children. This lysosomal storage disorder is caused by mutations in the *cln3* gene and patients show characteristic lysosomal storage of autofluorescent lipoprotein. The CLN3 protein is mostly described as having six transmembrane domains and being localized to endosomal and lysosomal subcellular compartments. The function of the CLN3 protein is so far unknown but it has been linked to autophagy, lysosomal homeostasis, lipid modification, protein and vesicular trafficking, and cytoskeletal organization.

In this thesis tagged CLN3 constructs were expressed in HeLa-cells and primary neuronal cultures. CLN3 localized primarily to lysosomal and late endosomal vesicular structures. There was little to no co-localization with markers for the Golgi, endoplasmatic reticulum or early endosomes. Moreover, in hippocampal neurons most CLN3 was found in somatic-dendritic areas with a minor population of CLN3-positive endosomes in spines. In the axon CLN3 is present to a lower degree. There it is involved in highly active fast axonal vesicular transport. To gain more insights into the cellular role of CLN3, the interaction of CLN3 with two new putative interaction partners, SorCS1 and Pen2, identified in TAP-tag screens, was analyzed. SorCS1 is a member of the Vps10p-Domain family of sorting receptors. Pen2 is a subunit of the  $\gamma$ -secretase. This protein complex consisting of four subunits – Pen2, Aph-1, Nicastrin and Presenilin – is a protease that cleaves transmembrane proteins with a single transmembrane domain. The best-known substrates are amyloid-precursor protein (APP) and Notch. Both putative new interaction partners for CLN3 have been associated with the neurodegenerative Alzheimer's disease. In the course of this study the interaction of CLN3 with Pen2 was confirmed, but not the interaction with SorCS1. Co-expression of CLN3 and Pen2 mRNA in developing mice and co-localization of the proteins to the same subcellular structures, which were mainly late endosomes or lysosomes, was demonstrated. CLN3 and Pen2 were co-immunoprecipitated from cell lysates and co-trafficking of both proteins was observed. CLN3 and Pen2 show co-transport along axons and dendrites of primary hippocampal neurons and are involved in trafficking events in the somatic region of these neurons.

In order to gain functional insight about the newly identified interaction the potential role of CLN3 in association with the  $\gamma$ -secretase complex was analyzed. CLN3 also shows partial co-localization with the  $\gamma$ -secretase associated proteins Presenilin 1 and APP. To assess if CLN3 regulates cleavage activity of the  $\gamma$ -secretase I established an assay that analyses  $\gamma$ -secretase-substrate-cleavage under CLN3-knockdown conditions. The results of

---

this assay show a tendency which suggests an influence of CLN3-presence on  $\gamma$ -secretase cleavage activity. In conclusion, the presented data strongly supports a functional interaction of CLN3 and Pen2. This interaction may not only modulate  $\gamma$ -secretase cleavage activity. In addition, this interaction could play a role in recently discussed  $\gamma$ -secretase-independent activities of Presenilin 1 or Pen2 such as autophagy associated functions which in turn may be related to the development of neurodegeneration as observed in JNCL.

## Zusammenfassung

Die Juvenile Neuronale Ceroid Lipofuscinose (JNCL) ist die häufigste neurodegenerative Erkrankung bei Kindern. Diese lysosomale Speichererkrankung wird durch Mutationen in dem Gen *cln3* hervorgerufen und führt zu einer charakteristischen Ablagerung von lysosomalem Speichermaterial, welches aus autofluoreszentem Lipoprotein besteht. Das Protein CLN3 wurde als Transmembranprotein mit sechs Transmembrandomänen beschrieben und hauptsächlich in endosomalen und lysosomalen subzellulären Kompartimenten gefunden. Die Funktion von CLN3 ist bisher nicht bekannt. Es wurde mit der Autophagy, der lysosomalen Homeostase, der Modifikation von Lipiden, dem Transport von Proteinen und Vesikeln sowie mit der Organisation des Zytoskelettes in Zusammenhang gebracht.

In dieser Arbeit wurden getaggte CLN3-Konstrukte in HeLa-Zellen und primären hippocampalen Neuronen exprimiert. Lokalisiert wurden diese Konstrukte hauptsächlich in Lysosomen und späten Endosomen. Im Gegensatz dazu fand sich weniger CLN3 im Golgi, dem endoplasmatischen Retikulum oder frühen Endosomen. In hippocampalen Neuronen war CLN3 vor allem in der somato-dendritischen Region lokalisiert, wobei ein sehr geringer Anteil an Spines ebenfalls eine CLN3-Fraktion aufwies. Im Axon konnte eine kleine Population von CLN3-positiven vesikulären Strukturen beobachtet werden, die am schnellen axonalen Transport beteiligt waren. Um mehr über die funktionelle Rolle von CLN3 in der Zelle zu erfahren, wurden im Rahmen dieser Arbeit mögliche Interaktionspartner für CLN3 untersucht. Zwei neue putative Interaktionspartner – SorCS1 und Pen2 – wurden in TAP-tag Screens gefunden. SorCS1 ist ein Mitglied der Vps10p-Domänen Proteinfamilie, welche Sortierungs-Rezeptoren umfasst. Pen2 ist eine Untereinheit der  $\gamma$ -Sekretase. Dieser Proteinkomplex besteht aus den vier Untereinheiten Pen2, Aph-1, Nicastrin und Presenilin. Die  $\gamma$ -Sekretase wurde als Protease für Proteine mit einer Transmembrandomäne charakterisiert. Die am besten beschriebenen Substrate dieser Protease sind das Amyloid-Vorläufer Protein (APP) und Notch. Beide putativen neuen Interaktionspartner von CLN3 haben eine Verbindung zu der neurodegenerativen Alzheimer Erkrankung. In dieser Arbeit wurde die Interaktion von CLN3 mit Pen2 bestätigt, jedoch konnte die Interaktion mit SorCS1 nicht untermauert werden. In Koexpressionsstudien von CLN3 und Pen2 mRNA wurde ein sehr ähnliches Expressionsmuster gefunden. Ebenso konnte eine Kollokalisierung von CLN3- und Pen2-Protein in denselben subzellulären Strukturen beobachtet werden. Bei diesen handelt es sich hauptsächlich um späte Endosomen oder Lysosomen. CLN3 und Pen2 wurden aus Zelllysaten koimmunopräzipitiert und mittels Lebend-Zell-Mikroskopie wurde ihr

---

Kotransport gezeigt. CLN3 und Pen2 werden in den gleichen Vesikeln entlang von Axonen und Dendriten von primär kultivierten Neuronen transportiert und sind an Fusionsprozessen in der somatischen Region dieser Neurone beteiligt.

Um eine funktionelle Verbindung dieser neu identifizierten Interaktion zu zellulären Prozessen herzustellen, wurde die mögliche Bedeutung von CLN3 für den  $\gamma$ -Sekretase-Komplex untersucht. CLN3 zeigt eine partielle Kolokalisation mit den  $\gamma$ -Sekretase-assoziierten Proteinen Presenilin und APP. Um zu untersuchen, ob CLN3 einen Einfluss auf das Protease-Verhalten der  $\gamma$ -Sekretase hat, wurde in dieser Arbeit ein Assay etabliert, der die Spaltungsfähigkeit der  $\gamma$ -Sekretase auf Substrate unter CLN3-knockdown Bedingungen testet. Die Ergebnisse dieses Assays geben erste Hinweise auf den Einfluss von CLN3 auf die Protease-Aktivität der  $\gamma$ -Sekretase.

Die Resultate dieser Arbeit weisen zum ersten Mal auf eine funktionelle Interaktion von CLN3 und Pen2 hin. Diese Interaktion moduliert möglicherweise nicht nur die Protease-Aktivität der  $\gamma$ -Sekretase, sondern könnte weiterhin auch bei anderen -  $\gamma$ -Sekretase unabhängigen – Funktionen von Presenilin 1 oder Pen2, eine Rolle spielen. So wurde Presenilin als Faktor für Autophagy diskutiert und eine Störung dieser Zellfunktion wurde auch mit der Neurodegeneration in JNCL assoziiert.

---



# 1 Introduction

## 1.1 Lysosomal storage disorders

Juvenile neuronal ceroid lipofuscinosis (JNCL) is a neurodegenerative disease in children that belongs to the large family of lysosomal storage disorders (LSDs). The lysosomal storage disorders are metabolic disorders that affect lysosomal homeostasis or in some cases pathways associated with other membrane-bound organelles. Each of them is a relatively rare disease but they have a combined incidence of 1:5000 live births (Fuller et al. 2006). The name-giving lysosomal storage describes the accumulation of undigested molecules in membrane structures of the endosomal-lysosomal-autophagic system (Platt et al. 2012). This might alter metabolism and trafficking in the cell and results in most LSDs in effects on the central nervous system (CNS) such as neurodegeneration. The diseases are recessively inherited monogenic disorders with mutations affecting genes coding for lysosomal proteins such as enzymes, membrane proteins or associated proteins that catalyse post-translational modifications or trafficking (Schultz et al. 2011).

The Classical clinical picture in LSDs is a neurodegenerative disease with onset in infancy or childhood in children that appeared normal at birth (Wraith 2002), but there are also rare forms with adult onset (Spada et al. 2006; Nixon et al. 2008; Shapiro et al. 2008). Treatments are only available for few forms of LSDs. They include enzyme replacement therapy, substrate reduction therapy and bone marrow transplantation. Research strategies also focus on gene therapy and stem cell therapy (Strulovici et al. 2007; de Filippis 2011; Valayannopoulos 2013; Lund 2013; Sondhi et al. 2014)

## 1.2 Neuronal Ceroid Lipofuscinosis

The Neuronal Ceroid Lipofuscinosis (NCL) also called Batten disease are a group of lysosomal storage disorders mainly affecting children with a combined incidence of about 1:12.500 life birth'. They lead to characteristic autofluorescent storage material - so-called lipofuscin - in cells of the body and gradual neurodegeneration in affected patients. The first cases of this broad range of neurodegenerative diseases have been described by Stengel in 1826 (Stengel 1826). The clinical picture he drew is in agreement with most of the aetiopathologies of the so far described forms of NCL caused by mutations in 14 different genes. Affected patients show usually progressive blindness, cognitive decline and epileptic seizures. The age of onset of the disease differs between the disease forms caused by mutations in different genes but also within the defined types (Table 1) (Jalanko & Brulke 2009; Kollmann et al. 2013).

The patients show characteristic storage material that is either predominantly composed of subunit C of the mitochondrial ATP synthase (SCMAS) or of the sphingolipid activator proteins A and D (SAPs). The ultrastructure of the storage bodies is in relation to the main component of the storage material and presents a fingerprint like, curvilinear or rectilinear pattern. Other components of the storage material that have been described are lysosomal proteins like palmitoyl protein thioesterase 1 (PPT1), tripeptidyl peptidase 1 (TPP1) and Cathepsin D (CTSD) (Anderson et al. 2013) and amyloid precursor protein (APP) and beta-A4 amyloid protein (A- $\beta$ ) (Wisniewski, Maslinska, et al. 1990; Wisniewski, Kida, et al. 1990; Herva et al. 2000). The storage material can be found in neuronal tissues but also in some other parts of the body.

Most of the cases start in young children at the age of zero to ten and lead to premature death of the patients.

**Table 1. Described forms of NCL**

Disease	Clinical phenotype	Main component of storage material	Ultrastructure of storage material	Gene	Gene product, synonyms	Function of protein
<b>CLN1</b>	Infantile classic, late infantile, juvenile, adult	SAPs	GRODs	<i>cln1</i> / <i>pp1</i>	CLN1, Palmitoyl protein thioesterase 1 (PPT1)	Palmitoylthioesterase, lysosomal enzyme
<b>CLN2</b>	Late infantile classic, juvenile	SCMAS	CL	<i>cln2</i> / <i>tpp1</i>	CLN2, Tripeptidyl peptidase 1 (TPP1)	Serine protease, lysosomal enzyme
<b>CLN3</b>	Juvenile classic	SCMAS	FP (CL, RL)	<i>cln3</i>	CLN3	Unknown; modulation of vesicular trafficking and fusion, pH regulation; late endosomal/lysosomal transmembrane protein
<b>CLN4</b>	Adult autosomal dominant	SAPs	GRODs	<i>cln4</i> / <i>dnajc5</i>	CLN4, Cysteine-string protein alpha (CSP $\alpha$ ), DNAJC5	Hsc70 co-chaperone, involved in exocytosis and endocytosis, soluble cytosolic protein associated with lysosomal membranes
<b>CLN5</b>	Late infantile variant, juvenile, adult	SCMAS	RL, CL, FP	<i>cln5</i>	CLN5	Unknown; modulation of vesicular trafficking predicted; soluble lysosomal protein
<b>CLN6</b>	Late infantile variant, adult (Kufs type A)	SCMAS	RL, CL, FP	<i>cln6</i>	CLN6	Unknown; ER-membrane protein
<b>CLN7</b>	Late infantile variant, juvenile, adult	SCMAS	RL, FP	<i>cln7</i> / <i>mfsd8</i>	CLN7, MFSD8	Unknown; transmembrane transporter function predicted; lysosomal membrane protein

Disease	Clinical phenotype	Main component of storage material	Ultrastructure of storage material	Gene	Gene product, synonyms	Function of protein
CLN8	Late infantile variant, progressive epilepsy with mental retardation	SCMAS	CL-like, FP granular	<i>cln8</i>	CLN8	Unknown; regulation in lipid metabolism predicted; ER/ERGIC-membrane protein
CLN9	Juvenile variant			<i>cln9</i>		Unknown; role in ceramide synthesis postulated
CLN10	Congenital classic, late infantile, adult	SAPs	GRODs	<i>cln10 / ctsd</i>	CLN10, Cathepsin D (CTSD)	Aspartyl endopeptidase, lysosomal matrix / extracellular protein
CLN11	Adult		FP	<i>cln11 / grn</i>	CLN11, Progranulin, proepithelin, acrogranin	Unknown; roles in inflammation, embryogenesis, cell motility and tumorigenesis postulated; extracellular protein
CLN12	Juvenile, Kufor-Raheb syndrome		FP	<i>cln12 / atp13a2</i>	CLN12, ATPase 13A2, KRPPD, PARK9, HSA9947, RP-37C10.4	Unknown; regulation of ion homeostasis postulated; lysosomal membrane protein
CLN13	Adult Kufs type			<i>cln13 / ctsd</i>	CLN13, Cathepsin F (CTSF)	Cysteine protease, lysosomal matrix protein
CLN14	Infantile, progressive myoclonus epilepsy 3			<i>cln14 / kctd7</i>	CLN14, Potassium channel tetramerisation domain-containing protein 7 (KCTD7)	Unknown; modulation of ion channel activity predicted, partially membrane-associated cytosolic protein

GRODs, granular osmiophilic deposits; CL, curvilinear profiles; FP, fingerprint bodies; RL, rectilinear profiles; SCMAS, subunit c of mitochondrial ATP synthase; SAPs, sphingolipid activator proteins. (Jalanko & Braulke 2009; Kollmann et al. 2013)

### 1.2.1 Juvenile Neuronal Ceroid Lipofuscinosis

The classical juvenile form of NCL - Juvenile Neuronal Ceroid Lipofuscinosis (JNCL) - starts mostly at the age of about six years in affected children with normal early development. The patients show progressive blindness and cognitive decline accompanied by epileptic seizures. Death occurs between the ages of 20 to 40. As a diagnostic marker for the disease the enlarged vacuoles in peripheral lymphocytes that do not occur in other NCLs but in JNCL and rarely in CLN7 disease are used (Siintola et al. 2007; Kohlschütter & Schulz 2009).

JNCL is inherited in an autosomal recessive manner. It is caused by mutations in the *cln3* gene that was first described in 1995 by the International Batten Disease Consortium (Int. Batten Disease Consortium 1995). So far about 60 different mutations in this gene have been found in affected patients (Kousi et al. 2012; Drack et al. 2013; Pebrel-Richard et al.

---

2014). The most frequent mutation is a 1.02 kb deletion of exons 7 and 8 of the gene leading to a frameshift resulting in 28 novel amino acids and a premature stop codon (Int. Batten Disease Consortium 1995). This mutation was found in about 81 % of disease chromosomes. If the residual protein is actually translated or stable is under debate. It has been suggested that the protein translated from this mutated gene might retain some of its function (Kitzmüller et al. 2008) but other studies describe that it is retained in the endoplasmic reticulum (ER) and not targeted to its normal localization in the late endosome and lysosome (Järvelä et al. 1999).

The autofluorescent storage material occurring in JNCL patients is mostly composed of subunit c of mitochondrial ATP synthase (SCMAS) and shows a fingerprint-like structure. Storage bodies can be found in various cell types all over the body but the main affected tissue is the CNS which also shows massive cell loss during the course of the disease. This is primarily observed in cerebral and cerebellar cortices. In JNCL small neurons in the cortex are earlier and more severely depleted than larger ones. This does not necessarily correspond to the occurrence of storage material that is more prevalent in large neurons such as pyramidal cells in the cerebral cortex but not in the large Purkinje cells of the cerebellum (Anderson et al. 2013). In the hippocampus more neuronal loss is found in Cornu Ammonis area (CA) 2-4 than in CA-1 or the dentate gyrus (DG). This is accompanied by a corresponding storage body distribution. In areas with more neuronal loss and storage material occurrence, an increased microglial and astrocytic activation has been observed and more interneurons are lost in CA-2 and -3 compared to CA1 and DG (Tyynelä et al. 2004). During the loss of neurons patient brains undergo severe reduction in mass (Anderson et al. 2013). A magnetic resonance imaging study by Tokola et al. showed progressive hippocampal atrophy and a greater volume loss in the hippocampus than in whole brain volume in JNCL patient brains (Tokola et al. 2014). Another region that is often affected by neuronal loss in JNCL is the substantia nigra, which can lead to Parkinsonian features in patients. In the cerebellum, Purkinje cells and granular cells degenerate and in the dentate nucleus granular cells are lost. No severe neurodegeneration was observed in the subcortical grey matter in the cerebrum, the brainstem or the spinal cord. The neurodegeneration is accompanied by microglial activation and the presence of macrophages and astrocytes containing storage material. On a cellular level, storage bodies were found in nerve cell bodies and in axonal parts such as proximal axonal segments, axon hillock and terminal axonal spindles. In electron microscopy it might also be possible to find storage material in dendritic processes. Patient brains can be analysed on the cellular level only post-mortem. Therefore many questions on the molecular and cellular pathology of JNCL still remain unanswered (Anderson et al. 2013). Another severely affected region

of the CNS is the retina, which is mostly responsible for the first clinical sign – the visual failure – in patients. Here, atrophy progresses from the outer photoreceptor layer to the ganglionic inner layer. Other parts of the body where storage material can be detected are the heart, which is also affected by the disease (Ostergaard et al. 2011), blood, skin, skeletal muscle and ganglionic neurons (following rectal biopsy) (Figure 1) (Anderson et al. 2013).

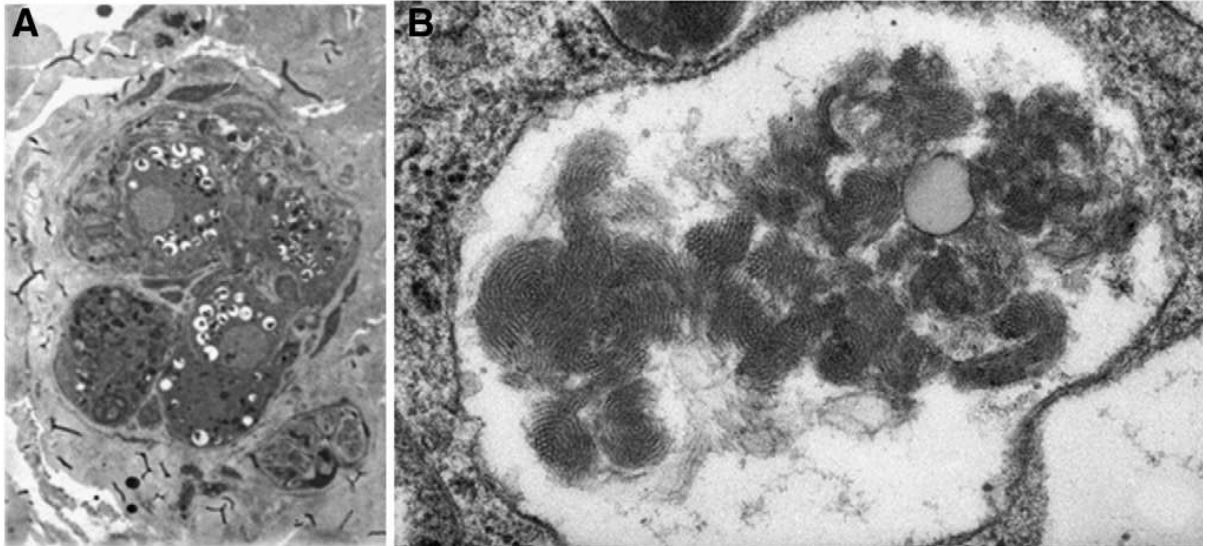


**Figure 1. Cells from rectal biopsy from JNCL patients.**

A: The cytoplasm of ganglionic neurons in JNCL patients shows vacuolations. Magnification: 900x. B: Fingerprint-like membrane structures in a single membrane-limited vacuole. Magnification: 113,000x. (Anderson et al. 2013)

For experimental purposes, four different mouse (*Mus musculus*) models for JNCL have been generated (Katz et al. 1999; Mitchison et al. 1999; Cotman et al. 2002; Eliason et al. 2007). In all of them storage material like in human patients has been observed, although to a different degree. In these mouse models the onset of neurological signs is variable from two months to over 16 months. Moreover, average age at death differs from under seven months to 20 months (Bond et al. 2013). Another animal model to analyse CLN3 function is *Drosophila melanogaster*. The development of a JNCL-model in *Caenorhabditis elegans* proved to be fruitless because knockouts of the three different homologues for CLN3 showed no phenotype. Other models not dependent on genetically modified animals are primary and secondary cell culture systems and in recent times iPS cells derived from JNCL patients (Bond et al. 2013; Lojewski et al. 2014).

CLN3 protein function has also been studied in the baker's yeast *Saccharomyces cerevisiae* and fission yeast *Schizosaccharomyces pombe*. Yeast expresses the CLN3 homologue Btn1. Unlike the human protein with six transmembrane domains Btn1 supposedly has twelve transmembrane domains (Nugent et al. 2008) but specific functional deficits found in Btn1 $\Delta$ -cells were rescued by expression of human CLN3 (Gachet et al. 2005).

---

### 1.2.2 CLN3 – Ceroid Lipofuscinosis, neuronal 3

The gene that is defective in JNCL is called *cln3*. It codes for the protein Ceroid Lipofuscinosis, Neuronal 3 (CLN3). The human gene is spanning 15 kb organized in at least 15 exons on chromosome 16 in the region 16p12.1 in the human genome (Int. Batten Disease Consortium 1995; Mitchison et al. 1997).

In mammals *cln3* is expressed on a low level ubiquitously in the body with the highest levels of *cln3* mRNA in the placenta (Int. Batten Disease Consortium 1995; Chattopadhyay & Pearce 2000; Su et al. 2004). Due to the low expression level and so far no good antibodies the analysis of protein levels of CLN3 is difficult and studies gave conflicting results (Margraf et al. 1999; Ezaki et al. 2003). The investigation of a *cln3*-deficient  $\beta$ -galactosidase reporter mouse confirmed results on the ubiquitous expression of *cln3* (Eliason et al. 2007; Stein et al. 2010; Ding et al. 2011). The most prominent expression of  $\beta$ -galactosidase under the *cln3* promoter was found in epithelial cells of skin, colon, lung and kidney with the kidney showing the highest expression level. The authors also observed a potential osmoregulation of the *cln3* locus (Stein et al. 2010). In the nervous system the highest expression of *cln3* was observed in the hippocampus (in particular in the granular cells of the DG), cortex, and the cerebellum (in particular in the granular cell layer and Purkinje cells). In the retina *cln3* reporter expression was found in the inner and outer nuclear layers (Pane et al. 1999; Chattopadhyay & Pearce 2000; Luiro et al. 2001; Cotman et al. 2002; Ding et al. 2011).

CLN3 has been predicted to be a transmembrane protein with six transmembrane domains with the amino (N-) and carboxyl (C-) terminus projecting into the cytoplasm (Mao et al. 2003; Nugent et al. 2008). There are presumably one large cytoplasmic loop and three large luminal loops of which one contains an amphipathic helix (Nugent et al. 2008). This topology has recently been confirmed by Förster Resonance Energy Transfer (FRET)-assisted microscopy studies (Ratajczak et al. 2014).

The function of CLN3 has so far not been specified, but on the subcellular level it seems to be mainly localized to the late endosomal and lysosomal compartments of the cell where it might have its key functions (Getty & Pearce 2011; Kollmann et al. 2013). The CLN3 protein presumably travels after its synthesis in the endoplasmic reticulum (ER) and processing in the Golgi to various cellular compartments. Different lysosomal targeting motifs – a cytosolic di-leucine motif, an unconventional C-terminal targeting motif and C-terminal prenylation - have been described (Kyttälä et al. 2004; Storch et al. 2004). Other structural features of the protein are four potential *N*-glycosylation sites of which two have been experimentally confirmed and nine potential phosphorylation sites (Figure 2) (Int.

Batten Disease Consortium 1995; Storch et al. 2007; Nugent et al. 2008). Although CLN3 has most often been described to reside in the late endosomal and lysosomal compartments it was also found at the plasma membrane, lipid rafts, ER, Golgi, mitochondria, early endosomes, recycling endosomes, synaptosomal fractions from neurons, nucleus and the cytoplasm (Phillips et al. 2005).

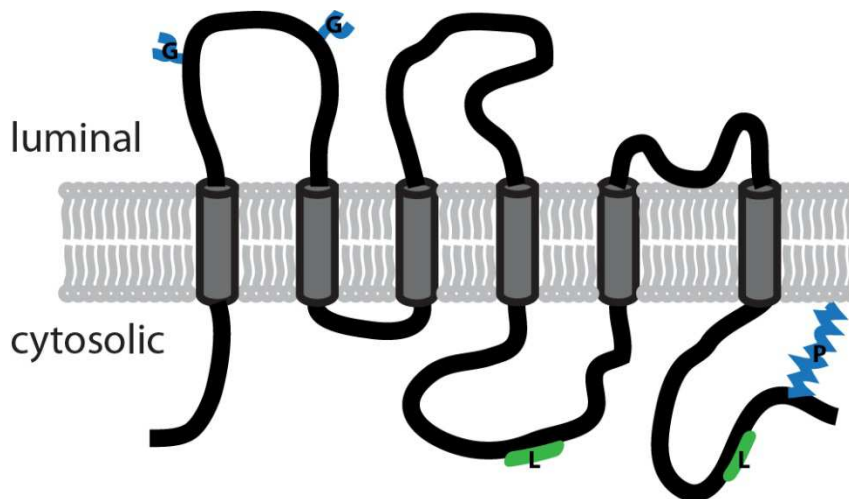


**Figure 2. The CLN3 protein and its transmembrane topology**

The CLN3 protein is a transmembrane-protein with presumably six transmembrane domains, two N-glycosylation sites (G), two lysosomal targeting motifs (L) and C-terminal prenylation (P). (Modified after Cotman & Staropoli 2012)

### 1.2.2.1 Described cellular functional implications of CLN3

The key functions of CLN3 are likely to be found in the late endosomal-lysosomal system but so far they have not yet been specified. No closely related protein has been identified by sequence comparison. Only a distant relation to members of the major facilitator superfamily and a fatty acid desaturase domain have been found (Nugent et al. 2008; Cotman & Staropoli 2012). The authors of one study also observed a deficient palmitoyl-protein  $\Delta$ -9 desaturase activity in the pancreas of *cln3*-knockout mice (Narayan et al. 2006). Alterations in *cln3*-mutant cells include a deficiency in amino acid transport into the lysosome (Kim et al. 2003), in bulk endocytosis (Luiro et al. 2004; Fossale et al. 2004; Codlin et al. 2008) and in Mannose-6-Phosphate receptor targeting (Metcalf et al. 2008), defects in lysosomal acidification (Pearce & Sherman 1998; Holopainen et al. 2001; Gachet et al. 2005) and in biometal homeostasis (Grubman et al. 2014) and a defective maturation of autophagosomes (Cao et al. 2006). CLN3 was also described to have an antiapoptotic role (Puranam et al. 1999) and to protect cells in ER stress (Wu et al. 2014). Apart from lysosome-associated functions, in neurons of *cln3* mouse models alterations in neurotransmitter and receptor levels, altered responses to neurotransmitters and alterations in astrocytic hemichannel activity and intracellular calcium concentration after potassium

---

chloride induced depolarization have been observed (Kovács et al. 2006; Herrmann et al. 2008; Finn et al. 2011; Warnock et al. 2013; Burkovetskaya et al. 2014). A large proportion of the listed deficits points to a role in membrane and protein trafficking and in cytoskeleton associated functions. This is also supported by the observation of motility defects in *cln3* deficient cells (Getty et al. 2011), a link to the small GTPase Arf1-Cdc42 pathway (Schultz et al. 2014) and trafficking defects of microdomain-associated proteins in *cln3*-null cells (Tecedor et al. 2013).

### **1.2.2.2 Described interaction partners for CLN3**

Several interaction partners have been found for CLN3. Some of those link CLN3 to the endosomal-lysosomal system such as CLN5, TPP1 (Lyly et al. 2009), Rab7 and RILP (Uusi-Rauva et al. 2012). Others provide a connection to trafficking functions through interactions with cytoskeleton-associated proteins like Myosin IIB (Getty et al. 2011),  $\beta$ -Fodrin (Uusi-Rauva et al. 2008), Dynein intermediate chain, Kif3A (Uusi-Rauva et al. 2012) and Hook1 (Luiro et al. 2004). Links to trafficking processes are also provided by putative interactions with adaptor protein (AP) 1 and 3 (Kyttälä et al. 2005) and the lipid raft marker protein flotilin-1 (Rakheja et al. 2004). Other interaction partners are the Na<sup>+</sup>/K<sup>+</sup>-ATPase-Fodrin-complex (Uusi-Rauva et al. 2008) and Shwachman-Bodian-Diamond syndrome protein (SBDS) – a protein with ribosomal functions (Vitiello et al. 2010; Wolfe et al. 2011). Calsenilin (Chang et al. 2007) and Atg7 (Behrends et al. 2010) might link CLN3 function to autophagy.

The described interaction partners for CLN3 provide a broad range of putative involvement of CLN3 in cellular processes but none of those so far provided a satisfying explanation for the development of neurodegenerative disease.

In conclusion subcellular localization and molecular function of CLN3 are still elusive. Therefore, additional efforts are needed to unravel subcellular localization and molecular function of CLN3 to understand the mechanisms underlying molecular pathology in JNCL.

## **1.3 Intracellular compartmentalization and trafficking processes**

### **1.3.1 General principles**

Many of the symptoms in JNCL are linked to the correct functionality of the subcellular compartmentalization and trafficking of proteins and membranes to their cellular destinations. In eukaryotic cells different membrane compartments exist that differ in their

function, protein content, membrane composition and also physiological characteristics like pH. Specific sorting processes that involve small GTPases of the Rab- and Arf-protein families and membrane components like phosphoinositides define the identity of the membrane compartments (Stenmark 2009; Jean & Kiger 2012). A central role in trafficking processes is held by the endosomal system. It is composed of a number of different membrane compartments namely early endosomes, late endosomes, recycling endosomes and intermediates between the listed. The endosomal system gets input from the biosynthetic compartment comprising the Golgi apparatus and the ER and of the plasma membrane. Input into the system does not only come in form of newly synthesized factors but also by recycling and redistribution. Cargo is delivered through the endosomal system to degradative compartments like autophagosomes and lysosomes – where the protein CLN3 is likely to be localized - and other subcellular compartments with distinct functions like synapses of neurons. The cytoskeleton plays an important role in this context, because cargo is transported along its major components actin and microtubules (Stenmark 2009; Lasiecka & Winckler 2011).

If taking the Golgi and ER as a starting point for protein biosynthesis and therefore delivery, non-cytosolic proteins can be directly secreted through the constitutive secretory pathway by vesicular transport to the plasma membrane or they can enter the endocytic pathway through early endosomes to recycling endosomes where sorting to a specific destination compartment takes place. In this process vesicles emerging from the trans-Golgi network (TGN) are transported to early endosomes where they fuse with this compartment. The function of the early endosome is mainly the sorting of the incoming cargo. Early endosomes fade to recycling endosomes that consist of different parts. The vacuolar part – named the vacuolar sorting endosome – and a tubular part that emerges from the vacuolar part. The tubular sorting endosome is responsible for recycling of cargo to the TGN or the plasma membrane whereas cargo destined for the lysosome remains in the vacuolar part of the early endosome. The lysosomal cargo travels through late endosomes, also called multivesicular bodies (MVBs) due to the numerous intraluminal vesicles, which then fuse with lysosomes. Some of the transported cargo is transported to the lysosome for degradation other proteins can execute their function in the degradation process here (Saftig & Klumperman 2009).

### **1.3.2 Defining vesicular identities**

Important factors in the sorting of membranes and proteins are Rab GTPases and phosphoinositides which are both facing the cytosolic side of membrane compartments.

The latter are phospholipids that can be found in seven different forms differing in their phosphorylation status. Membrane identities are defined by distinctions in the phosphoinositide composition (Di Paolo & De Camilli 2006). Phosphoinositides have important functions in membrane trafficking but also in signalling and scaffolding.

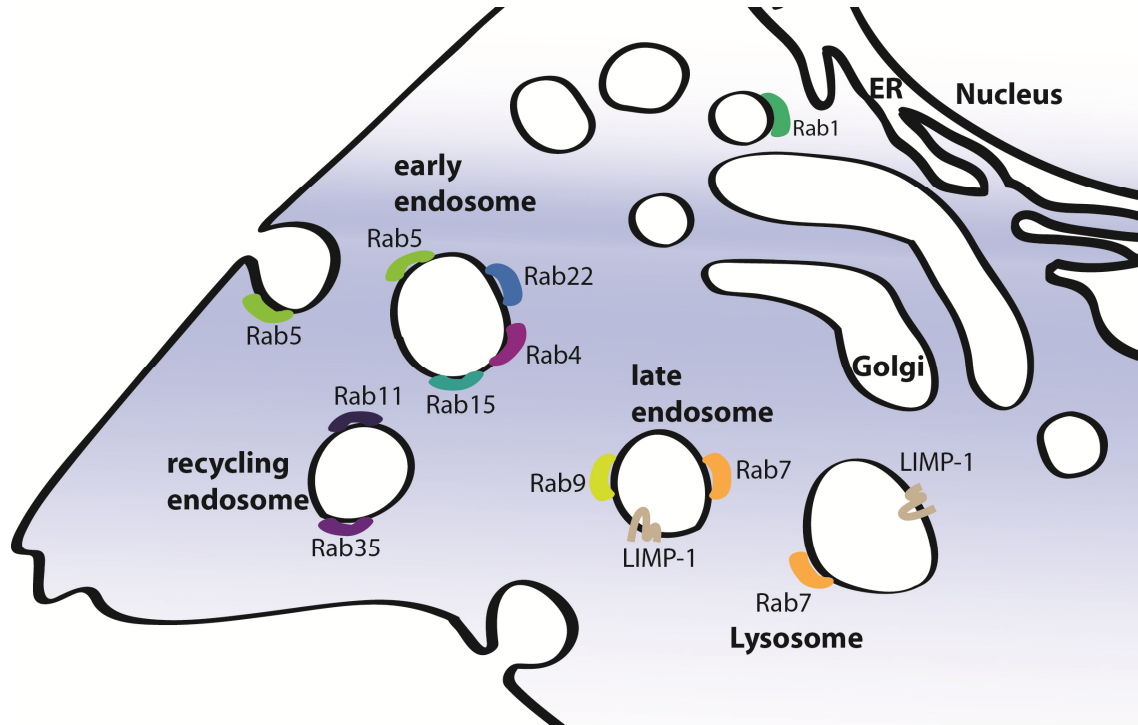


**Figure 3. Major endosomal compartments of mammalian cells and a fraction of their specific Rab GTPases.**

On early endosomes Rab5, Rab4, Rab22 and Rab15 can be found. Recycling endosomes are characterized by Rab11 and Rab35. Rab7 is localized at late endosomes that can also be positive for Rab9 and LIMP-1. Rab7 and LIMP-1 can also be found on lysosomes. Rab1 is present at ER-to-Golgi-transition sites. (Modified after Stenmark 2009)

Rab GTPases can be membrane associated by a geranylgeranyl anchor but also have a non-membrane bound form. In their role as GTPases they function as molecular switches that exist in a GTP-bound active - and membrane bound - form, and a GDP-bound 'off'-form - the non-membrane bound form (Stenmark 2009). Effector molecules like sorting adaptors, tethering factors, motor proteins, kinases and phosphatases can interact with Rab proteins to cooperate in cellular functions. In humans more than 60 members of the Rab GTPase family have been described (Stenmark 2009). They are localized to distinct subcellular compartments and analysis of the Rab population on membrane compartments can help defining their nature (Pfeffer 2003; Ali & Seabra 2005). The above described early endosomes which are positive for the marker protein early endosome antigen 1 (EEA1) (Mu et al. 1995) are dominated by Rab5 and Rab4 on their membranes but also Rab22 and Rab15 were found there (Figure 3). Rab5 is important during endocytosis whereas Rab4 has its functional role in fast recycling to the plasma membrane. The recycling endosome is characterized by Rab11 and Rab35 which regulate slow endocytic, recycling but also Rab15.

On the membranes of late endosomes Rab9 and Rab7 can be found (Figure 3). Rab7 has its role in the maturation of late endosomes and autophagosomes to lysosomes and also stays on the membrane after fusion with the lysosomal compartment (Stenmark 2009).

In the process of membrane trafficking Rab GTPases are major players but they could not act without a large network of other proteins involved in transport, signalling and membrane formation. Membrane trafficking starts with the formation of vesicles. This step is supported by transmembrane proteins specific for the cargo that can recruit adaptor proteins. These adaptor proteins provide for the binding of coat proteins (like clathrin or COPI or II) that enclose the vesicle which can then be constricted from the membrane. The vesicle is uncoated after budding and directed transport along actin filaments or microtubules can be mediated by Rab GTPases, adaptors and motor proteins, among others. When reaching a destination compartment with the right composition of molecules on the acceptor membrane SNARE protein complexes initiate membrane fusion.

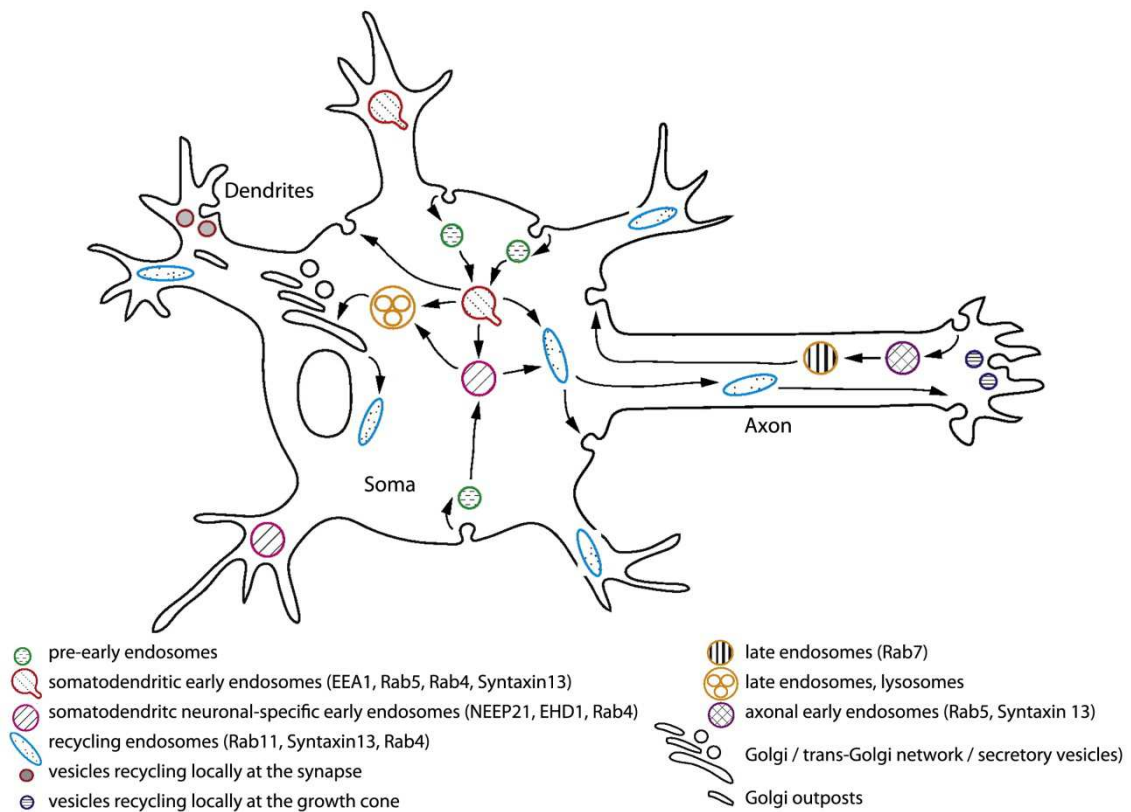


**Figure 4. The neuronal endosomal system**

Neurons are highly polarized cells with also the endosomal system showing a strong polarization between the axon and the somatodendritic compartment. Some endosomal structures localize specifically to one compartment or are absent from a compartment. Some endosomal markers show neuronal specificity and are not found in other cell types of the body. Delivery of cargo to the ends of the processes can be mediated by endosomal transport. (Modified after Lasiecka & Winckler 2011)

In neurons the endosomal-lysosomal system displays a strong polarization due to the nature of the cell itself with differences between the somatodendritic and the axonal compartment (Yap & Winckler 2012) (Figure 4). The early endosomal marker EEA1 which

---

is also a Rab5 effector was only found on endosomes in the somatodendritic compartment but not in axons (Wilson et al. 2000). The primarily neuronal protein Neuronal Early Endosome Protein 21 (NEEP21) can be found on an early endosome population that is largely not EEA1 positive (Steiner et al. 2002). A number of studies describe parts of the biosynthetic compartments in neuronal processes – so-called Golgi-outposts that are localized to a subset of dendrites (Gardioli et al. 1999; Horton & Ehlers 2003). Another difference is the even distribution of recycling endosomes in neuronal cells whereas these organelles are clustered near the nucleus and the TGN in non-neuronal cells (Prekeris et al. 1999; Park et al. 2006; Thompson et al. 2007; Ascaño et al. 2009) (Figure 4).

The long range transport in neurites has - like in other cell types - a retrograde and an anterograde direction. In axons endosomes carrying cargo for degradation acidify on their way to the soma (Overly and Hollenbeck 1996) whereas other endocytosed cargo is trafficked in not-acidifying endosomes (Lalli & Schiavo 2002). Rab 5 and Rab 7 seem to have a role in retrograde trafficking along the axon (Deinhardt et al. 2006) but also in endosomal trafficking at postsynaptic sites (Brown et al. 2005) and neuronal migration (Kawauchi et al. 2010). Anterograde trafficking in the axon can be used for the delivery of biosynthetic cargo and was shown for transport of axonal adhesion molecules like L1/NgCAM (Yap et al. 2008), tropomyosin-related kinase (Trk) receptors (Ascaño et al. 2009), integrins (Eva et al. 2010), and endosomal regulators such as syntaxin 13 (Prekeris et al. 1999) and Rab 11 (Ascaño et al. 2009). In dendrites bidirectional transport of vesicles has been shown.

The general endocytic machinery has a central role in neuronal organization. Neuron specific functions have been described for some of the components of the endocytic machinery and neuron-specific proteins have been found in the endosomal sorting machinery in neurons (Fariás et al. 2012).

## **1.4 The Lysosome**

The primary degradative compartment in the cell with a pH below 5 is the lysosome. Substrates reach the lysosome through endocytosis, phagocytosis and autophagy. In multiple cell types similar organelles called lysosome-related organelles (LROs) including melanosomes, lytic granules, major histocompatibility complex (MHC) class II compartments and platelet-dense granules exist and contain cell-type specific proteins and a subset of lysosomal proteins. Additional functions of the lysosome apart from degradation contribute to cell signalling, cell death, cholesterol homeostasis, plasma

membrane repair, bone and tissue remodelling and pathogen defence (Saftig & Klumperman 2009).

#### 1.4.1 The active protein content of the lysosome

The protein content of the lysosome consists of soluble and integral membrane proteins. Among the soluble proteins are lysosomal hydrolases of which 50 have been described (Saftig & Klumperman 2009). They are involved in the degradation of specific substrates. About 25 lysosomal membrane proteins (LMPs) have been identified but it is likely that there are still more to be found (Schröder et al. 2007; Saftig & Klumperman 2009). Their functional capacities lie in acidification of the lysosomal luminal space, membrane fusion, protein import from the cytosol and export of degraded products. The LMPs with the highest prevalence are lysosome-associated membrane protein 1 (LAMP1), LAMP2, lysosome integral membrane protein 2 (LIMP2) and LIMP1 (also called CD63) (Saftig & Klumperman 2009). Many of the lysosomal proteins, including CLN3, are part of the CLEAR (Coordinated Lysosomal Expression and Regulation) network. This group of proteins contains a CLEAR element in the promoter region that is regulated by the master gene transcription factor EB (TFEB) (Sardiello et al. 2009).

A central and the most well-known receptor responsible for sorting of lysosomal hydrolases is the mannose-6-phosphate receptor (M6PR). This receptor recognizes with its luminal moiety a mannose-6-phosphate-tag that is bound to lysosomal hydrolases in the Golgi. The complex of receptor and lysosomal protein forms in the TGN and binding of the cytoplasmic domain of the M6PR to AP1 or GGA (Golgi-localized,  $\gamma$ -ear-containing, Arf-binding protein) leads to clathrin-mediated membrane budding. The M6PR-cargo complex is targeted to the endosomal system and sorted to late endosomes where the cargo is released due to the acidic pH (Pfeffer 2009). Low pH is also essential for the activity of the lysosomal hydrolases (Mindell 2012). The “empty” M6PR is retrieved from late endosomes to the TGN - a process in which AP1 (Meyer et al. 2000) and Rab9 are involved (Díaz et al. 1997). There are likely to be multiple routes and responsible proteins for recycling of the M6PR.

In disease models deficient for M6PR or for other proteins important in M6PR-dependent protein sorting a fraction of lysosomal hydrolases can still reach the lysosome (Owada & Neufeld 1982; Waheed et al. 1982; Little et al. 1987) which means that there must be alternative mechanisms of sorting. One possibility is the constitutive secretory pathway where proteins are secreted through the plasma membrane and subsequently available for

---

reuptake by binding to other mannose-receptors and endocytosis (Allavena et al. 2004; Elvevold et al. 2008).

Another protein family that might be involved in sorting of lysosomal hydrolases is the Vps10p-Domain receptor family named after their Vps10p domain which is homologous to the luminal part of the yeast sorting protein Vps10p (vacuolar protein sorting defective protein 10). Members of this family of mammalian type-I transmembrane receptors comprise Sortilin, SorLA, SorCS1, -2 and -3 (Hermeijer 2009). The acid sphingomyelinase and sphingolipid activator proteins (SAPs) have been suggested to be targeted directly to the lysosome by Sortilin (Ni & Morales 2006). The lysosomal sorting capacity of Sortilin has been further supported by its co-localization with CI-M6PR (cation-independent M6PR) in the TGN, the identification of functional AP1- and GGA-binding motifs essential for lysosomal targeting in the cytoplasmic domain of Sortilin (Nielsen et al. 2001; Lefrançois et al. 2003; Mari et al. 2008), and co-immunoprecipitation of Sortilin with the lysosomal hydrolases Cathepsin D and H (Canuel et al. 2008)

Apart from the listed trafficking guidance receptors, LMPs can also support the transport of lysosomal proteins. One example is the transport of  $\beta$ -glucocerebrosidase to the lysosome which can be mediated by LIMP2 (Reczek et al. 2007). Less is known about the transport of LMPs themselves to the lysosome. A large portion of LMPs travel from the TGN through the secretory pathway to the plasma membrane and are delivered to the lysosome through the endocytic pathway (Janvier & Bonifacino 2005). Another route is the endosomal-lysosomal system. Sorting motifs prime the proteins for distinct trafficking pathways such as the lysosomal sorting motifs in CLN3 (Kyttälä et al. 2004; Storch et al. 2004). Di-leucine- or tyrosine-based sorting motifs for AP1- and GGA-clathrin dependent TGN exit can be found in many LMPs (Bonifacino & Traub 2003) but it is likely that there are additional ways for direct TGN-to-lysosome transport (Saftig & Klumperman 2009).

#### **1.4.2 Autophagy – the route to lysosomal degradation**

The delivery of substrate to the lysosome is maintained through autophagic pathways. There are three different forms of autophagic streams:

- Microautophagy
- Chaperone-mediated autophagy (CMA)
- Macroautophagy

In the process of microautophagy cytoplasmic material is engulfed by the lysosome by invagination of the lysosomal membrane. CMA is mediated by the chaperone heat shock

cognate 70 (Hsc70). This protein recognizes the amino acid signal sequence KFERQ on soluble proteins and translocates the target proteins through the lysosomal membrane for degradation. The third autophagic stream is macroautophagy. In macroautophagy a double membrane – the so-called phagophore - forms in the cytoplasm and engulfs cytosolic material. This newly formed double-membrane-surrounded organelle is called autophagosome and can contain defective organelles and oligomerized proteins (Boya et al. 2013).

Autophagic processes can be activated by cellular stress such as amino acid deprivation, growth factor deficiency, low energy levels, oxidative stress, ER stress, hypoxia, pathogens or organelle damage (Burman & Ktistakis 2010). It is also a general cellular process in the turnover of cytoplasmic constituents and organelles (Klionsky 2007). Macroautophagy shares a common signalling pathway with protein synthesis – both are regulated by the kinase mTOR (mammalian target of rapamycin) (Beugnet et al. 2003). Autophagy activation is achieved by dephosphorylation of mTOR. The phosphorylation on the other hand leads to phosphorylation of p70S6 kinase and thereby to induction of protein synthesis and cell proliferation (Hartmann 2012). The suppression of mTOR by dephosphorylation results in the activation of the ULK1 (Unc51-like kinase) complex. At least one other kinase is able to induce the phosphorylation of ULK1 - the AMP-activated protein kinase (AMPK) – meaning that there is also a possible mTOR-independent activation of autophagy. The phosphorylated ULK1 complex can sequester a complex containing beclin-1 and class III phosphoinositide 3-kinase (PI3K CIII or Vps34) to the phagophore membrane. This in turn leads to formation of the autophagosome (Nixon 2013). One of the proteins involved in autophagosome formation – more precisely in phagophore expansion (Boya et al. 2013) – is Atg7. Atg7 was shown to be linked to CLN3 in a proteomic assessment of the autophagy system (Behrends et al. 2010). The origin of the membrane for the phagophore formation is presumably the ER but also mitochondria have been suggested to supply membranes (Hailey et al. 2010; Burman & Ktistakis 2010). The phagophore membranes are enriched in membrane bound LC3-II that is derived from LC3-I which resides on the cytoskeleton and is distributed evenly in the cell body. LC3-II is often used as a marker for autophagosome accumulation (Boland & Nixon 2006).

In neurons normally there are few autophagosomes and the ratio of LC3-II compared to LC3-I is low. But autophagy is still an essential process for neuronal survival involved in several neuronal cellular processes. Hollenbeck showed the progressive maturation of autophagosomes along neurites resulting in fusion with lysosomes, and autophagy is thought to be an important mechanism in neurite remodeling, growth cone formation and neuroprotection (Hollenbeck 1993). At hippocampal dendrites mTOR is abundant and

---

might be essential for the local regulation of protein synthesis and autophagy in plasticity-related processes like long-term potentiation (LTP) and long-term depression (LTD) (Boland & Nixon 2006).

In many neurodegenerative diseases alterations in autophagy-associated molecules or organelles have been observed. In relation to CLN3, an increase in the autophagosome marker LC3-II was observed in CLN3<sup>Δex7/8</sup>-knock-in mice (Cao et al. 2006). This could either mean an induction of autophagy or a defect in a later step in autophagy that prevents the degradation of LC3-II in the lysosome. In the case of CLN3 it was suggested that there is a defect in autophagosome-lysosome fusion. It was suggested that autophagy is upregulated in certain neurodegenerative diseases as a protective mechanism to clear the neuron from toxic compounds. In Alzheimer's' disease patients an accumulation of autophagy intermediates was observed and mice lacking the autophagy genes *atg5* or *atg7* undergo severe neurodegeneration (Boland & Nixon 2006). In other LSDs apart from JNCL - including Pompe disease, Niemann–Pick type C, other NCLs, mucopolysaccharidosis type IV, GM1-gangliosidosis and sulphatase deficiency – autophagy has also been found to be impaired (Schultz et al. 2011).

In conclusion there is evidence for a link between CLN3 and cellular processes in the lysosomal and autophagy pathway. The association of autophagy with other neurodegenerative diseases provides an interesting context for the analysis of CLN3 in this process.

## 1.5 Aim of this study

The rare disease Juvenile Neuronal Ceroid Lipofuscinoses (JNCL) is the most common neurodegenerative disease affecting children. This lysosomal storage disorder is caused by mutations in the *cln3* gene. The function of the CLN3 protein is so far unknown but it has been linked to autophagy, lysosomal homeostasis, lipid modification, protein and vesicular trafficking, and cytoskeletal organization.

The aim of this study is to identify and characterize new interaction partners for CLN3. This should result in new insights into the cellular role of CLN3 and help to elucidate the function of CLN3 in the not-defective neuronal cell. This characterization will promote the understanding of molecular mechanisms in neurodegeneration in JNCL and will in consequence support the development of therapies.

## 2 Materials

### 2.1 Solutions and buffers

#### Solutions for molecular biology

	<b>component</b>	<b>concentration</b>
<b>TELT-lysisbuffer</b>	Tris HCl pH 7.5	50 mM
	EDTA	62.5 mM
	Triton X 100	0,40%
	LiCl	2.5 M
<b>DNA-Loading buffer (10x)</b>	TrisHCl, pH 7.6	10 mM
	Glycine	50 %
	EDTA, pH 8	60 mM
	Bromphenolblue	0,25 %
	Xylenecyanole	0,25 %
<b>DIC-medium</b>	Trypton	16 g/l
	Yeast extract	10 g/l
	NaCl	5 g/l
<b>SOC-medium</b>	Pepton	0.002%
	Yeast extract	0,0005%
	NaCl	8.56 mM
	KCl	2,5 mM
	MgCl <sub>2</sub>	10 mM
	Glucose	20 mM
	in H <sub>2</sub> O, adjust to pH 7	
	NaCl	3 M
<b>20x SSC</b>	Trisodium citrate (*2H <sub>2</sub> O)	0.3 M
	DEPC	0.10%
	in H <sub>2</sub> O, adjust to pH 7	

<b>antibiotics</b>	<b>final concentration</b>
<b>anamycin</b>	50 µg/ml
<b>ampicillin</b>	100 µg/ml
<b>chloramphenicol</b>	34 µg/ml

#### Solutions for cell culture

	<b>component</b>	<b>concentration</b>
<b>HANKS' medium</b>	HANKS balanced salt solution	1 bottle for 1000 ml
	NaHCO <sub>3</sub>	4.17 mM
	HEPES	1 mM
	in H <sub>2</sub> O, adjust to pH 7.3 – 7.4	
<b>for HANKS' medium plus FCS</b>	FCS	20%
	<b>Digestion buffer</b>	
	NaCl	137 mM
	KCl	5 mM

	<b>component</b>	<b>concentration</b>
	Na <sub>2</sub> HPO <sub>4</sub> (*2H <sub>2</sub> O)	7 mM
	HEPES	25 mM
	Papain	1 mg/ml
	in H <sub>2</sub> O, adjust to pH 7.2	
	DNase solution	0.02 %
<b>Dissociation buffer</b>	HANKS' medium	1 x
	MgSO <sub>4</sub> (7*H <sub>2</sub> O)	12 mM
	DNase solution	0.02 %
<b>DNase solution</b>	DNase (Sigma)	75 kU/ml
	NaCl	150 mM
<b>permeabilization and washing buffer</b>	PBS	1x
	FCS	5%
	Saponin	0.50%
<b>PFA-fixation solution</b>	PBS	1x
	Paraformaldehyde (PFA)	4 %
	Sucrose	4 %

#### Solutions for biochemistry

	<b>component</b>	<b>concentration</b>
<b>PBS</b>	NaCl	1.73 M
	KCl	27 mM
	Na <sub>2</sub> HPO <sub>2</sub> (*2H <sub>2</sub> O)	81 mM
	KH <sub>2</sub> PO <sub>4</sub>	14.7 mM
<b>buffers for IP</b>		
<b>Lysisbuffer 1</b>	NaCl	50 mM
	Tris-HCl pH7.5	50 mM
	NP40	0.1 %
	ProtInh	1 x
	PMSF	1 mM
	in H <sub>2</sub> O	
<b>Lysisbuffer 2</b>	NaCl	100 mM
	Tris-HCl pH7.5	50 mM
	NP40	0.5 %
	CaCl <sub>2</sub>	1 mM
	MgCl <sub>2</sub>	1 mM
	ProtInh	1 x
	PMSF	1 mM
	in H <sub>2</sub> O	
<b>Dilutionbuffer 1</b>	NaCl	50 mM
	Tris-HCl pH7.5	50 mM
	Triton X 100	0.01 %
	ProtInh	1 x
	PMSF	1 mM
	in H <sub>2</sub> O	

	<b>component</b>	<b>concentration</b>
<b>Dilutionbuffer 2</b>	NaCl	100 mM
	Tris-HCl pH7.5	50 mM
	Triton X 100	0.01 %
	CaCl <sub>2</sub>	1 mM
	MgCl <sub>2</sub>	1 mM
	ProtInh	1 x
	PMSF	1 mM
	in H <sub>2</sub> O	
<b>Laemmli-sample buffer (1x)</b>	SDS	2 %
	Glycerol	10 %
	2-Mercaptoethanol	5 %
	Bromphenolblue	0.002 %
	Tris-HCl	0.0625 M
	in H <sub>2</sub> O	
<b>SDS-PAGE</b>		
<b>stacking gel</b>	Acrylamid:Biacylamid (29:1; 30 % w/v)	4 %
	Tris-HCl, ph 6.8	125 mM
	SDS	0.1 %
	APS	0.05 %
	Temed	0.05 %
<b>running gel</b>	Acrylamid:Biacylamid (29:1; 30 % w/v)	10-12 %
	Tris-HCl, ph 8.8	380 mM
	SDS	0.1 %
	APS	0.05 %
	Temed	0.05 %
<b>running buffer</b>	Tris-Base	250 mM
	Glycine	1.92 M
	SDS	1 %
<b>blotting buffer</b>	Tris-Base	25 mM
	Glycine	192 mM
	Methanol	10 %

## 2.2 Antibodies

<b>primary antibodies</b>			
<b>anti</b>	<b>species</b>	<b>supplier</b>	<b>dilution</b>
<b>HA</b>	mouse	Covance	1:1000
<b>GFP</b>	chicken	Abcam	1:10000
<b>dsRed</b>	rabbit	Clontech	1:500
<b>IL-2</b>	mouse	Abcam	1:1000
<b>SorCS1</b>	rabbit	home-made	1:1000
<b>GPR78/BiP</b>	rabbit	Abcam	1:1000
<b>TGN46</b>	rabbit	Abcam	1:500
<b>GM130</b>	mouse	Abcam	1:1000
<b>Map2</b>	rabbit	Synaptic Systems	1:1000

<b>coupled secondary antibodies</b>			
<b>anti</b>	<b>species</b>	<b>supplier</b>	<b>dilution</b>
<b>chicken-488</b>	goat	Life Technologies	1:500
<b>chicken-633</b>	goat	Life Technologies	1:250
<b>mouse-488</b>	goat	Life Technologies	1:500
<b>mouse-555</b>	goat	Life Technologies	1:500
<b>mouse-633</b>	goat	Thermo Scientific	1:250
<b>rabbit-555</b>	goat	Life Technologies	1:500
<b>chicken-HRP</b>	goat	Promega	1:10000
<b>mouse-HRP</b>	goat	Vector Laboratories	1:10000

## 2.3 Technical laboratory equipment

<b>Instrument / Equipment</b>	<b>Supplier</b>
Agarose-gel electrophoresis chamber PerfectBlue	PaqLab
ImageQuant LAS4000mini chemiluminescence detector	GE Healthcare
LS6000 Sc Scintillation counter	Beckmann
Mini-Twin SDS-gel electrophoresis chamber	Biometra
Nanodrop 2000 spectrophotometer	ThermoScientific
T-Professional Trio Thermocycler for PCR	Biometra
Trans-cell blotting chamber	BioRad
UV-gel-documentation system for DNA-gels	BioRad
Victor3 Multilabel Luminescence Counter	Perkin Elmer

## 2.4 Microscopes

### Epifluorescence microscope:

Zeiss Axio Imager Epifluorescence microscope

HXP 120C mercury short-arc lamp

Apotome

Software: Axiovision / ZEN

### Confocal laser scanning microscopes:

Olympus Fluoview 1000

AR Laser (458nm, 476nm, 488nm, 514nm); GreNE Laser (543nm); HeNe

Laser (633nm)

Three PMTs (epifluorescence, reflection) and one PMT for transmission mode

Scanformat up to 2048 x 2048 pixel, 12 bit, scanfield rotatable -5 up to +95

Software: Olympus Fluoview

---

Leica TCS SP5 confocal laser scanning microscope

Laser lines: Diode 405 nm / Multi-Ar 458 nm / 467 nm / 488 nm / 514 nm;

DSS: 561 nm; HeNe 633 nm

Software: Leica LAS

### **Spinning disc microscopes:**

Visitron Systems Spinning Live Cell Confocal

lasers (solid state): 488, 561, 647 or 405

two charge-coupled device EM-CCD cameras (Hamamatsu Photonics)

optical image splitter for simultaneous dual image acquisition

Perkin Elmer spinning disc microscope

Laser lines: 405nm/440nm/488nm/515nm/561nm/640nm

Software: Volocity 6

## **2.5 Software**

Image processing and analysis:

Image J, Fiji

DNA and protein analysis:

DNASTar Lasergene9

Statistics:

SigmaPlot

others:

Microsoft Office

Adobe creative suite



### 3 Methods

#### 3.1 Molecular biology

In the course of this study, several different recombinant expression-constructs and plasmids were used. Most of them were created or altered during this thesis.

##### 3.1.1 Amplification of DNA-fragments by polymerase chain reaction (PCR)

Amplification of DNA-fragments was needed for the creation and alteration of expression constructs or other plasmids. For the polymerase chain reaction (PCR) a standard mixture of template, primers, deoxynucleotide triphosphates (dNTPs), the proof-reading polymerase Pwo (Peqlab), 10x Pwo reaction buffer (Peqlab) and distilled water was used. The reaction mixture constituents were added in the amounts listed in Table 2

**Table 2. Standard mixture for PCR-reactions**

Reagent	stock concentration	volume /amount
forward primer	10 $\mu$ M	1 $\mu$ l
reverse primer	10 $\mu$ M	1 $\mu$ l
dNTPs	25 mM	1 $\mu$ l
reaction buffer	10 x	5 $\mu$ l
Pwo polymerase	1 U/ $\mu$ l	0,5 $\mu$ l
Template DNA		200 ng
H <sub>2</sub> O		ad 50 $\mu$ l

The basic protocol for amplification of the template is shown in Table 3. The primer annealing temperature was adapted to the primers used and calculated by the following equation:

$$69,3 + \left( \frac{41 * \# \text{ of GC bp}}{\# \text{ of total bp}} - \frac{650}{\# \text{ of total bp}} \right)$$

The amplification time depended on the length of the PCR fragment and was roughly proportional to 45 seconds for 1 kb of DNA.

**Table 3. Amplification protocol for PCR-reactions**

step	purpose of step	time (seconds)	temperature (°C)	repeats
1	initial denaturation	120	95	1
2	denaturation	15	95	30 cycles of step2 - 4
3	primer annealing	30	dependent on primers	
4	amplification	30 – 250	68	
5	terminal amplification	420	68	1
6	resting temperature	-	4	1

---

### **3.1.2 Agarose-gel electrophoresis**

DNA fragments were separated on agarose-gels for the purpose of analysis and extraction of fragments of specific sizes. Agarose-gels were prepared with 0.5 - 2 % agarose (depending on the size of the relevant fragment) in TAE-buffer. The mixture was heated and GelRed (Biotium) was added in a dilution of 1:20,000 before casting the gel. DNA was mixed with loading buffer before being run on the gel. To assess the sizes of DNA-fragments in the gel GeneRuler 1 kB plus DNA ladder (Fermentas) was loaded in parallel to the DNA of interest. The gel was run at 10 V/cm and documentation followed in the UV- transilluminator (BioRad).

### **3.1.3 Restriction digestion**

For cloning purposes and for the inspection of cloned plasmids digestions with restriction endonucleases were executed. Either conventional restriction endonucleases (Fermentas, NEB) were used for digestion in 1 hour or fast digest enzymes (Fermentas) were used for a digestion in 10 minutes. Restriction reactions were performed according to the product manual. For specific reactions the digested DNA was incubated with 1 unit FastAP-thermosensitive alkaline phosphatase (Fermentas) for the removal of 5'-phosphate groups to prevent re-ligation of the plasmid. The digested DNA was separated on an agarosegel.

### **3.1.4 Gelextraction and purification of PCR reactions**

After restriction digestion and separation on an agarosegel the relevant fragments were extracted from the agarosegel with the NucleoSpin® Gel and PCR Clean-up kit (Macherey-Nagel) according to the guidelines of the manufacturer. The kit was also used to purify DNA from PCR reactions.

### **3.1.5 Ligation of DNA-fragments**

For the ligation of DNA fragments for cloning purposes 1 unit of T4-DNA ligase (Fermentas) was used to ligate 50 ng of vector-DNA and suitable insert-DNA in a molar ratio of 3:1 to the vector. The reaction was set up according to the manufacturer's protocol and incubated for 20 minutes at room temperature or overnight at 4°C.

### 3.1.6 Transformation of chemically competent *E. coli* bacteria

For the propagation of cloned DNA-plasmids the DNA was transformed into chemically competent *E. coli* Top10 (for most cloning reactions) or *ccdB Survival*<sup>TM</sup> 2 T1R bacteria (for propagation of pDEST vectors without expression-inserts). All bacteria were kindly provided by Ute Süsens and stored at -80 °C. The bacteria were defrosted on ice and for the transformation 1.5 µl of DNA were added to 50 µl of bacteria. After mixing and 15 minutes incubation on ice a heat shock was performed for 40 seconds at 42 °C. 250 µl of room temperature SOC medium were added to the bacteria and they were incubated for 1 hour at 37°C and 250 rpm to induce growth of the bacteria and translation of the antibiotic resistance gene on the transformed plasmid. Selection of clones was performed through plating of the bacteria on LB-agar plates with appropriate antibiotics. The plates were incubated at 37 °C overnight.

### 3.1.7 DNA-preparation

For DNA-preparation in a small scale the “TELT”-method (modified boiling method after Maniatis et al.) was applied. An overnight culture of a picked colony from an LB-agar-plate in 4 ml of LB medium with antibiotics (concentration see materials) was pelleted for 15 seconds at 13,000 rpm in a tabletop centrifuge. The pellet was stored on ice, resolved in 250 µl of TELT-lysis-buffer and incubated on ice for 5 minutes. 5 µl of 50 mg/ml lysozyme (Roche) in water were added before 5 further minutes of incubation on ice. After boiling of the mixture for 1 minute at 99°C and cooling on ice for 5 minutes a centrifugation step of 10 minutes at 14,000 rpm followed. The mucous pellet was removed and 500 µl of absolute ethanol was added to precipitate the DNA from the supernatant. After a centrifugation step at 14,000 rpm for 20 minutes the pellet was washed with 1 ml of 70 % ethanol and dried. The DNA was dissolved in 20 to 40 µl of distilled water.

The preparations of larger scales of DNA were conducted with the NucleoBond<sup>®</sup> Xtra Midi Kit (Machery-Nagel) and performed according to the manufacturer’s protocol.

### 3.1.8 DNA-concentration assessment

The DNA concentration and purity in DNA preparations from TELT-preparations, Midi preparation, PCR or gel-extraction was determined with the NanoDrop 2000 spectrophotometer (Peqlab) by measurement of the optical density.

---

### 3.1.9 DNA-sequencing

To test the correctness of amplified DNA and cloned plasmids the DNA was analysed by Sanger sequencing (Sanger et al. 1977). Sequencing was executed by Eurofins MWG Operon in Martinsried or in house by the service group Bioanalytics of PD Dr. Sabine Hoffmeister-Ullerich. Sequence alignment and verification was then done with help of the software package DNASTAR Lasergene 9 Core Suite.

### 3.1.10 Gateway cloning

Expression constructs for recombinant protein expression in mammalian cells were mostly generated with the Gateway system (Life Technologies).

In the first cloning step, the sequence of interest was amplified with the addition of a Kozak consensus sequence (CACC) at the 5' end of the sequence. The PCR-product was cloned into a pENTR<sup>TM</sup>/D-TOPO-vector according to the manufacturer's protocol. After 5 to 20 minutes of incubation 1.5 µl of the reaction were transformed into Top10 E. coli bacteria. Correct integration of the sequence of interest into the pENTR<sup>TM</sup>/D-TOPO-vector was assessed by antibiotic selection conditions for the bacteria, restriction digestion of the purified plasmids and sequencing.

pENTR<sup>TM</sup>/D-TOPO-constructs can be cloned into various destination vectors (pDEST) with the Gateway LR Clonase II Enzyme Mix (Life Technologies) by DNA recombination. The pENTR<sup>TM</sup>/D-TOPO-construct was combined with the desired pDEST-vector in a recombination reaction which was set up according to the manufacturer's protocol. After an incubation time of 1 hour 1.5 µl of the reaction were transformed into Top10 E. coli bacteria. Correct recombination was assessed by the same methods as for the TOPO-cloning reaction.

### 3.1.11 Cloning of shRNAs

For the knockdown of mRNAs of CLN3 and Pen2 shRNAs were produced with the BLOCK-iT<sup>TM</sup> U6 RNAi Entry Vector Kit (Life Technologies) in combination with the psiCHECK<sup>TM</sup> Vector system and the Dual-Glo<sup>®</sup> Luciferase Assay System (Promega) as a testing system (see below).

Sequences for shRNAs were selected in comparison with the literature and with the help of the following web-tools:

- siRNA Wizard by Invivogen
- shRNA designer by Biosettia

- shRNA design tool by Life Technologies

The selected sequences were cloned into the BLOCK-iT™ U6 RNAi Entry Vector (Life Technologies) according to the manufacturer's guidelines. The sequences selected for 3 different shRNAs for each murine CLN3 and murine Pen2 are listed in Table 4

**Table 4. Sequences of shRNAs for murine CLN3 and Pen2**

shRNA	Sequence
mCLN3-1	GTTGCCGAATACGGTTCACCTcgaaAGGTGAACCGTATTCGGCAAC
mCLN3-2	GCAGCACACCCTACTTTCTATcgaaATAGAAAGTAGGGTGTGCTGC
mCLN3-3	GCCGCTTACGTGAATACCTTCgaaGAAGGTATTCACGTAAGCGGC
mPen2-1	GCGGGTATCCAATGAGGAGAAcgaaTTCTCCTCATTGGATACCCGC
mPen2-2	GAACCTGTGCCGGAAGTACTAcgaaTAGTACTTCCGGCACAGGTC
mPen2-3	GCCAAATCAAAGGCTATGTTTcgaaAAACATAGCCTTTGATTTGGC

For assessment of the knockdown-capabilities of the cloned shRNAs the target cDNAs were cloned into psiCHECK™ vectors (Promega) that harbour cDNAs for two different luciferases. By comparison of their activity with the Dual-Glo® Luciferase Assay System (Promega) the knockdown-capability of a shRNA on the target gene which is cloned in frame with one of the luciferases can be tested.

## 3.2 Biochemistry

### 3.2.1 Immunoprecipitation with anti-GFP-coupled beads

Co-immunoprecipitation of proteins was carried out with the GFP-Trap-technology (Chromotek). GFP-coupled fusion proteins can be purified efficiently with the anti-GFP lama-nanobodies coupled to magnetic beads.

For immunoprecipitations double transfected HeLa-cells were used and cell lysates were collected after the following protocol. Transfected cells were harvested on ice by scraping in ice-cold PBS and transferred to a 1.5 ml reaction tube. After a centrifugation step at 1200 g for 2 minutes at 4°C the pellet was incubated in 250 µl lysisbuffer on ice for 30 minutes with several times of pipetting up and down. The cell lysate was centrifuged for 10 minutes at 20,000 g at 4°C and the supernatant was then mixed with 400 µl dilution buffer. 40 µl of this "Input" fraction was kept for the analysis by SDS-PAGE and the rest was transferred to a reaction tube with 15 µl of the 3 times in 250 µl dilution buffer washed magnetic particles. The beads were incubated with the "Input" for 20 minutes under constant mixing. 40 µl of the supernatant were kept for analysis after the precipitation. After 3 washing steps in 300 µl ice-cold dilution buffer the beads were mixed with 15 µl of dilution buffer and 15 µl of 4x SDS-sample buffer as well as the other samples. The

---

samples were heated to 95°C for 5 minutes and then either stored at -20°C or directly transferred to an SDS-polyacrylamide gel.

For certain immunoprecipitations the proteins were crosslinked by the crosslinking agent DSP (dithiobis[succinimidylpropionate]; Thermo Scientific) prior to the precipitation. The transfected cells in their normal growing environment were washed 2 times in PBS and incubated on ice for 2 hours with 1 mM DMSO dissolved DSP in PBS. To stop the crosslinking reaction 1 M Tris, pH 7.5 was added to a final concentration of 15 mM and an incubation for 15 minutes on ice followed. The cells were then treated as described above and used for the co-immunoprecipitation.

### **3.2.2 Separation of proteins and their detection**

#### **3.2.2.1 SDS-polyacrylamide-gel electrophoresis (SDS-PAGE)**

The separation of proteins according to molecular weight was conducted by SDS-polyacrylamide-gel electrophoresis (SDS-PAGE). Discontinuous 10 or 12 % SDS-gels were prepared with a polymerization time of 30 minutes for each separating and stacking gel. The separating gel part was overlaid with isopropanol after casting to create a clean edge. After polymerization, the isopropanol was discarded and the stacking gel was casted around a comb for the creation of pockets for the samples. The protein-samples were loaded into the pockets of the stacking gel and the SDS-PAGE was run in running buffer at 80 V to allow focusing of the proteins above the separating gel. For the following separation in the separating gel 150 V were applied for about 1.5 hours. For molecular weight-comparison of the proteins PageRuler prestained protein Ladder (Thermo Scientific) was used.

#### **3.2.2.2 Western Blot**

After the completed separation process on the SDS-PAGE the proteins from the gel were transferred to a PVDF membrane (Immobilon-P Transfer Membran, Millipore) by western blotting. Prior to setting up the western blot the PVDF membrane was activated for 15 seconds in methanol, washed with distilled water for 2 minutes and then equilibrated in precooled blotting buffer for 5 minutes. The composition of the transfer-system was fixed in a sandwich chamber and setup as follows:

1. 1 sponge
2. 2x Whatmann-3MM-paper

3. PVDF membrane
4. SDS-gel
5. 2x Whatmann-3MM -paper
6. 1 sponge

The proteins were transferred onto the PVDF membrane in blotting buffer by the application of electric current at a tension of 100 V for 1.5 hours at 4 °C or at 80 mA overnight. Subsequently the PVDF-membrane with the transferred proteins was washed in water and treated with methanol for 10 seconds and dried for 15 minutes. Another reactivation with methanol for 5 seconds was followed by washing in water for 2 minutes. The membrane was incubated with ponceaured-solution for 15 minutes to visualize the transferred proteins. After scanning and 2 washing steps in PBS-Tween (1x PBS; 0.1 % Tween20) the membrane was incubated with 5 % skimmed milk powder in PBS-Tween to block unspecific binding of antibodies.

If necessary, the membrane was dissected into different parts and incubated with the primary antibody in PBS-Tween for either 1 hour at RT or overnight at 4 °C under slight agitation. After 3 washing steps in PBS-Tween the incubation with the horseradish-peroxidase-coupled secondary antibody followed for 1 hour at RT. The membrane was washed 3 times in PBS-Tween and subsequently incubated with ECL-solution (SuperSignal West Pico, Thermo Scientific) for 1 minute. The detection of the chemiluminescence signal was conducted with the LAS4000Mini system (GE Healthcare).

### 3.3 Cell culture

#### 3.3.1 Cultivation of secondary cell lines

Localization studies, analysis of interaction and luciferase assays were performed in secondary cell lines (Table 5). The cell lines were handled in a laminar flow hood according to good laboratory practice guidelines. The cells were cultivated in an environment of 5 % CO<sub>2</sub> and 95 % humidity at 37°C.

**Table 5. Secondary cell lines used in this study**

Cell line	Origin	growth medium
HeLa	derived from cervical cancer from the 31-year old woman Henrietta Lachs in 1951 (Gey et al. 1952)	DMEM (Dulbecco's modified eagle medium) + 10 % FCS (Biochrom)
N2A	mouse neuroblastoma cell line (Klebe & Ruddle 1969)	OptiMEM (Life Technologies) + 5 % FCS + 1% Penicillin/ Streptomycin (PAA)

---

Secondary cell lines were maintained in 10 cm plastic cell dishes (Cellstar<sup>®</sup>, Greiner Bio-one) and split when reaching 90 % confluence. Detachment of cells was achieved with the incubation with 1 ml of trypsin solution (PAA) for 3 minutes. The trypsin reaction was stopped by the addition of 10 ml growth medium and the cells were reseeded at a dilution of 1:10 in 10 ml growth medium or seeded for experimental purposes at a suitable density in 6-well, 24-well or 96-well plates (Greiner Bio-one).

For long-term storage cells were trypsinized cells were pelleted at 1500 g for 2 minutes and redissolved in cryoprotectant medium (20 % dimethyl sulfoxide (Sigma), 40% FCS, 40 % DMEM) and frozen at -80 °C before long-term storage in liquid nitrogen.

### **3.3.2 Cultivation of primary hippocampal mouse neurons**

For the cultivation of primary hippocampal mouse embryo neurons E17.5 embryos were prepared from timed-pregnant C57Bl/6J mice. Pregnant mice were sacrificed by cervical dislocation and embryos were prepared out of the uterus on ice in cold HANKS' medium without calcium and magnesium (Sigma). All following steps were carried out on ice or in cooled media. The embryonic brains were dissected out and transferred to HANKS' medium plus 20% FCS and the preparation of the hippocampi which were then collected in a new tube with HANKS' medium plus 20% FCS followed. The hippocampi were washed 2 times in HANKS' medium and incubated for 30 minutes in 2 ml digestion buffer supplemented with 1 mg DNase (Sigma). 3 washing steps with HANKS' medium followed and subsequently the hippocampi were dissociated with a pasteur pipette in dissociation buffer supplemented with DNase. After addition of 10 ml HANKS' medium plus 20% FCS the cells were pelleted for 5 minutes at 1000 g and redissolved in PNGM<sup>TM</sup>-medium with supplements (Lonza). The cells were seeded at a density of 40,000-60,000 cells/cm<sup>2</sup> on Poly-L-Lysine (0.5 mg/ml Poly-L-Lysine (Sigma) in H<sub>2</sub>O) coated glass coverslips (Carl Roth) or in glassbottom dishes (ibidi) in PNGM<sup>TM</sup>-medium with supplements. Neurons were grown for 7-21 days before fixation.

### **3.3.3 Transfection-methods**

#### **3.3.3.1 Transfection of secondary cell lines**

Secondary cell lines were transfected using Lipofectamine 2000 (Life Technologies) according to the manufacturer's protocol. For the transfection the cells were incubated in OptiMEM (Life Technologies) which was exchanged for normal growth medium 4-6 hours

after the transfection. N2A cells were kept in growth medium over the whole time of treatment.

Stably transfected HeLa cells were generated under antibiotic selection conditions with 150 µg/ml zeocin (Invivogen).

### **3.3.3.2 Transfection of primary hippocampal mouse neurons**

Primary hippocampal mouse embryo neurons were transfected at DIV (days in vitro) 3 to 7 using Lipofectamine LTX (Life Technologies) according to the guidelines of the manufacturer. For transfection 1 µl of Lipofectamine LTX reagent and 0,75 µg DNA were used. The cells were transferred to preequilibrated OptiMEM (Life Technologies) of 37 °C and 5 % CO<sub>2</sub>. After 45 minutes incubation time of the cells in OptiMEM the transfection mixture was added to the OptiMEM and left on the cells for 30 minutes. Subsequently the coverslips with the neuronal cells were transferred back into the old PNGM<sup>TM</sup>-medium.

### **3.3.4 Immunocytochemistry**

For the visualization of overexpressed proteins in HeLa cells and primary hippocampal neurons the cells were fixed and the proteins indirectly labelled with fluorescent antibodies. The overexpression in HeLa cells lasted 15 to 48 hours after transfection. Primary hippocampal neurons were fixed at DIV7 to DIV21. Before the fixation cells were washed 3 times in PBS. Fixation was conducted with 4 % paraformaldehyde (PFA) in PBS for 15 minutes or ice-cold methanol for 3 minutes. After the fixation cells were washed 3 times with PBS and afterwards incubated in PBS with 0.5% Saponin and 10 % FCS for permeabilization of membranes and blocking of unspecific antibody binding sites. Antibody labelling was performed on Parafilm (Bemis) in a damp environment. The antibody was diluted in PBS with 0.5% Saponin and 10 % FCS. For the primary antibody the incubation time was 1 to 2 hours. After 3 washing steps each lasting for 10 minutes in PBS with 0.5% Saponin the cell-covered coverslips were transferred onto the secondary antibody and incubated for 1 hour. 2 washing steps in PBS with 0.5% Saponin followed and one final washing was conducted in distilled H<sub>2</sub>O. The coverslips were then mounted with Immu-Mount (Thermo Scientific) containing 20 % ProlongGold anti fade with Dapi (Life Technologies) on a glass slide.

---

### 3.4 Luciferase-assays

Luciferase-assays were used for the assessment of knock-down efficiency of shRNAs and for the  $\gamma$ -secretase activity assay. Luciferase-assays for Dual-Glo<sup>®</sup> Luciferase Assay System (Promega) and Bright-Glo<sup>™</sup> Luciferase Assay System (Promega) were conducted according to the guidelines of the manufacturer.

#### 3.4.1 Test of shRNAs

The shRNAs constructed with the BLOCK-iT<sup>™</sup> U6 RNAi Entry Vector Kit (Life Technologies) were tested with the Dual-Glo<sup>®</sup> Luciferase Assay System in combination with the Promega psiCHECK<sup>™</sup> vectors system.

In the assay, knockdown-capacity of the constructed shRNAs was compared to the specific knockdown of the Renilla luciferase with a Renilla-specific shRNA (shRenilla). As negative controls the empty shRNA-vector (U6-vector) and a scrambled Renilla-shRNA (pS-Trono) were used. The assay was conducted in 96-well format with N2A-cells. The test-vector psiCHECK2<sup>™</sup> with the gene of interest and the suitable shRNAs (exemplary scheme: Table 6) were transfected into the cells with Lipofectamine2000 (Life Technologies) according to the manufacturer's protocol. Each reaction-mix was tested in 7 replicates. The cells in the 8<sup>th</sup> row of the 96-well plate remained untransfected for normalization-purposes.

**Table 6. Pipetting scheme for shRNA test (exemplarily listed for murine CLN3)**

Line 1	Line 2	Line 3	Line 4	Line 5	Line 6	$\mu$ g DNA per well
psiCHECK2-mCLN3	psiCHECK2-mCLN3	psiCHECK2-mCLN3	psiCHECK2-mCLN3	psiCHECK2-mCLN3	psiCHECK2-mCLN3	0.15
sh-mC-1	sh-mC-2	sh-mC-3	U6-vector	shRenilla	pS-Trono	0.15

The efficiency of the shRNAs was assessed with the Dual-Glo<sup>®</sup> Luciferase Assay System (Promega). The Dual-Glo<sup>®</sup> Luciferase Assay System (Promega) was administrated according to the guidelines of the manufacturer with the aberration that 25  $\mu$ l reagent were used per well in the 96-well format instead of 75  $\mu$ l. The luminosity was measured with the Victor<sup>3</sup> Light Luminescence Counter (PerkinElmer). The Renilla-caused luminosity was normalized to the measured Firefly-activity for each well.

#### 3.4.2 $\gamma$ -Secretase-assay

As sensors for  $\gamma$ -secretase activity  $\gamma$ -secretase-substrates were inserted into a vector I generated from a Gateway pDEST-vector template. This cloning reaction adds a C-

terminal nuclear localization sequence, a Gal-4-promoter-binding domain and a VP16 transcriptional activation domain to the peptide of interest. This C-terminal peptide of these constructs can induce transcription of a Gal-4-promoter-driven reporter-gene. Here the reporter is the Firefly luciferase and the activity is measured with the Bright-Glo™ reagent (Promega).

To test the assay-system the cloned constructs were transfected into N2A cells with the Lipofectamine2000 reagent (Life Technologies) according to the manufacturer's protocol. As a transfection control EGFP was co-transfected and in addition the reporter plasmid bearing the Gal-4-promoter-driven Firefly luciferase gene was transfected (Table 7). Each reaction-mix was tested in 7 replicates. The cells in the 8<sup>th</sup> row of the 96-well plate remained untransfected for normalization-purposes.

**Table 7. Pipetting scheme for  $\gamma$ -secretase-assay test**

Line 1	Line 2	Line 3	Line 4	Line 5	$\mu\text{g DNA per well}$
Notch-dEMV	Notch-ICD	APP-FL	APP-ICD	CLN3	0.0125 to 0.1
EGFP	EGFP	EGFP	EGFP	EGFP	0.1125
UAS	UAS	UAS	UAS	UAS	0.0125

To test the influence of CLN3 on the  $\gamma$ -secretase activity, CLN3 was knocked down by shRNAs in the assayed cells. As a positive control for an effect of a knockdown on the  $\gamma$ -secretase activity, Pen2 knock-down was conducted. As negativ-controls the empty-shRNA-vector and shRNAs targetting other genes were used. As a transfection control EGFP was co-transfected and in addition the reporter plasmid bearing the Gal-4-promoter-driven Firefly luciferase gene was transfected (Table 8). Each reaction-mix was tested in 7 replicates. The cells in the 8<sup>th</sup> row of the 96-well plate remained untransfected for normalization-purposes.

**Table 8. Pipetting scheme for  $\gamma$ -secretase-assay with Notch as the substrate**

Line 1	Line 2	Line 3	Line 4	Line 5	Line 6	Line 7	Line 8	Line 9	Line 10	Line 11	Line 12	$\mu\text{g DNA per well}$
Notch-dEMV (0.03125 $\mu\text{g/well}$ ) or Notch-ICD (0.02875 $\mu\text{g/well}$ )												
mC1	mC2	mC3	U6	hC1	mP1	mP2	mP3	ohne	C 1	C 2	C 3	0.025
EGFP	EGFP	EGFP	EGFP	EGFP	EGFP	EGFP	EGFP	EGFP	EGFP	EGFP	EGFP	0.1125
UAS	UAS	UAS	UAS	UAS	UAS	UAS	UAS	UAS	UAS	UAS	UAS	0.0125

The reporter-gene expression was assessed with the Bright-Glo™ Luciferase Assay System (Promega). The Bright-Glo™ reagent (Promega) and OptiMem (Life Technologies) were warmed to room temperature. The EGFP-fluorescence was measured with the Victor<sup>3</sup> Light Luminescence Counter (PerkinElmer). The media was removed from the wells and 25  $\mu\text{l}$  fresh OptiMem and 25  $\mu\text{l}$  Bright-Glo™ reagent were added to each well of the 96-well plate. After 5 minutes incubation with slight shaking, the liquid was transferred to a white

---

measuring plate and the luminosity was measured with the Victor<sup>3</sup> Light Luminescence Counter (PerkinElmer). The luminosity was normalized to the measured EGFP-intensity for each well.

### 3.5 In situ hybridization

pBSK plasmids containing parts of the cDNA sequence of the gene of interest were linearized and purified with the SureClean kit (Bioline). 1 µg of the linearized plasmid was used for in vitro transcription with the In Vitro transcription Riboprobe® System-T7 (Promega). 4 µl 5x transcription buffer, 2 µl 100 mM DTT, 1 µl of 10 mM ATP, 1 µl of 10 mM CTP, 1 µl of 10 mM GTP (Promega), 1 µl RNaseOUT™ (Life Technologies), 1 µl T7 or T3 polymerase (Roche) and 8 µl 80 µCi α[<sup>35</sup>S]-UTP (Hartmann Analytic GmbH) for labeling were incubated for 2 hours at 37 °C. After transcription the reaction was incubated for 20 minutes with 1 µl DNase I (Roche). After purification with mini Quick Spin RNA Columns (Roche), elution in 1 mM DTT and precipitation of RNA with 2 volumes of absolute ethanol at 20°C for 2 hours or overnight the RNA-pellet was dried and eluted in 100 µl 100 mM DTT. With the help of a scintillation counter the probe was diluted to a final concentration of 5000 cpm/µl with hybridization solution and 10 µl 1M DTT were added to 100 µl of probe. The probe was stored at -20°C and before the hybridization it was preheated to 55°C.

The cryosections were stored at -80 °C and dried for 20 minutes after removal from the freezer. A fixation step for 15 minutes in 4 % PFA at RT and 3 washing steps for 5 minutes in PBS followed. The fixed cryosections were acetylated by equilibration in 0.1 M Triethanolamin, pH 8 for 3 minutes and subsequent incubation in 0.1 M Triethanolamin, pH 8 with recent addition of 350 µl acetic anhydride for 10 minutes at RT. An ethanol-dehydration-sequence followed with 3 minute incubations in 30, 50, 80, 95 % and absolute ethanol. After drying of the cryosections they were covered with 100 µl of hybridization mixture with labelled probe and overcasted with a glass coverslip which was fixed with DPX mount. The slides were incubated for 30 minutes under a hood and subsequently at 55 °C overnight. On the following day the slides were cooled down for 10 minutes at RT. DPX mount was removed and the cryosections passed the following washing steps: 20 minutes in 4x SSC at RT (after this step the glass coverslips were removed), 2 times 10 minutes in 4x SSC, 30 minutes in RNase buffer with RNase A at 37 °C, 15 minutes in 2x SSC, 15 minutes in 1x SSC, 15 minutes in 0.5x SSC, 30 minutes in 0.1x SSC at 55 °C and 10 minutes in 0.1x SSC at RT. The cryosections were dehydrated for 5 minutes in 70 % and 95 % ethanol and dried at RT. X-ray films (Kodak BioMax MR, Amersham) were

exposed to the radioactive cryosections for 1 day to several weeks and developed in Kodak developing and fixation solution. The slides were dipped in Kodak NTB-2 nuclear track emulsion subsequently and developed after 6-10 weeks.

### **3.6 Statistics**

All experiments in this thesis were conducted at least three times for qualitative and quantitative evaluation. Statistical analysis of the data from the  $\gamma$ -secretase assay and shRNA-analysis was conducted using Microsoft Excel (for mean values and standard deviations) or with SigmaPlot (for the indicated statistical tests).



## 4 Results

### 4.1 Identification of new interaction partners

The specific function of CLN3 is still elusive. One way to get more insights into the function of a protein is to find its interaction partners. Knowledge about the role of the interaction partners in subcellular processes can give hints on the functionality of the probed protein. There are different methods to screen for putative interaction partners. One of them is the Tandem affinity purification or Tap-tag technology. By this method protein complexes can be purified from their physiological context in two steps.

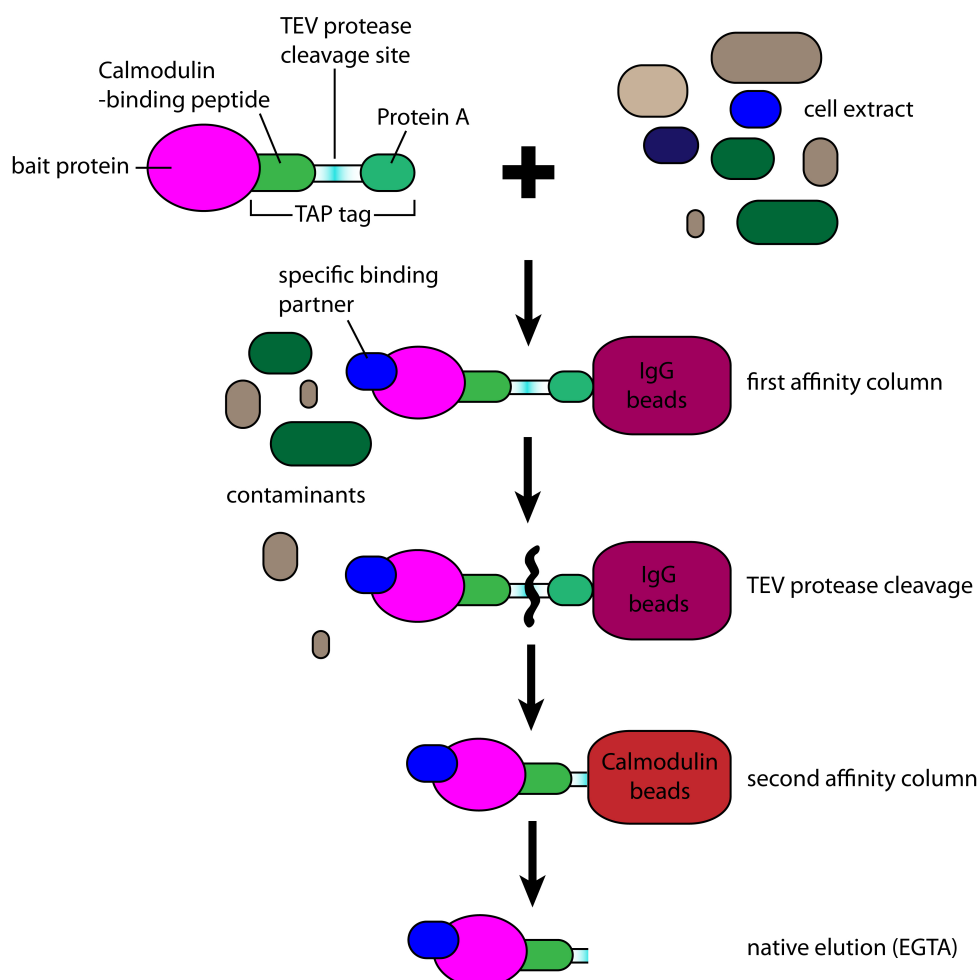


**Figure 5. Tandem Affinity Purification**

In the Tandem Affinity Purification (TAP-tag technology) bait and prey-protein complexes are purified in 2 steps by the TAP tag of the bait protein. On a first column the protein complexes are purified via the Protein A tag on IgG beads. After cleavage at the tobacco etch virus protease cleavage site, the complexes are run on a second column where they bind via their Calmodulin-binding peptide to Calmodulin beads. The native elution is conducted with EGTA. (Modified after Huber et al 2003)

The bait protein is expressed as a fusionprotein with a protein A-tag and a Calmodulin-binding peptide-tag. In the first purification step fusionproteins from cell lysates bind via their protein A-tag to IgG beads (Figure 5), (Huber 2003).

After cleavage at the Tobacco Etch Virus protease cleavage site another round of binding is carried out on calmodulin beads. The protein complexes can be eluted from these beads with the calcium chelator EGTA. The TAP-tag screen to identify new interaction partners for CLN3 was conducted in collaboration with the company Cellzome. The fusionproteins were expressed in neuroblastoma cells and CLN3 was used as the bait protein. Several different putative new interaction partners were identified in this screen. One of them was SorCS1. In only one other TAP-tag screen performed by Cellzome CLN3 was found as a putative interaction partner. In this screen Presenilin enhancer 2 (Pen2) was used as a bait protein.

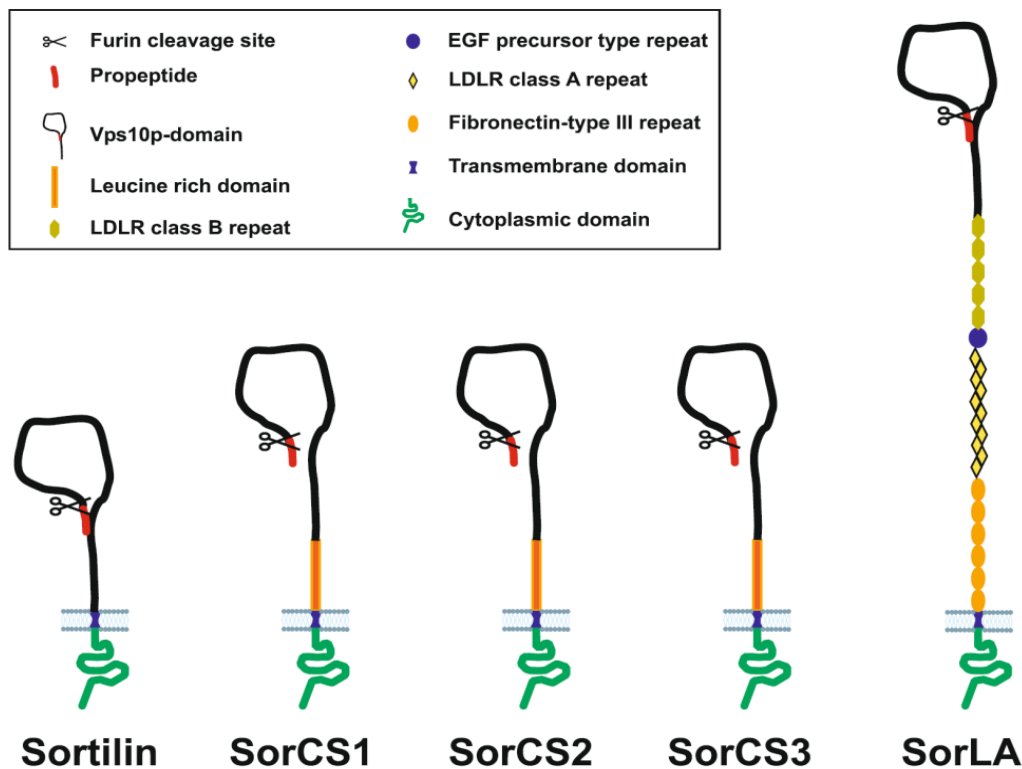


**Figure 6. The members of the Vps10p-Domain family of receptor proteins.** The members of the Vps10p-Domain family of receptor proteins are Sortilin, SorCS1, SorCS2, SorCS3 and SorLA. They all exhibit a Vps10p-domain, a propeptide that can be cleaved at the Furin cleavage site, a transmembrane domain, a cytoplasmic domain and various other domains that are specific for the particular family members. (Hermey 2009)

SorCS1 is a member of the Vps10p-Domain receptor family. Members of this family were also found to be involved in lysosomal trafficking. These receptor proteins are type-I transmembrane proteins with a large extracellular N-terminal part containing the Vps10p-domain and a short cytoplasmic domain (Figure 6). The Vps10p-Domain protein SorCS1 exists in at least 8 different splice variants. The splice variants all have identical extracellular and transmembrane parts, but different cytoplasmic domains. Some of the isoforms present functional internalization signals and mediate endocytosis (Nielsen et al. 2008). It has been demonstrated for human SorCS1a and -c that their internalization is adaptor-

protein-complex-2 (AP2) dependent (Nielsen et al. 2008). Several isoforms show prominent expression in the nervous system, but can also be found in other tissues (Hermeijer 2009). The expression in the hippocampus is regulated by neuronal activity (Hermeijer et al. 2004). The many different isoforms of SorCS1 are thought to have differential functions, but may share ligands. SorCS1 is genetically associated with Alzheimer's disease and Diabetes Type II. (Hermeijer 2009; Reitz et al. 2013). On the subcellular level most SorCS1 isoforms are localized to vesicular and perinuclear structures. These convey endocytosis and target internalized cargo to lysosomes (Nielsen et al. 2008). The protein is processed by proprotein convertases in the TGN and mature receptors traffic to the plasma membrane where they can internalize ligands to lysosomes. SorCS1 ability to internalize cargo may be a link to CLN3 sorting as it was shown that CLN3 is enriched at the cell surface after loss of C-terminal farnesylation (Storch et al. 2007; Hermeijer 2009).

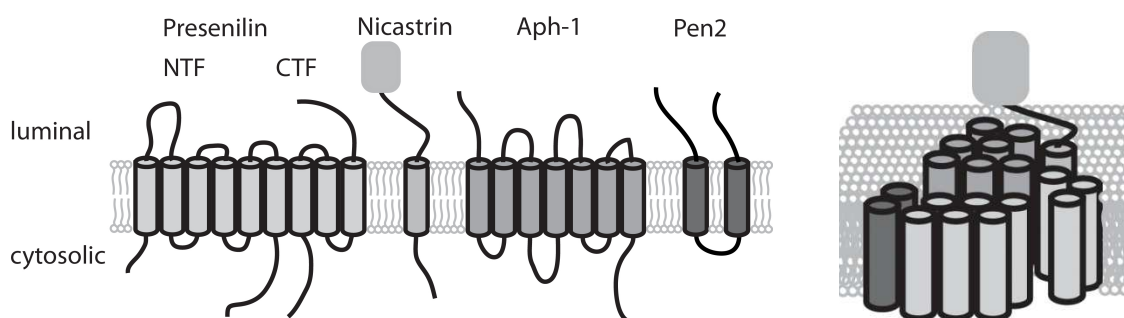


**Figure 7. The subunits of the  $\gamma$ -secretase complex and their assembly in the membrane.** The four subunits of the  $\gamma$ -secretase complex are Presenilin, Nicastrin, Aph-1 and Pen2. They assemble to a protein complex in the ER and build a water-containing pore where transmembrane-proteins can be cleaved. (Modified after Wolfe et al. 2006)

Pen2 is a small protein of 101 amino acids. It has presumably two hydrophobic domains and displays a hairpin topology (Wolfe 2006). Pen2 is the smallest subunit of the  $\gamma$ -secretase complex that catalyses the cleavage of transmembrane proteins with a single transmembrane domain (Beel & Sanders 2008) (Figure 7). The  $\gamma$ -secretase complex is assembled in the ER and Golgi. Pen2 is the last subunit that is added to the complex and the ER exit of the  $\gamma$ -secretase complex is dependent on Pen2. The fully assembled  $\gamma$ -secretase complex is localized to the ER and Golgi and to endosomes of different nature and to the plasma membrane. The optimal conditions for its activity are at an acidic pH at 4.5 which can be mainly found in late endosomes and lysosomes (Pasternak et al. 2003). The complex was also found in phagosomal structures (Jutras et al. 2005). The best-studied substrates of the  $\gamma$ -secretase complex are amyloid-protein precursor (APP) and Notch (Dries & Yu 2008). The  $\gamma$ -secretase complex is genetically associated with Alzheimer's disease (Haass et al. 2012). Alzheimer's disease as a neurodegenerative disease displays

similar features as JNCL with later in life occurring symptoms. This makes a connection between the two diseases through proteins potentially involved in cellular defects in both of them a relevant research subject.

## 4.2 Expression-pattern of CLN3-mRNA

One model system that was planned to be used during this thesis were primary hippocampal mouse embryo neurons. Since, to this date, CLN3 expression in mouse embryos was only analysed indirectly in  $\beta$ -galactosidase knock-in mice (Eliason et al. 2007) and not directly, I started my study with the analysis of mRNA expression of CLN3 in mice.

In radioactive in situ hybridizations the expression pattern of a specific gene can be visualized. To analyse the murine expression pattern of CLN3 two different probes for CLN3 were used. These showed similar results for the CLN3 mRNA expression pattern in 2 different experiments for each probe.

### 4.2.1 Expression of CLN3-mRNA during embryonic development

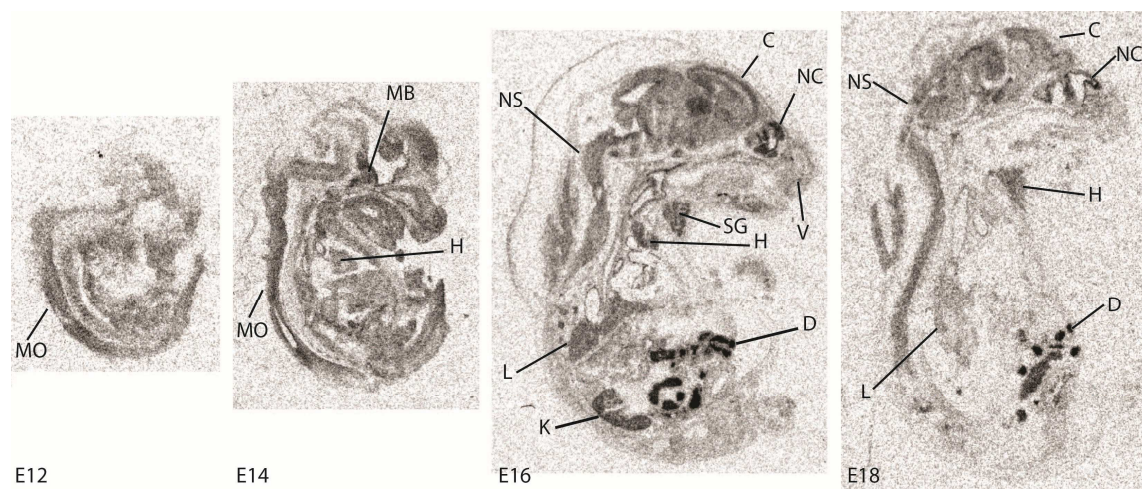


**Figure 8.** The expression pattern of CLN3 mRNA in radioactive in situ hybridizations on sections of embryonic mice at different developmental stages.

Sagittal sections of embryonic mice were probed for CLN3 mRNA with radioactively labelled mRNA-probes. The labelling was visualized on x-ray films which were exposed for 14 days. Expression maxima can be observed in the embryonic gastrointestinal tract, the kidney, liver, heart and thymus and a moderate expression in the medulla oblongata and the nervous system. C: Cortex; D: Duodenum; K: Kidney; L: Liver; MB: Midbrain; MO: Medulla oblongata; NC: Nasal cavity; SC: Spinal cord; SG: Submandibular gland; T: Thymus; V: Vibrissae.

The mRNA expression pattern of CLN3 was analysed in autoradiograms of sagittal sections of embryonic developmental stages E12, E14, E16 and E18 (Figure 8). CLN3 mRNA is ubiquitously expressed in all analysed developmental stages. In the autoradiograms expression maxima can be seen in the gastrointestinal tract, kidney, liver,

nasal cavity, and heart. Within the nervous system, medulla oblongata, embryonic midbrain and the cortex in older embryos show a moderate expression level.

#### 4.2.2 Expression of CLN3-mRNA in the developing and adult brain

In the mouse brain the expression levels for CLN3 mRNA are very homogenous (Figure 9). There is no especially high expression in any specific region. Areas of high cell density like the hippocampus and the cerebellum show highest radioactive labelling.

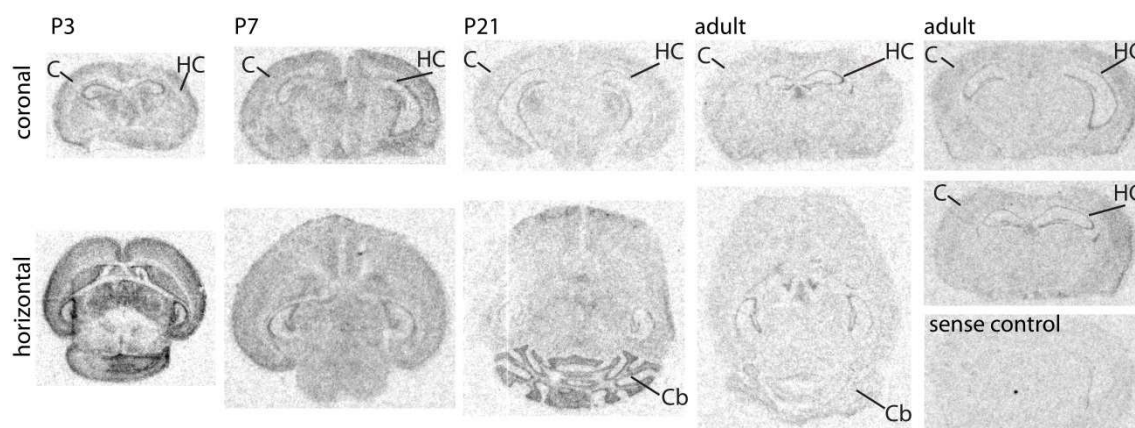


**Figure 9. The expression pattern of CLN3 mRNA in radioactive in situ hybridizations on sections of embryonic mouse brains at different developmental stages.**

Coronal and horizontal sections of brains at different developmental stages (P3, P7, P21 and adult) were probed for CLN3 mRNA with radioactively labelled mRNA-probes. The labelling was visualized on x-ray films which were exposed for 14 days. Expression maxima can be observed in the cerebellum and the hippocampal formation. For the adult brain a coronal section labelled with the sense-control for CLN3 mRNA is displayed and shows no signal. (C: Cerebral Cortex; Cb: Cerebellum; H: Hippocampus).

#### 4.2.3 Activity-regulation of CLN3-mRNA levels

Some of the other NCL-genes like Ppt1 and cathepsin D proved to be upregulated after kainic acid induced seizures (Hetman et al. 1995; Suopanki et al. 2002). Eliason et al. also found an upregulation of  $\beta$ -galactosidase expression in the hippocampus in their reporter CLN3 knock-in mouse 24 hours after seizure induction with pentylenetetrazole.

Since CLN3 mRNA was found to be expressed in the hippocampus in my studies, I tested the expression levels after kainic acid induced seizures. For this purpose mice were treated with kainic acid and sacrificed 1, 4, 8 or 24 hours after the seizure. No significant induction of mRNA-expression was observed for CLN3 (Figure 10). 4 hours after the onset of seizures there might be even a reduction in the CLN3 mRNA level but since the mRNA level is very low in general this is not clear.

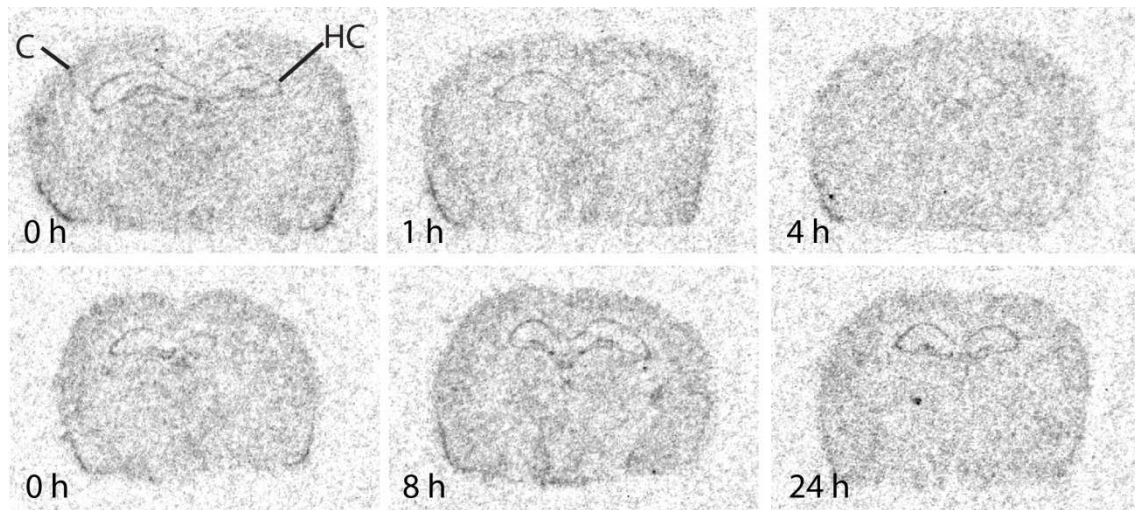


**Figure 10. The expression pattern of CLN3 mRNA in radioactive in situ hybridizations on sections of embryonic mouse brains after seizure induction by kainic acid.**

Mice were treated with kainic acid to induce seizures and sacrificed at different time points after the seizure (0 hours: control without induction, 1 hour, 4 hours, 8 hours, 24 hours after seizure). Coronal sections of the brains of the mice were probed for CLN3 mRNA with radioactively labelled mRNA-probes. The labelling was visualized on x-ray films which were exposed for 14 days. There is no significant induction of CLN3-mRNA expression after seizures. (C: Cerebral Cortex; H: Hippocampus).

### 4.3 Subcellular localization of CLN3

Proteins that display functional interactions in cellular processes show co-localization on a subcellular level. This can be tested by using specific antibodies or after labelling of the relevant proteins in transfected cells. Currently highly specific antibodies against CLN3 are not available. Therefore, different labelling of CLN3 was used to detect CLN3. The cellular system that is the easiest to be used for expression and localization of proteins are secondary cultured cells or cell lines. In this project HeLa and Hek293 cells were tested and HeLa cells proved to give the more consistent results. Proteins that were supposed to be analysed were either labelled through specific antibodies after the transfection and fixation of the cells or were labelled with fluorescent or HA-tags. In initial experiments, different N- or C-terminal tags were added to CLN3. N-terminal tags proved to give the more consistent and better results in comparison to the literature.

#### 4.3.1 Localization of CLN3 in comparison to organelle markers in HeLa cells

To test the trafficking and subcellular localization of the tagged CLN3 constructs different subcellular marker constructs were co-expressed with CLN3 in HeLa cells.

CLN3 shows most prominent co-localization with late endosomal and lysosomal markers. Lysosomal integral membrane protein 1 (Limp1) - also named CD63 - is a late

endosomal/lysosomal membrane protein. After co-expression with CLN3 in HeLa-cells the two proteins co-localize to a great extent to the same membranes (Figure 11a).

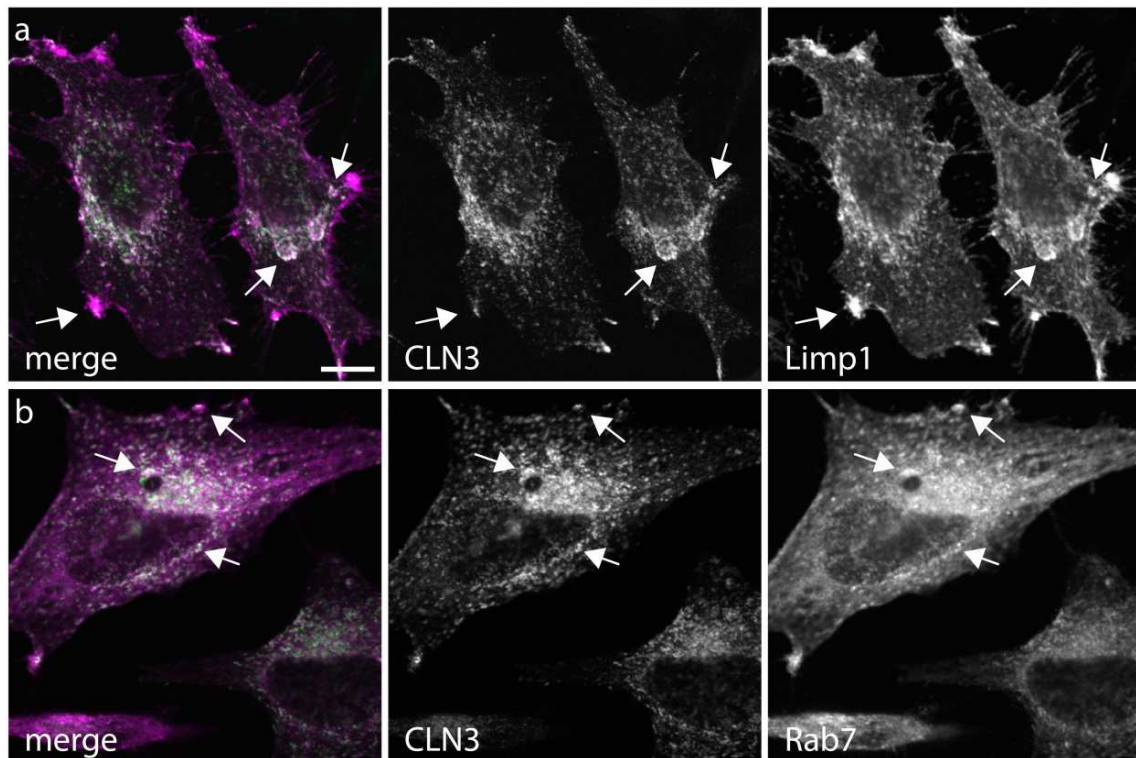


**Figure 11. Subcellular localization of CLN3 in comparison to subcellular marker proteins in lysosomal and late endosomal structures of transfected HeLa-cells.**

HeLa-cells were co-transfected with GFP-CLN3 and tdTomato-Limp1 or tdTomato-Rab7. After PFA-fixation the proteins were labelled by anti-GFP and anti-dsRed antibodies and fluorescently labelled secondary antibodies. For each co-expression experiment a merged image (CLN3 in green, Limp1 and Rab7 in magenta, white indicates overlapping staining) and the respective single images for both proteins are displayed. The arrows point to regions of interest. a: CLN3 shows strong co-localization with Limp1 in endosomal structures but less overlap on the plasma membrane. b: CLN3 and Rab7 display a strong overlap in endosomal structures which primarily localize to the perinuclear region. Scale bar in a (applies to all parts): 10  $\mu$ m. Confocal laser scanning microscope.

Particularly great overlap can be observed in the perinuclear region harbouring lysosomes. Some overlapping spots of localization also occur at the plasma membrane. Rab7 is a small GTPase that is localized to the late endosomal and lysosomal compartment and plays a role in the maturation of late endosomes and phagosomes to lysosomes. This protein shows co-localization with CLN3 in several vesicular structures in transfected HeLa-cells (Figure 11b).

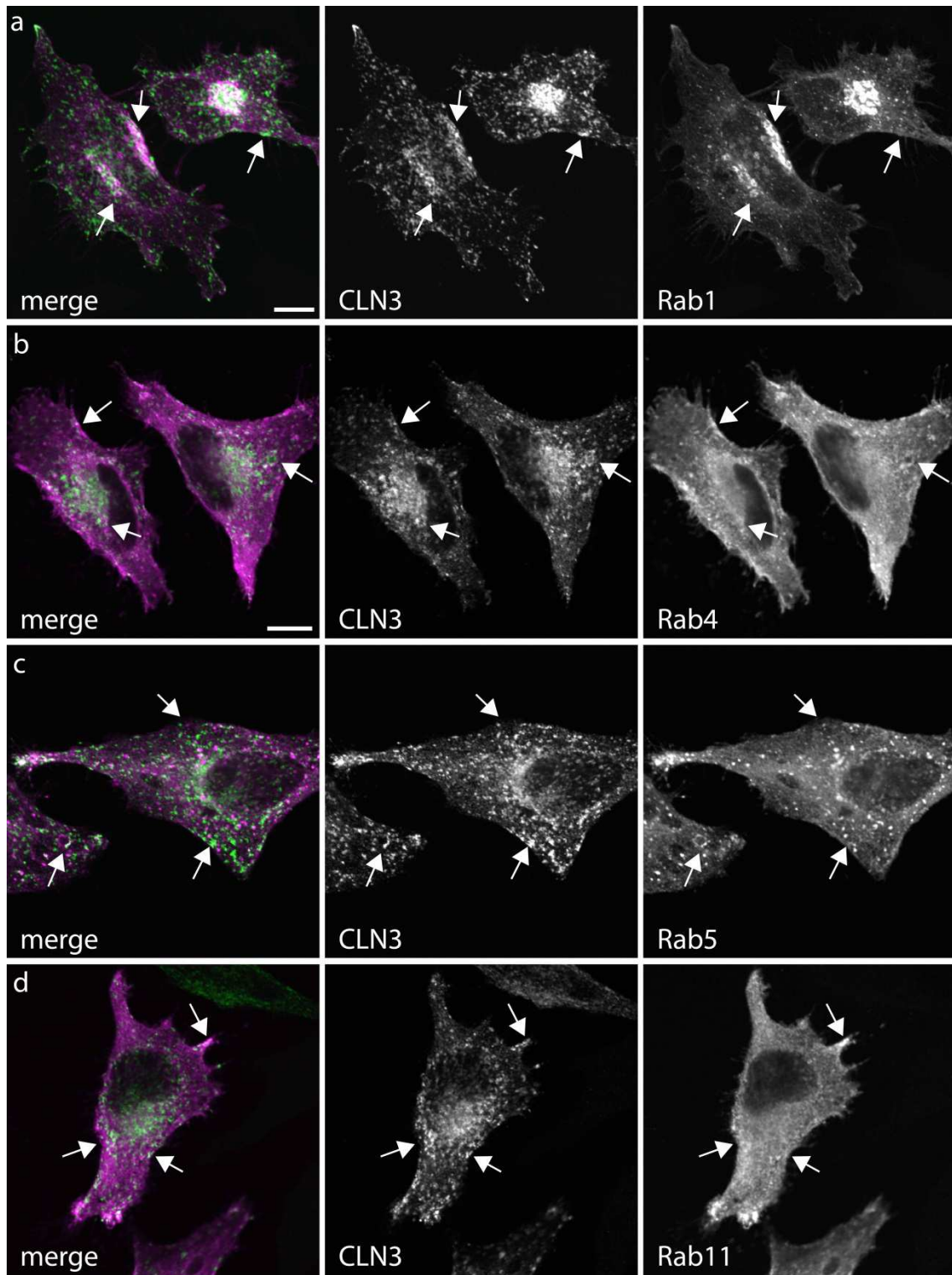


**Figure 12. Subcellular localization of CLN3 in comparison to subcellular marker proteins in transfected HeLa-cells.**

HeLa-cells were co-transfected with HA-CLN3 and GFP-Rab1, GFP-CLN3 and tdTomato-Rab4, tdTomato-Rab5 or tdTomato-Rab11. After PFA-fixation the proteins were labelled by anti-HA, anti-GFP and anti-tdRed antibodies and fluorescently labelled secondary antibodies. For each co-expression experiment a merged image (CLN3 in green, Rab1, Rab4, Rab5 and Rab11 in magenta, white indicates overlapping staining) and the respective single images for both proteins are displayed. The arrows point to regions of interest. a: CLN3 shows neighbouring localization with Rab1. b: Some co-localization of CLN3 and Rab4 in endosomal structures can be found in the cell periphery. c: CLN3 and Rab5 display little overlap but some adjacent localization. d: There is no co-localization between CLN3 and Rab11. Scale bar in a and b: 10  $\mu\text{m}$  (scale bar in a applies to a, c and d). Confocal laser scanning microscope.

CLN3 supposedly reaches its final localization after passing the Golgi. In order to analyse a Golgi-localization of CLN3 it was co-expressed with the small GTPase Rab1 which associates with structures in the ER-to-Golgi transition area. The two proteins both show a strong localization to the perinuclear region but are rather localized next to each other than at identical spots (Figure 12a). The small GTPase Rab4 mostly localizes to early endosomes and has its functional role in fast recycling to the plasma membrane. CLN3 and Rab4 do not co-localize to a great extent, but do in some smaller vesicular structures. Some endosomal compartments show localization of CLN3 on one side and localization of Rab4 on another part of the structure (Figure 12b). Rab5 is also a marker for early endosomes and is important during endocytosis. CLN3 again shows little co-localization with this protein but some vesicular structures are labelled for both (Figure 12c). The small GTPase Rab11 localizes to the recycling endosome and regulates slow endocytic recycling. With Rab11 CLN3 shows the least co-localization in co-expression experiments in HeLa-cells (Figure 12d).

### **4.3.2 Global localization of CLN3 in primary hippocampal neurons**

JNCL is a neurodegenerative disease. Thus the localization pattern of CLN3 in neurons might be relevant for understanding the development of JNCL. The localization of tagged CLN3 was analysed in dissociated primary hippocampal mouse embryo neurons. The neuronal cells were co-transfected with GFP as a filler for the whole neuron and stained with an antibody against Map2 as a marker for dendritic microtubules. CLN3 localizes to roundish endosomal structures that vary in size in almost every region of primary hippocampal mouse embryo neurons (Figure 13). The expression is more prominent in the somatic and dendritic region where relatively large CLN3-positive structures can be observed. Smaller and fewer CLN3-positive structures can be found in the axon (Figure 13).

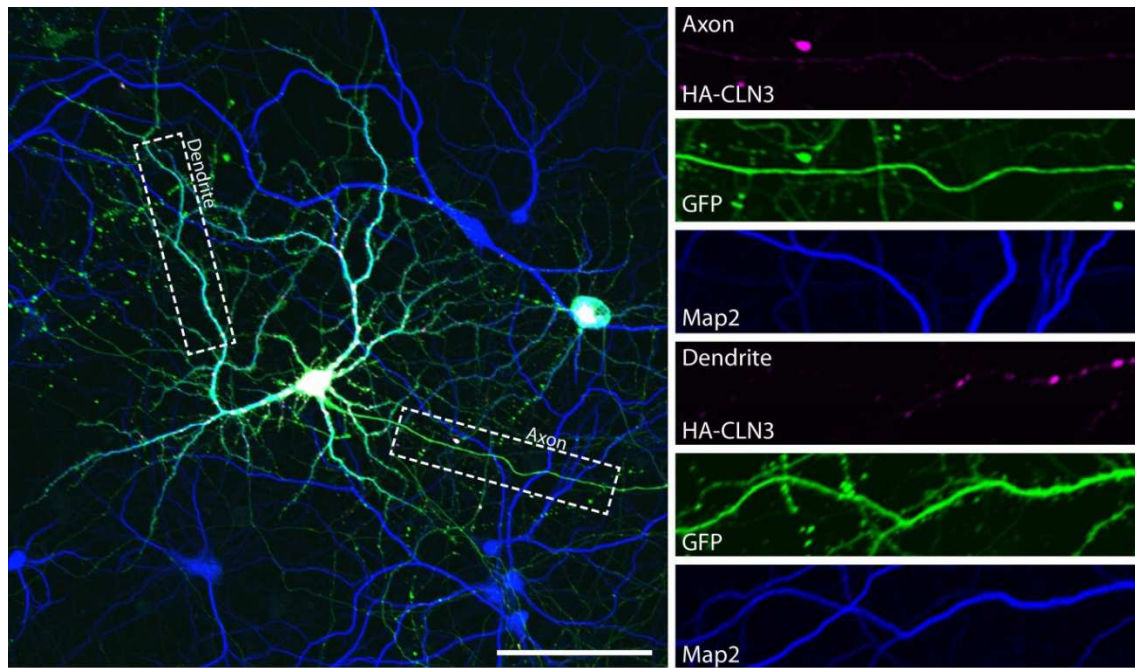


**Figure 13. HA-CLN3 shows somatic, dendritic and axonal localization in primary hippocampal mouse neurons.**

Dissociated hippocampal neurons were transfected at DIV3 with HA-CLN3 (shown in magenta) and EGFP (shown in green). After PFA-fixation at DIV15 the labelling with anti-HA, anti-GFP and anti-Map2 (for dendritic microtubules, shown in blue) and fluorescently labelled secondary antibodies was conducted. Stack-images of the neuronal cells were taken by confocal laser scanning microscopy. Maximum intensity projections of a merge overview and the respective single images for the zoom-in of the dotted boxes on axon and dendrite are shown. CLN3 can be found in axons and dendrites. In the axon the vesicular structures positive for CLN3 are smaller than the ones in dendrites. Scale bar in overview: 100  $\mu$ m.

For the functionality of the nervous system the propagation of electric signals is crucial. These signals are transferred by chemical signalling from one cell to another at synapses. For this purpose dendrites of neurons harbour spines that receive synaptic input from axonal presynapses. Synaptic contacts and their usage are important for neuronal growth and plasticity. Neurons can show degeneration when they do not receive input from other neurons anymore. Since the reason for neurodegeneration in JNCL has so far not been identified it is relevant to determine if CLN3 localizes to synaptic structures like dendritic spines. Primary hippocampal mouse embryo neurons were co-transfected with HA-tagged murine CLN3 and GFP as a filler and labelled with an antibody against Map2. The dendritic spines are visualized by the GFP that localizes to dendrites and spines. CLN3-positive punctae can be seen in distant dendritic regions (Figure 14a, b). In dendritic spines mostly very little or no CLN3 signal is visible. A small fraction of spines can be identified that harbours CLN3. In comparison to CLN3 the receptor protein SorCS3 shows prominent localization to dendritic spines (Figure 14c, d).

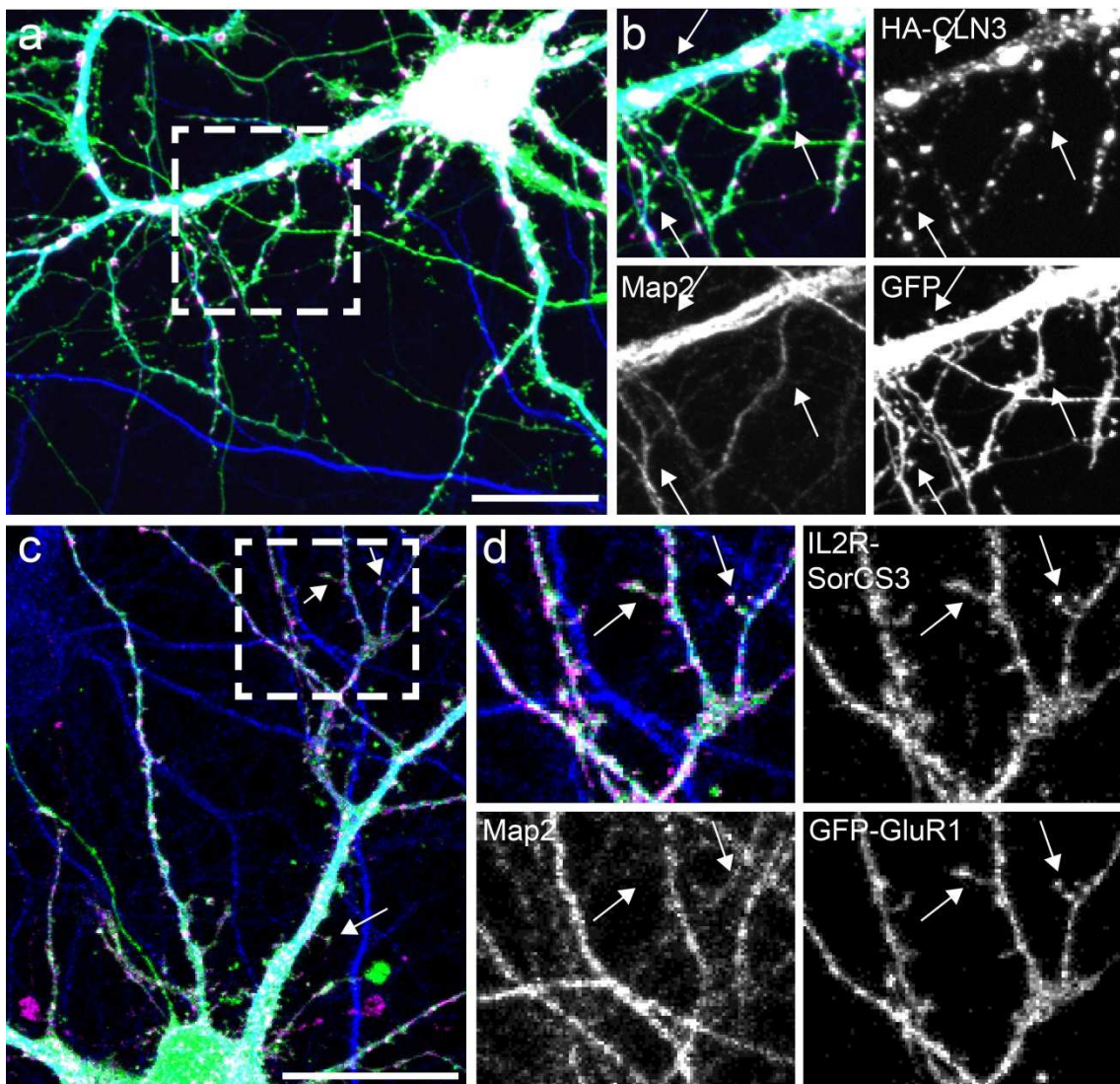


**Figure 14. HA-mCLN3 does not localize to dendritic spines in primary hippocampal mouse neurons as extensively as SorCS3.**

Dissociated hippocampal neurons were transfected at DIV3 with HA-CLN3 (shown in magenta), IL2-SorCS3 (shown in magenta) and GFP (for CLN3 (a, b) shown in green) or GFP-mGluR1 (for SorCS3 (c, d), shown in green). After PFA-fixation at DIV15 (CLN3) or DIV10 (SorCS3) the labelling with anti-HA, anti-IL2, anti-GFP and anti-Map2 (for dendritic microtubules, shown in blue) and fluorescently labelled secondary antibodies was conducted. Stack-images of the neuronal cells were taken by confocal laser scanning microscopy. Maximum intensity projections of a merge overview and the respective single images for the zoom-in of the dotted boxes on dendritic regions are shown. a, b: CLN3 shows localization to large endosomal structures in the shaft of the displayed dendrite. In some spines (arrows) a small fraction of CLN3 can be found but from most spines CLN3 is absent. c, d: SorCS3 shows a distribution over the whole area of the dendrite and also a strong localization to dendritic spines (arrows). Scale bar in a and c: 20  $\mu\text{m}$ .

### 4.3.3 Localization of CLN3 in comparison to organelle markers in primary hippocampal neurons

CLN3 localizes to endosomal structures of various sizes in the soma and neurites of primary hippocampal mouse embryo neurons. To test of what nature these structures are, co-localization analysis with subcellular marker proteins was conducted.

In previous publications a localization of CLN3 to the Golgi-apparatus was discussed. CLN3 was found in the Golgi by some research groups but others observed a localization

to the endosomal / lysosomal system in secondary cell culture or yeast. In my studies I analysed the co-localization of CLN3 with the Golgi-markers TGN46 and GM130 in primary hippocampal neurons (Figure 15a, b)..

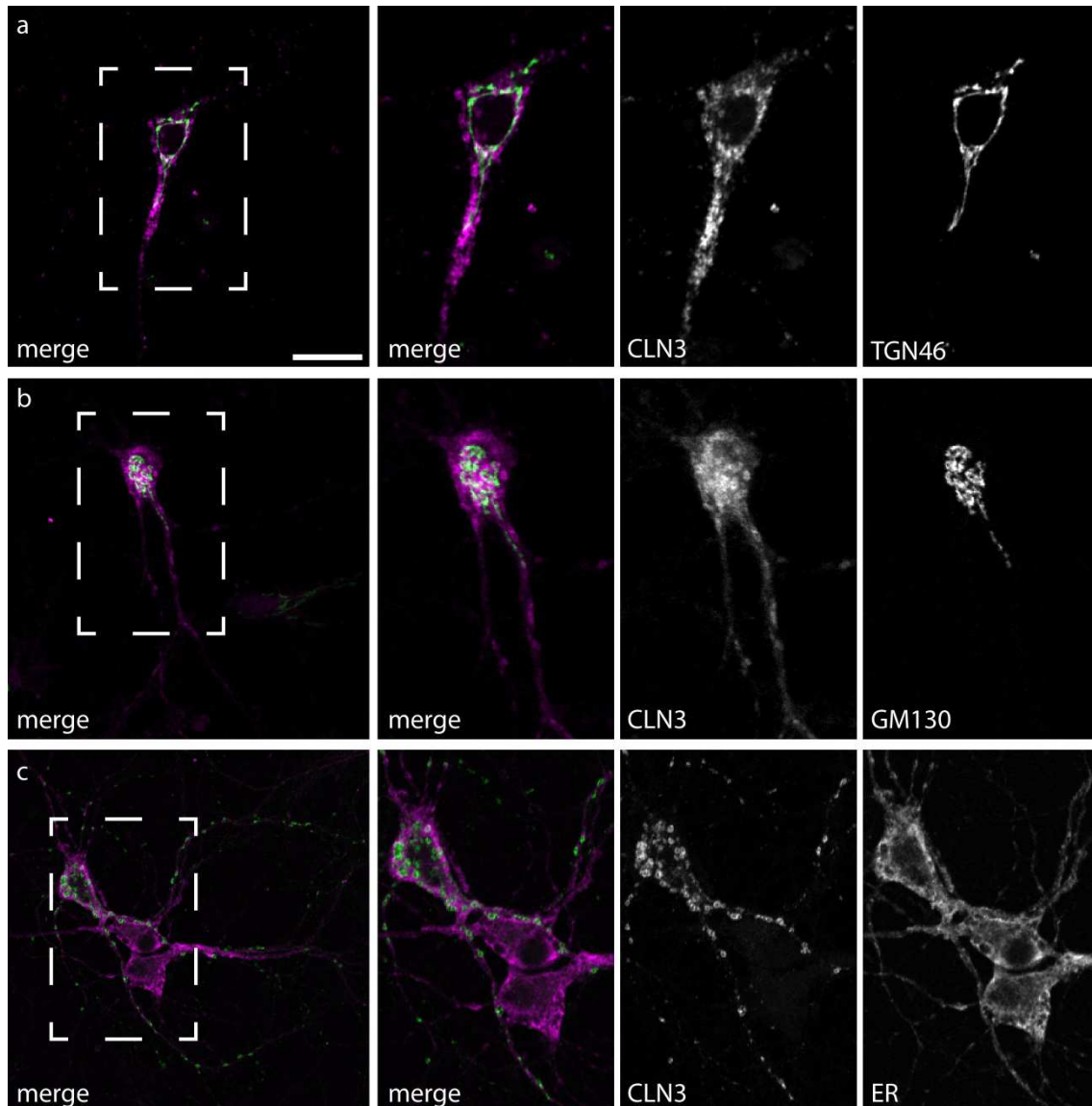


**Figure 15. Subcellular localization of CLN3 in comparison to the major cellular organelles Golgi and ER in transfected primary hippocampal mouse neurons.**

Primary hippocampal mouse embryo neurons were transfected with HA-CLN3 or GFP and after PFA-fixation stained for TGN46 (at DIV17), GM130 (at DIV16) and ER (at DIV14) and fluorescently labelled secondary antibodies. For each experiment a merged image and zoom-in of the merge with the respective single images for both proteins are displayed. a: CLN3 (red) shows no co-localization with the trans-Golgi-marker TGN46 (green). b: CLN3 (red) and the cis-Golgi-marker GM130 (green) show little overlap. c: There is no overlap between GFP-CLN3 (green) and the ER-staining (red). Scale bar in a (applies to a, b and c): 20  $\mu$ m. Confocal laser scanning microscope.

There was no overlap of CLN3 with the trans-Golgi-marker TGN46 in hippocampal neurons (Figure 15a). The analysis of CLN3 in comparison with the cis-Golgi-marker GM130 showed some very small regions that showed overlap but these in total are negligible (Figure 15b). In the course of this thesis the interaction of CLN3 with Pen2 was going to be analysed. Since Pen2 was to a major part found in the ER, I analysed the localization of CLN3 in the ER. In GFP-CLN3-transfected neurons stained for the ER-

marker protein Binding immunoglobulin protein (BiP) there was no overlap between CLN3- and BiP-localization (Figure 15c). In addition to the major cellular synthesizing organelles Golgi and ER the co-localization of CLN3 with other marker proteins was tested in cultured hippocampal neurons. Like in HeLa-cells, CLN3 co-localizes with the late endosomal / lysosomal marker Limp1 to almost 100 % in primary hippocampal mouse embryo neurons (Figure 16a). CLN3 and the late endosomal marker Rab7 do largely localize to the same vesicular structures but do not show total overlap on every single one of these structures (Figure 16b).

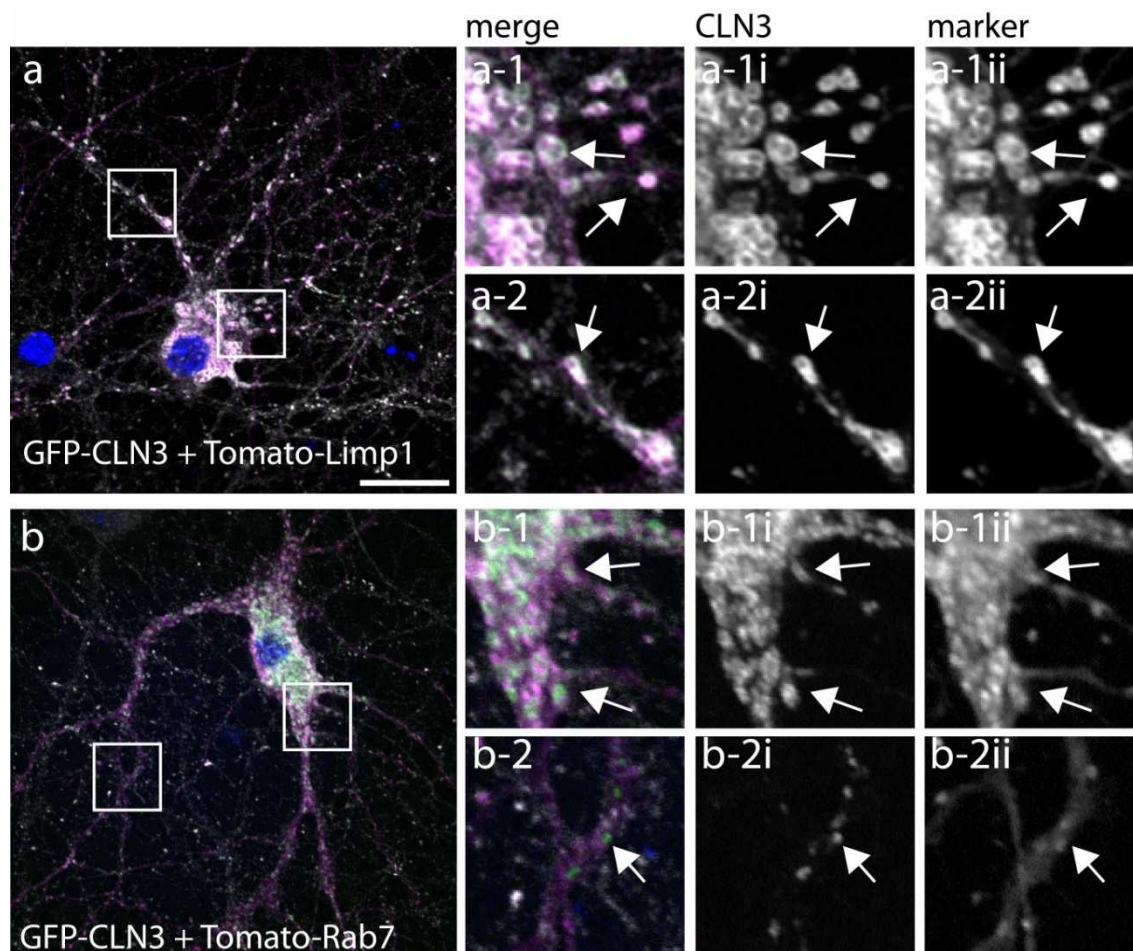


**Figure 16. Subcellular localization of CLN3 in comparison to subcellular marker proteins in lysosomal and late endosomal structures of transfected primary hippocampal mouse neurons.**

Primary hippocampal mouse embryo neurons were co-transfected with GFP-CLN3 (shown in green) and tdTomato-Limp1 (shown in magenta) or tdTomato-Rab7 (shown in magenta) at DIV13. After PFA-fixation at DIV15 the proteins were labelled by anti-GFP and anti-dsRed antibodies and fluorescently labelled secondary antibodies and mounted with Dapi. For each co-expression experiment a merged image and a somatic and a neuritic zoom-in with the respective single images for both proteins are displayed. The arrows point to regions of interest. a: CLN3 (green) shows strong co-localization with Limp1 in endosomal structures in the somatic as well as the neuritic region. b: CLN3 and Rab7 display a strong overlap in endosomal structures particularly in the somatic region. In the dendritic region the overlap does not apply to all structures. Scale bar in a (applies to a and b): 20  $\mu$ m. Confocal laser scanning microscope.

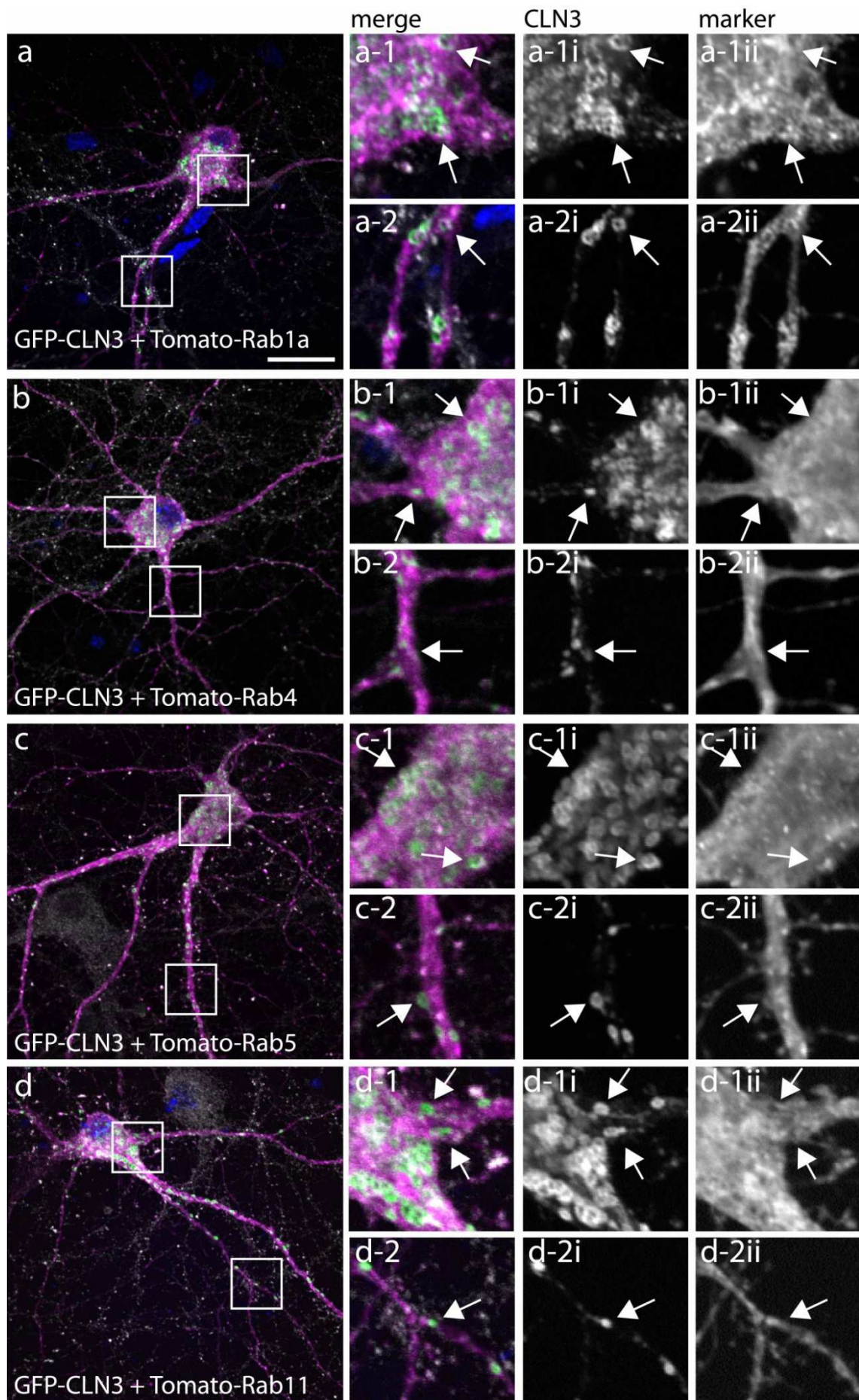


Figure 17. Subcellular localization of CLN3 in comparison to subcellular marker proteins in transfected primary hippocampal mouse neurons.

Primary hippocampal mouse embryo neurons were co-transfected with GFP-CLN3 (shown in green) and tdTomato-Rab1, tdTomato-Rab4, tdTomato-Rab5 or tdTomato-Rab11 at DIV13 (Rab1, Rab4, Rab5 and Rab11 shown in magenta). After PFA-fixation at DIV15 the proteins were labelled by anti-GFP and anti-dsRed antibodies and fluorescently labelled secondary antibodies and mounted with Dapi. For each co-expression experiment a merged image and a somatic and a neuritic zoom-in with the respective single images for both proteins are displayed. The arrows point to regions of interest. a: CLN3 and Rab1 show adjacent localization in the somatic and neuritic region. b: Some co-localization of CLN3 and Rab4 can be found in endosomal structures in the neuritic regions. c: CLN3 and Rab5 display little overlap but some neighbouring localization in the soma and the neurite. d: There is very little to no co-localization between CLN3 and Rab11. Scale bar in a (applies to overviews a, b, c and d): 20  $\mu\text{m}$ . Confocal laser scanning microscope.

The small GTPase Rab1a – a marker for ER-to-Golgi transition areas and CLN3 do not show large areas of overlap. Some structures are positive for both proteins and at some spots they are localized very close to each other (Figure 17a). The localization patterns of CLN3 and Rab4 also show little overlap. There are small spots of co-localization in neuritic regions. The stronger overlap between the two proteins in the somatic region is likely to be due to more total protein content. Rab5 shows less overlap with CLN3 than Rab4 (Figure 17b, c). In neuritic regions there are again a few structures that are positive for both proteins. Like Rab4 and CLN3, Rab11 and CLN3 show some overlapping localization in the somatic region. There is little to no co-localization in neurites (Figure 17d). These localization studies demonstrate that CLN3 localizes primarily to lysosomal and late endosomal vesicular structures in transfected cell lines as well as in primary cultured neurons. There is little to no co-localization with markers for the Golgi, ER or early endosomes. Moreover, in hippocampal neurons most CLN3 can be found in somatic-dendritic areas with a minor population of CLN3-positive endosomes in spines. In the axon CLN3 is also present but to a smaller ratio.

## 4.4 Trafficking of CLN3

CLN3 localizes to endosomal structures that are primarily of lysosomal or late endosomal nature in HeLa-cells and primary hippocampal mouse embryo neurons. Life-cell-imaging experiments are a valuable tool to determine the nature and physiology of these structures.

### 4.4.1 Trafficking of CLN3 in HeLa-cells

To analyse CLN3-positive structures in living cells GFP-tagged CLN3 was first expressed in HeLa cells. Most of the CLN3-positive vesicles show a fast movement within the cell. A large portion is localized to the perinuclear lysosomal region but GFP-positive structures can also be found in the cell periphery and near the plasma membrane. A lot of these structures show fast movement from the plasma membrane to the perinuclear space or vice versa. There is also movement along the edges of the cell where the submembranous actin

---

cytoskeleton is localized (Figure 18a). The trafficking of CLN3 positive endosomes seems to be directed as shown by tracking with the Fiji plugin Trackmate. Some of the tracks follow the same path and overlap as can be seen by the colored lines (Figure 18b).

For the analysis, GFP-tagged CLN3 was overexpressed in HeLa-cells and visualized by spinning disc laser scanning microscopy in living cells. Video sequences lasted for up to 3 minutes in HeLa-cells. The moving GFP-positive endosomal structures were then tracked with the Trackmate-Plugin. The LoG detector was used to find spots of around 1  $\mu\text{m}$  diameter and for these tracks were retrieved with a maximal gap distance of 2  $\mu\text{m}$  and a maximal frame gap of 2. For the displayed cell 809 tracks were found in the 3 minute sequence. Of those 154 tracks that had a mean velocity over 0.3  $\mu\text{m}/\text{second}$  are displayed. Some of the spots show a migration on a similar track as others. This points to a directed movement of the CLN3-positive endosomal structures. The mean maximum speed found in this cell for a CLN3-positive structure is 1.27  $\mu\text{m}/\text{sec}$  with a standard deviation of 0.008  $\mu\text{m}/\text{sec}$ . For other cells the maximum speed also spread around this value.

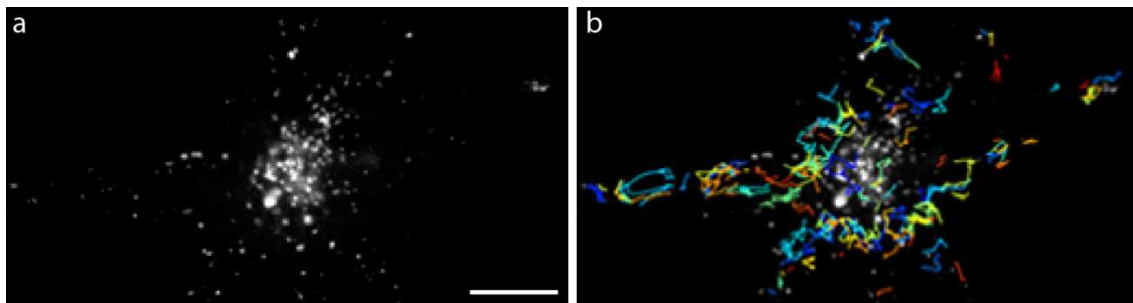


**Figure 18. Subcellular trafficking of CLN3 in in transfected HeLa cell.**

Living HeLa-cells overexpressing GFP-CLN3 were imaged for 1 min. GFP-CLN3 is localized to endosomal structures moving less or more fast in the cell (a). The moving endosomal structures were tracked with the ImageJ tool TrackMate and the tracks are labelled by coloured lines (b). Scale bar: 10  $\mu\text{m}$ . Visitron Systems Spinning Live Cell Confocal, 37 °C and 5 % CO<sub>2</sub>.

#### 4.4.2 Trafficking of CLN3 in neurons

To get further information on the endosomal structures harbouring CLN3 in neurons, the vesicular transport of CLN3 positive structures was analysed in live-cell spinning disk microscopy in primary hippocampal mouse embryo neurons. The dissociated neuronal cultures were transfected with fluorescently tagged CLN3 at DIV3 to DIV6 and visualized in life-cell-imaging at DIV6 to DIV12. CLN3 was detected in mobile endosomal structures all over the cell in neurons and in HeLa cells. The somatic CLN3-positive endosomes show a similar behaviour as those seen in HeLa-cells. In neurites of younger neurons (DIV6 to DIV8) CLN3 positive structures show fast movement of retrograde and anterograde direction. This trafficking behaviour was observed in more than five independent experiments with a total number of CLN3-transfected neurons of over 30. The trafficking

along a neurite of DIV7 neuron is visualized in Figure 19. The imaged sequence lasted for 180 seconds. The trafficking of CLN3-positive structures was analysed with the ImageJ MultipleKymograph plugin. The kymograph (Figure 19b) was created for the dotted line displayed in Figure 19a and has a spatial length of 93  $\mu\text{m}$ . In the retrograde direction towards the soma of the neuron the movement of some larger structures was observed. Trafficking in the anterograde direction is mostly performed by smaller CLN3-positive structures.

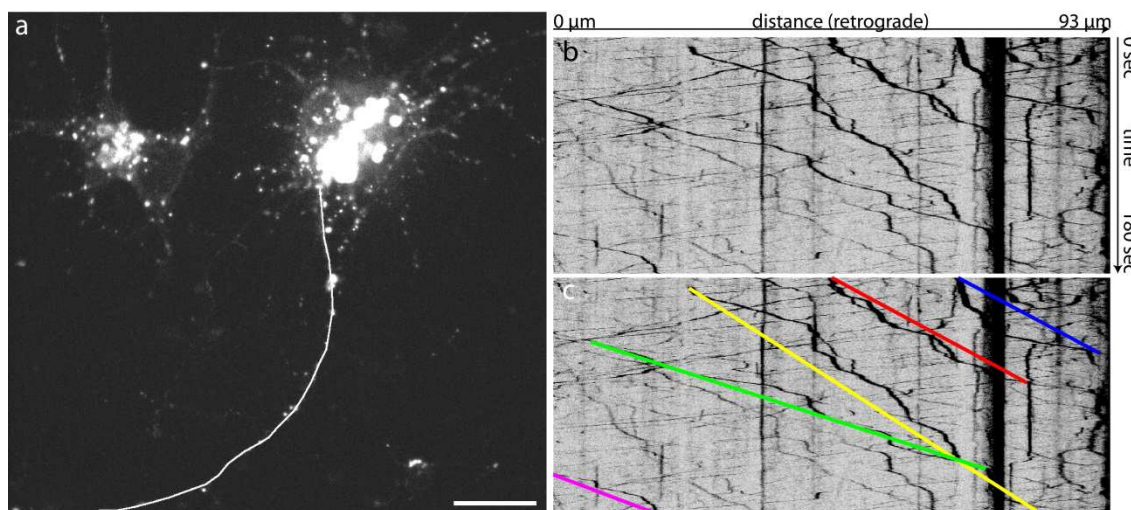


**Figure 19. Subcellular trafficking of CLN3 in transfected primary hippocampal neurons.** Living neurons overexpressing GFP-CLN3 were imaged for 3 min. GFP-CLN3 is localized to endosomal structures moving less or more fast in the cell soma and processes. The first image of the sequence is displayed with a white line marking the neurite where vesicles were tracked in (a). Along the line a kymograph was generated with the ImageJ plugin MultipleKymograph. The kymograph shows the movement of vesicles in retrograde and anterograde direction in the neurite along a distance of 93  $\mu\text{m}$  (b). The mean velocity of GFP-CLN3-positive vesicles was measured by assessing the length of tracks over time (c). Timeframe of imaging sequence: 180 sec. Scale bar in a: 17  $\mu\text{m}$ . Perkin Elmer Spinning Disk Confocal microscope, 37  $^{\circ}\text{C}$  and 5 %  $\text{CO}_2$ .

**Table 9. Velocity of moving CLN3-positive vesicular structures in 4 different neurons**

	cell 1 (DIV8)	cell 2 (DIV7)	cell 3 (DIV7)	cell 4 (DIV8)
Velocity ( $\mu\text{m}/\text{sec}$ )	0.736	0.340	1.27	0.848
	0.642	0.675	0.846	1.1
	0.874	0.409	1.186	0.343
	1.417	0.413	0.948	0.739
	0.723	0.574	0.458	0.99
average	0.878	0.482	0.942	0.804
standard deviation	0.313	0.138	0.320	0.292
all values:				
average:	0.776			
standard deviation:	0.311			

To get more detailed information about the trafficking of CLN3-positive structures in primary hippocampal mouse neurons the velocity of a representative fraction of

retrogradely moving endosomal structures was measured (Figure 19c). The mean speed of these structures lies at  $0.776 \mu\text{m}/\text{sec}$  with a standard deviation of  $0.311$ . The maximal velocity that was observed in the retrograde trafficking of CLN3-positive endosomes is  $1.27 \mu\text{m}/\text{sec}$  (Table 9).

#### 4.4.2.1 Cotrafficking of CLN3 with organelle markers in primary hippocampal neurons

The trafficking of CLN3 in HeLa cells and the neuritic and somatic compartment of primary hippocampal mouse embryo neurons is carried out in endosomal structures. In fixed cells CLN3 was shown to co-localize with different marker proteins. Most co-localization was detected with the late endosomal and lysosomal marker proteins Rab7 and Limp1. Little co-localization was seen with the early endosomal marker proteins Rab5 and Rab11.

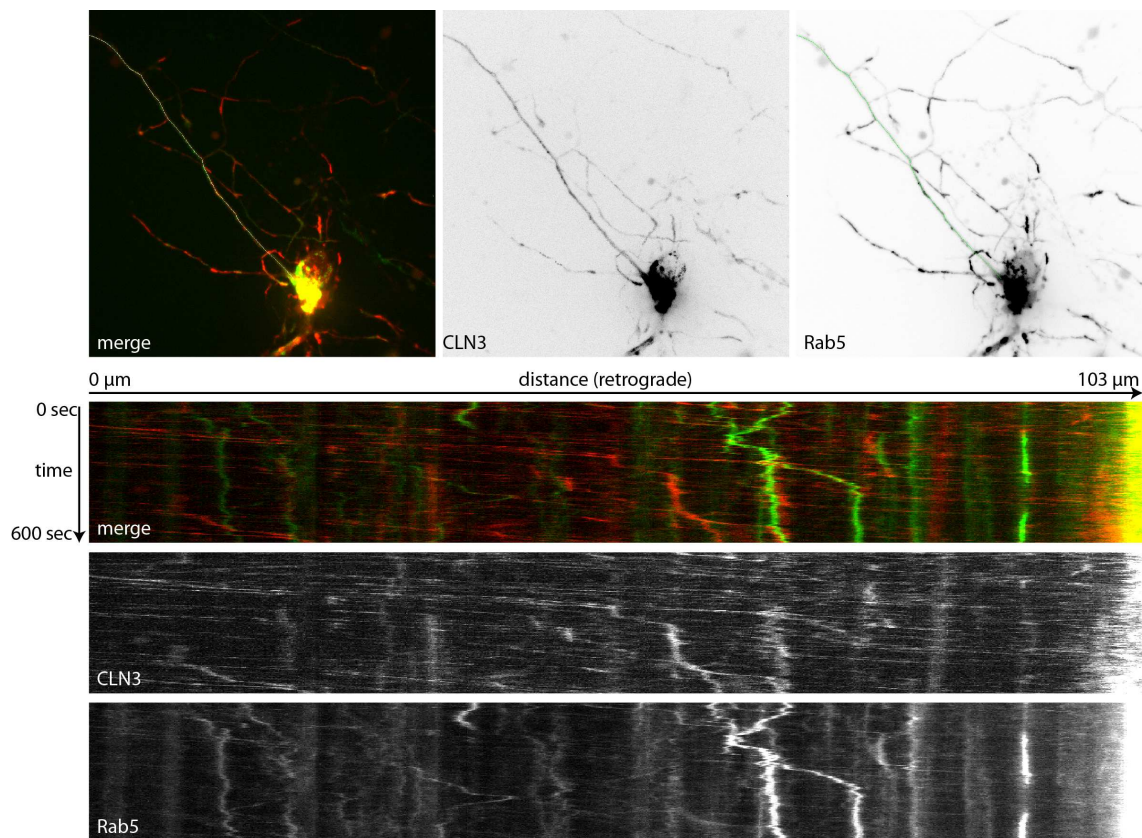


**Figure 20. Subcellular trafficking of CLN3 and Rab5 in transfected primary hippocampal neurons.** Living neurons overexpressing GFP-CLN3 and tdTomato-Rab5 were imaged for 10 min. GFP-CLN3 (green) and tdTomato-Rab5 (red) are localized to not overlapping endosomal structures moving more or less fast in the cell soma and processes. A merge and single channels of the first image of the sequence is displayed with a line marking the neurite vesicles where tracked in. Along the line a kymograph was generated with the ImageJ plugin MultipleKymograph. The kymograph shows the movement of vesicles in retrograde and anterograde direction in the neurite along a distance of  $103 \mu\text{m}$ . A merge and single channels kymographs are displayed showing little overlap of GFP-CLN3 and tdTomato-Rab5 vesicle trafficking. Timeframe of imaging sequence: 600 sec. Perkin Elmer Spinning Disk Confocal microscope,  $37^\circ\text{C}$  and  $5\% \text{CO}_2$ .

To test whether this observation withstands in living cells, neuronal cultures were co-transfected with fluorescently tagged CLN3 and fluorescently tagged marker proteins. The cells were visualized by spinning disc microscopy and the trafficking of the fluorescently labelled proteins was visualized in kymographs. mCherry-CLN3 shows as well as in fixed cells little to no overlap with GFP-Rab5 (Figure 20). Like in the single transfection experiments in neuronal cultures CLN3 can again be detected in moving vesicles of fast velocity during long-range-transport. Rab5 positive vesicular structures are less mobile and show shorter periods of movement.

GFP-CLN3 shows strong overlap with tdTomato-Rab7 in neurons (Figure 21). The proteins localize to the same vesicular structures that mostly show retrograde movement. Anterogradely moving CLN3 positive structures are not positive for Rab7. These data was obtained in 5 different experiments with more than 30 different cells.

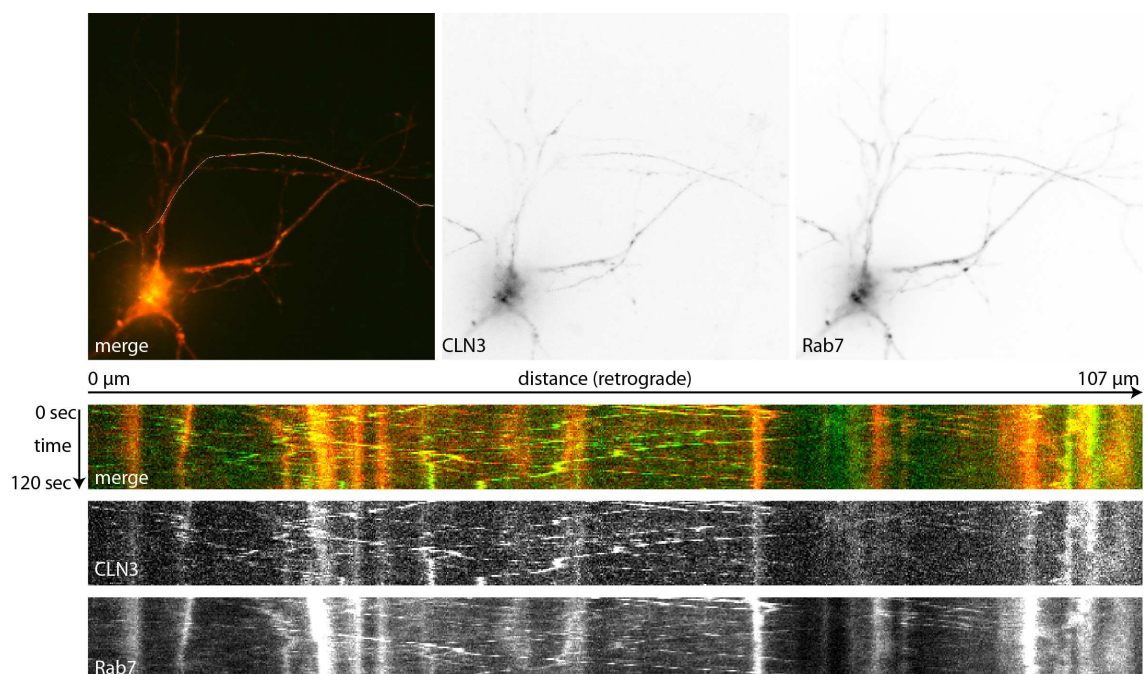


**Figure 21. Subcellular trafficking of CLN3 and Rab7 in transfected primary hippocampal neurons.** Living neurons overexpressing GFP-CLN3 and tdTomato-Rab7 were imaged for 2 min. GFP-CLN3 (green) and tdTomato-Rab7 (red) are localized to overlapping endosomal structures moving more or less fast in the cell soma and processes. A merge and single channels of the first image of the sequence are displayed with a line in the merged image marking the neurite where vesicles were tracked in. Along the line a kymograph was generated with the ImageJ plugin MultipleKymograph. The kymograph shows the movement of vesicles in retrograde and anterograde direction in the neurite along a distance of 107  $\mu\text{m}$ . A merge and single channel kymographs are displayed showing co-localization in retrograde trafficking of GFP-CLN3 and tdTomato-Rab7. Timeframe of imaging sequence: 120 sec. Perkin Elmer Spinning Disk Confocal microscope, 37  $^{\circ}\text{C}$  and 5 %  $\text{CO}_2$ .

In conclusion the localization of CLN3 to late endosomal / lysosomal vesicular-like structures that are positive for Rab7 was confirmed in live-cell video microscopy. This is in agreement with my experiments in fixed cells.

## 4.5 CLN3 and the putative interaction partner SorCS1

The aim of this study was the identification of new interaction partners for CLN3 and the characterization of the interactions. One putative new interaction partner for CLN3 is SorCS1. This protein was identified in a TAP-tag screen and the putative interaction was investigated here by co-localization analysis and by co-immunoprecipitation.

### 4.5.1 Expression patterns of CLN3 and SorCS1 in mouse embryos

An interaction of two proteins can be physiologically relevant if the two proteins are expressed in the same tissues and in the same compartments on the subcellular level. The expression of CLN3 and SorCS1 mRNA in mouse embryos and mouse adult brains was analysed by radioactive in situ hybridization. CLN3 is expressed on a very low level both embryonically and in the adult brain. In mouse E16 sections CLN3 mRNA is expressed ubiquitously and the highest expression level was detected in the gastrointestinal tract and kidney (Figure 22).

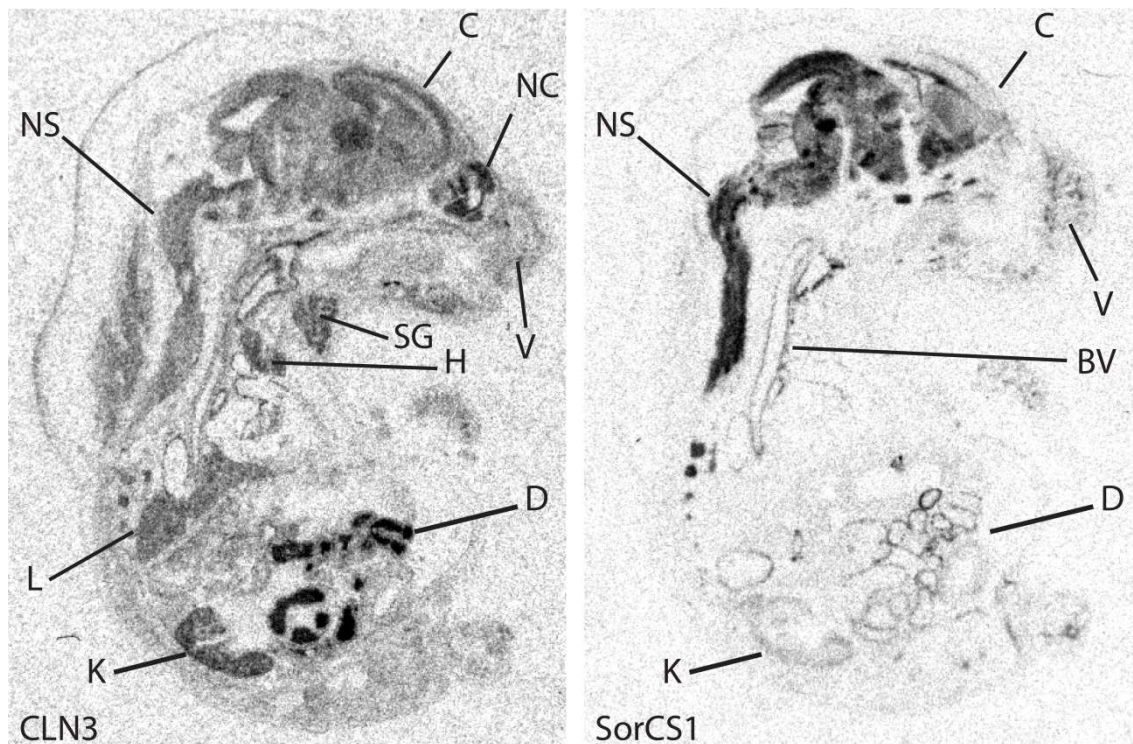


**Figure 22. The expression patterns of CLN3 and SorCS1 mRNA in radioactive in situ hybridizations on E16 embryonic mice show overlapping expression.**

Sagittal sections of embryonic mice were probed for CLN3 and SorCS1 mRNA with radioactively labelled mRNA-probes. The labelling was visualized on x-ray films, which were exposed for 14 days for CLN3 and 2 days for SorCS1. The expression pattern for CLN3 shows maxima in the embryonic gastrointestinal tract, the kidney, liver, heart and thymus and a moderate expression in the nervous system. The mRNA of SorCS1 shows the highest expression in the nervous system and a moderate expression in the kidney and blood vessels. BV: Blood vessels; C: Cortex; D: Duodenum; K: Kidney; L: Liver; NC: Nasal cavity; SC: Spinal cord; SG: Submandibular gland; T: Thymus; V: Vibrissae.

In most other tissues CLN3 mRNA is expressed on a low level with the thymus, submandibular gland, liver, nasal cavity and some parts of the nervous system showing a slightly higher expression. SorCS1 mRNA is expressed almost exclusively in the nervous system. Some expression can also be detected in the gastrointestinal tract and the kidney.

In the adult mouse brain CLN3 mRNA shows a weak expression. In the hippocampal formation a higher signal can be detected. This can be due to the high cell number in this region. SorCS1 mRNA is expressed on a high level in the cerebral cortex and can be detected in the CA1 region of the hippocampus (Figure 23).

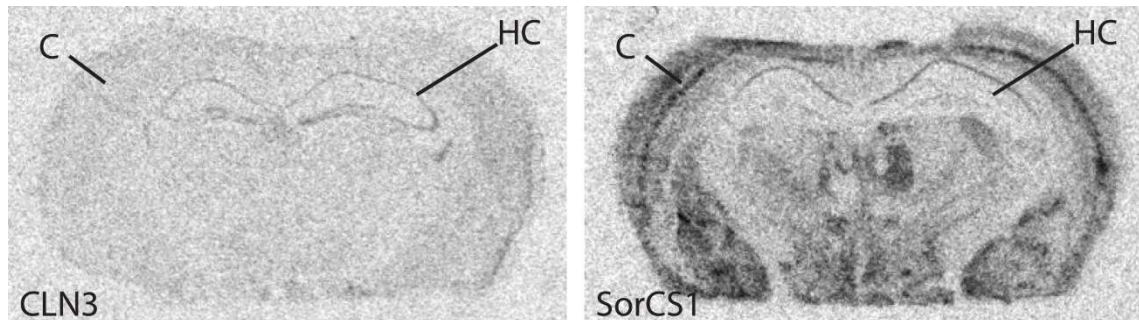


**Figure 23. The expression patterns of CLN3 and SorCS1 mRNA in radioactive in situ hybridizations on adult mouse brains show overlapping expression.**

Coronal sections of embryonic mice were probed for CLN3 and SorCS1 mRNA with radioactively labelled mRNA-probes. The labelling was visualized on x-ray films, which were exposed for 14 days for CLN3 and 2 days for SorCS1. Both expression patterns show maxima in the hippocampal formation. SorCS1 mRNA is also expressed on a high level in the cortex. (C: Cerebral Cortex; H: Hippocampus)

In total there is little congruence between the mRNA expression patterns of CLN3 and SorCS1. Still, the high expression of SorCS1 mRNA in the nervous system can be a crucial functional link to the effect of CLN3 deficiency on this tissue in JNCL patients.

#### 4.5.2 Co-localization of CLN3 and SorCS1

The co-localization of CLN3 and SorCS1 in subcellular compartments was investigated in co-transfected HeLa-cells. SorCS1 was found in several different splice variants that are named SorCS1a, SorCS1b, SorCS1 $\alpha$ , SorCS1 $\beta$ , SorCS1 $\gamma$ , SorCS1 $\delta$  and SorCS1e in humans (Hermey 2009). The different splice variants show different intracellular localization. Some can be found primarily in intracellular vesicular structures and some localize primarily to the plasma membrane where they can internalize cargo.

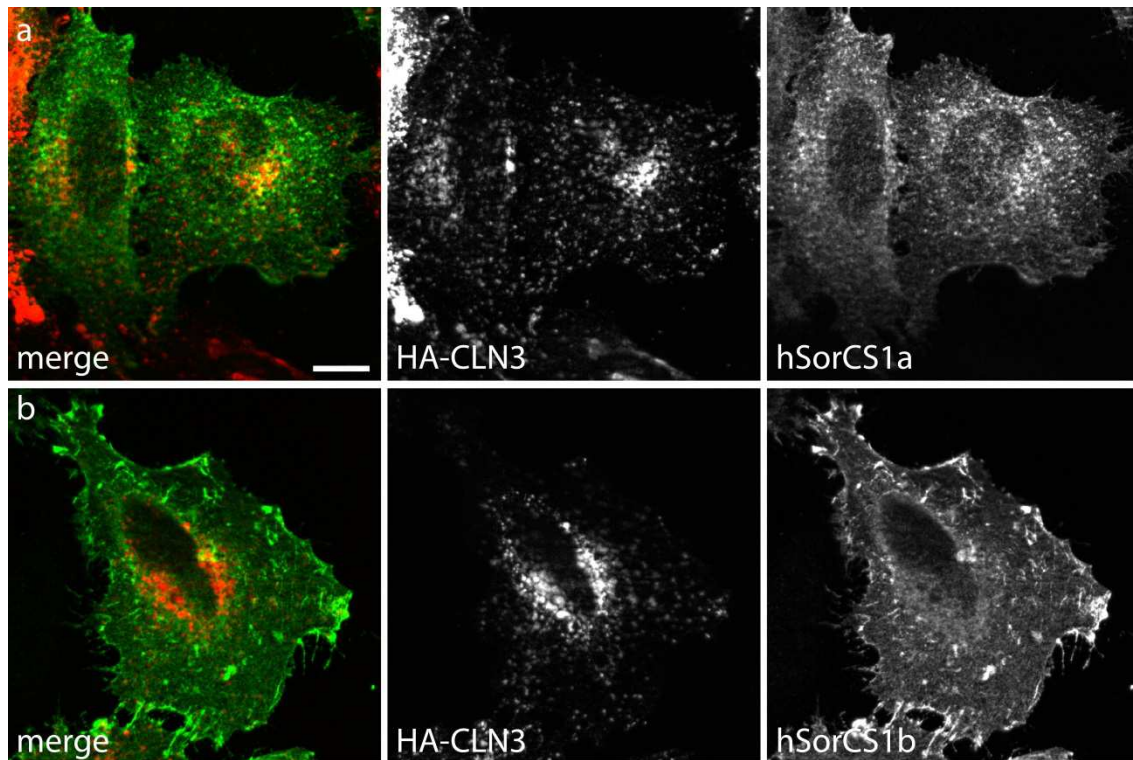


**Figure 24. Subcellular localization of CLN3 and SorCS1 in transfected HeLa-cells.**

HeLa-cells were co-transfected with HA-CLN3 (red) and human SorCS1 variants (green). After PFA-fixation the proteins were labelled by anti-HA and anti-SorCS1 antibodies and fluorescently labelled secondary antibodies. For each co-expression experiment, a merged image and the respective single images for both proteins are displayed. a: CLN3 and human SorCS1a show small regions of co-localization in some vesicular structures. b: CLN3 and human SorCS1b show little to no overlapping subcellular localization. Scale bar in a: 10  $\mu\text{m}$  (applies to all panels). Zeiss Axiovert microscope with ApoTome.

Human and mouse variants of SorCS1 were co-expressed with HA-CLN3 in HeLa-cells. SorCS1 was then labelled with a specific antibody whereas HA-CLN3 was labelled through its HA-tag by an anti-HA-antibody. SorCS1a and CLN3 do both localize to intracellular endosomal structures but their localization pattern does not show significant overlap (Figure 24a). Although some vesicular structures that harbour both proteins do occur too. In these structures there can be an interaction of CLN3 and SorCS1a.

SorCS1b is mainly found at the plasma membrane. There seems to be no co-localization of SorCS1b with CLN3 (Figure 24b).

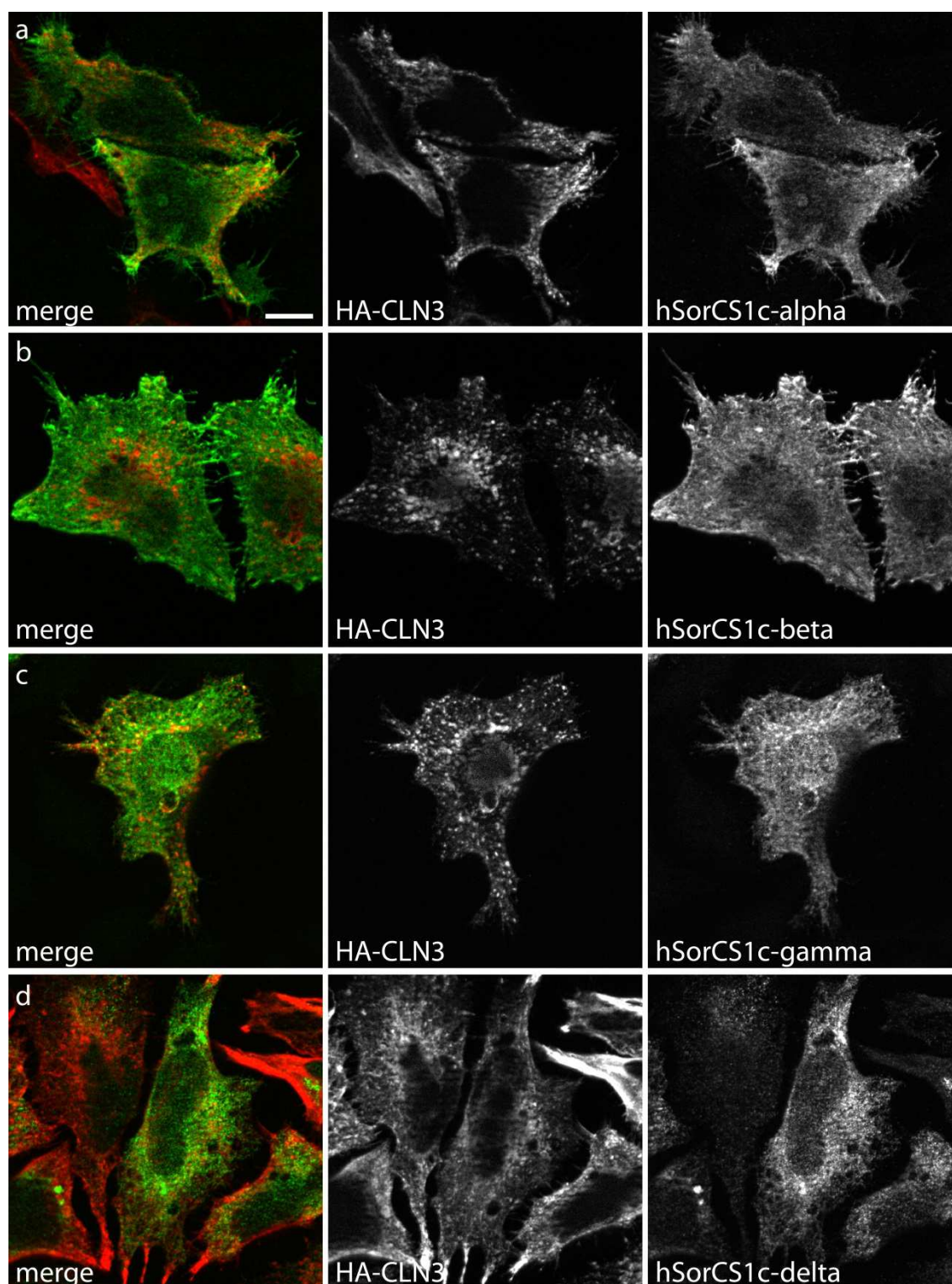


**Figure 25. Subcellular localization of CLN3 and SorCS1 in transfected HeLa-cells.**

HeLa-cells were co-transfected with HA-CLN3 (red) and human SorCS1 variants (green). After PFA-fixation the proteins were labelled by anti-HA and anti-SorCS1 antibodies and fluorescently labelled secondary antibodies. For each co-expression experiment a merged image and the respective single images for both proteins are displayed. CLN3 shows co-localization with different SorCS1c isoforms in endosomal structures (a-d). Scale bar in a (applies to all panels): 10  $\mu\text{m}$ . Zeiss Axiovert microscope with ApoTome.

The human variant of SorCS1c has several different subforms of which the localization pattern in HeLa cells of four is displayed in Figure 25. The different subforms of SorCS1c $\alpha$ , SorCS1c $\beta$ , SorCS1c $\gamma$  and SorCS1c $\delta$  can primarily be found on intracellular

---

endosomes and only a small fraction localizes to the plasma membrane. Some of the vesicular structures positive for SorCS1c are also positive for HA-CLN3 antibody-staining (Figure 25). The mouse variants of SorCS1 were also tested for co-localization with CLN3 and the different mouse isoforms displayed a similar co-localization pattern with CLN3 as the human variants (data not shown). Some of the SorCS1 splice variants show regions of overlapping localization with HA-tagged CLN3. This partial co-localization can be a hint to a joint functional role in the respective compartment.

### **4.5.3 Co-immunoprecipitation of CLN3 and SorCS1**

Some of the splice variants of SorCS1 showed a partial overlap with the subcellular localization of CLN3. The putative interaction was subsequently analysed on the biochemical level with co-immunoprecipitations. The protein interaction of different splice variants of SorCS1 with CLN3 was analysed. Co-immunoprecipitations were established for CLN3 with two different techniques. Precipitations with protein A coupled magnetic beads and anti-GFP-nanobody coated magnetic beads were tested under different buffer conditions. Since the immunoprecipitations with anti-GFP-nanobody-coated beads produced more clear and consistent results they are shown here. In these experiments GFP-CLN3 was used as the bait protein and SorCS1 as the prey protein. For SorCS1 terminal addition of a protein-tag is not established due to the processing and shedding of the protein. The co-immunoprecipitations were conducted with cell lysates from double-transfected HeLa-cells. In Figure 26 exemplary western blots of co-immunoprecipitations of SorCS1a and SorCS1b with GFP-CLN3 are shown. All three proteins show strong labelling in the input lane on the western blot. In the GFP-IP only CLN3 can be detected but not SorCS1a. For SorCS1b there is a weak signal in the GFP-IP but this can also be found in the control-IP. Therefore this cannot be regarded as a specific co-precipitation of SorCS1b with CLN3.

Neither SorCS1a nor SorCS1b showed a positive result for the interaction with CLN3 in co-immunoprecipitations. Other buffer conditions and splice variants of SorCS1 were also tested but for those the interaction of CLN3 could not be shown with co-immunoprecipitations either.

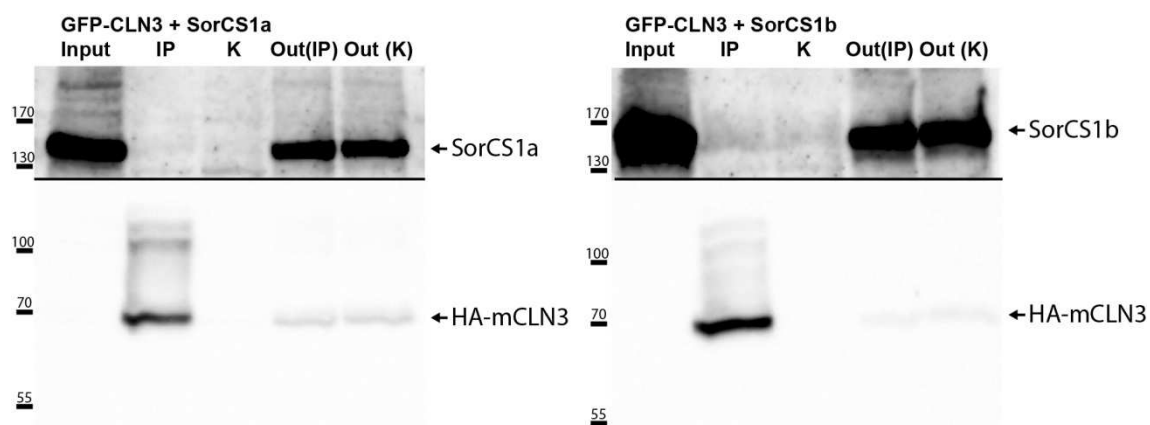


**Figure 26. Co-immunoprecipitations of CLN3 and SorCS1a and SorCS1b.**

GFP-tagged human CLN3 was co-expressed with SorCS1a or SorCS1b in HeLa-cells and cell lysates were collected after 24 hours. The co-immunoprecipitation was conducted with anti-GFP-nanobody-coupled magnetic beads binding the GFP-tag of CLN3. The protein-fractions were separated by SDS-PAGE and transferred to PVDF-membranes by western blotting. The proteins were visualized on the blots through antibodies and chemiluminescence. The input presents the used cell lysates and shows the strong expression of SorCS1 in both experiments. The IP-fraction represents the precipitated protein and the control precipitation. The IP shows a strong band for GFP-CLN3 but no specific bands for SorCS1. In the “Output”-fraction the supernatants of the co-immunoprecipitations are plotted. The marker-bands for 170, 130, 100, 70 and 55 kDa are indicated.

#### 4.5.4 CLN3 and other members of the Vps10p-Domain receptor family

Since there are more members in the Vps10p-Domain protein family that are in close relation to the analysed SorCS1 variants also SorCS3, SorLA and Sortilin were co-expressed with CLN3. For SorLa and Sortilin some areas of co-localization with CLN3 can be detected especially on endosomal structures (Figure 27a, b). SorCS3 showed little to no co-localization with CLN3 with SorCS3 mostly being localized to the TGN, the plasma membrane and some endosomal structures (Figure 27c). A potential interaction with these members of the Vps10p-Domain family was not investigated further but could be a future step.

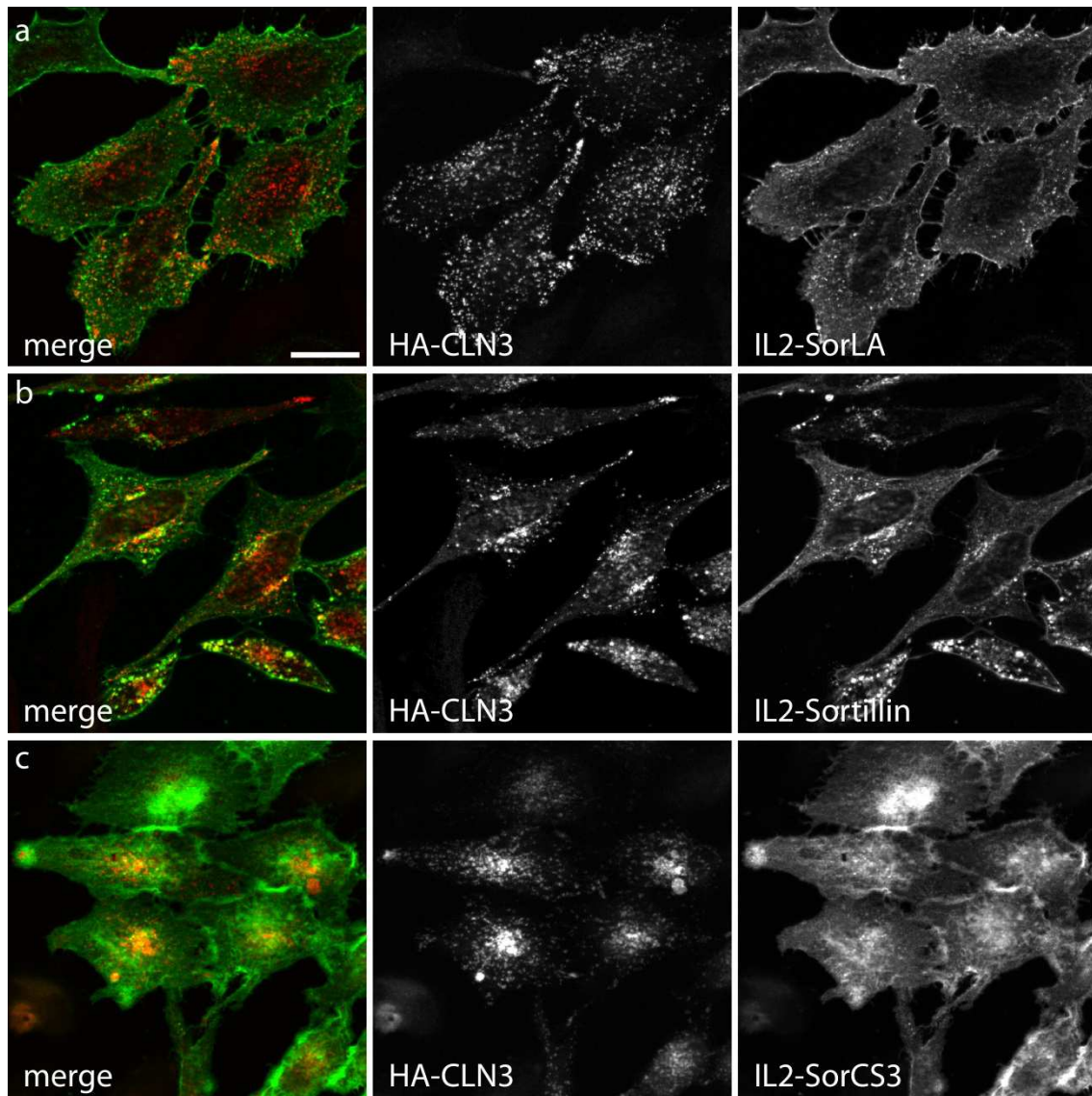


**Figure 27. Subcellular localization of CLN3 and SorLA, Sortilin or SorCS3 in transfected HeLa-cells.**

HeLa-cells were co-transfected with HA-CLN3 (red) and IL2-SorLA, IL2-Sortilin or IL2-SorCS3 chimeric receptors (green). After methanol-fixation the proteins were labelled by anti-HA and anti-IL2 antibodies and fluorescently labelled secondary antibodies. For each co-expression experiment a merged image and the respective single images for both proteins are displayed. a: CLN3 shows co-localization with SorLA in some endosomal structures in the cell periphery. b: There is co-localization of CLN3 with Sortilin in small parts of endosomal structures mainly in the perinuclear region. c: CLN3 and SorCS3 show little co-localization. Scale bar a (applies to all panels): 20  $\mu$ m. Zeiss Axiovert microscope with ApoTome.

#### 4.6 CLN3 and the putative interaction partner Pen2

The second protein for which the putative interaction with CLN3 was found in a TAP-tag screen is Pen2. Here the interaction of the two proteins was investigated by co-localization analysis, by co-immunoprecipitation and by co-trafficking studies.

#### 4.6.1 mRNA expression patterns of CLN3 and Pen2 in mouse embryos

In order to analyse the interconnection of CLN3 and Pen2 on tissue level radioactive in situ hybridizations were performed on sections of embryonic mice and adult mouse brains. The overall expression patterns of the mRNAs for CLN3 and Pen2 in E16 embryonic mice are very similar (Figure 28). Both mRNAs show the highest expression levels in the gastrointestinal tract, kidney, liver, heart and thymus and a moderate expression in the central nervous system.

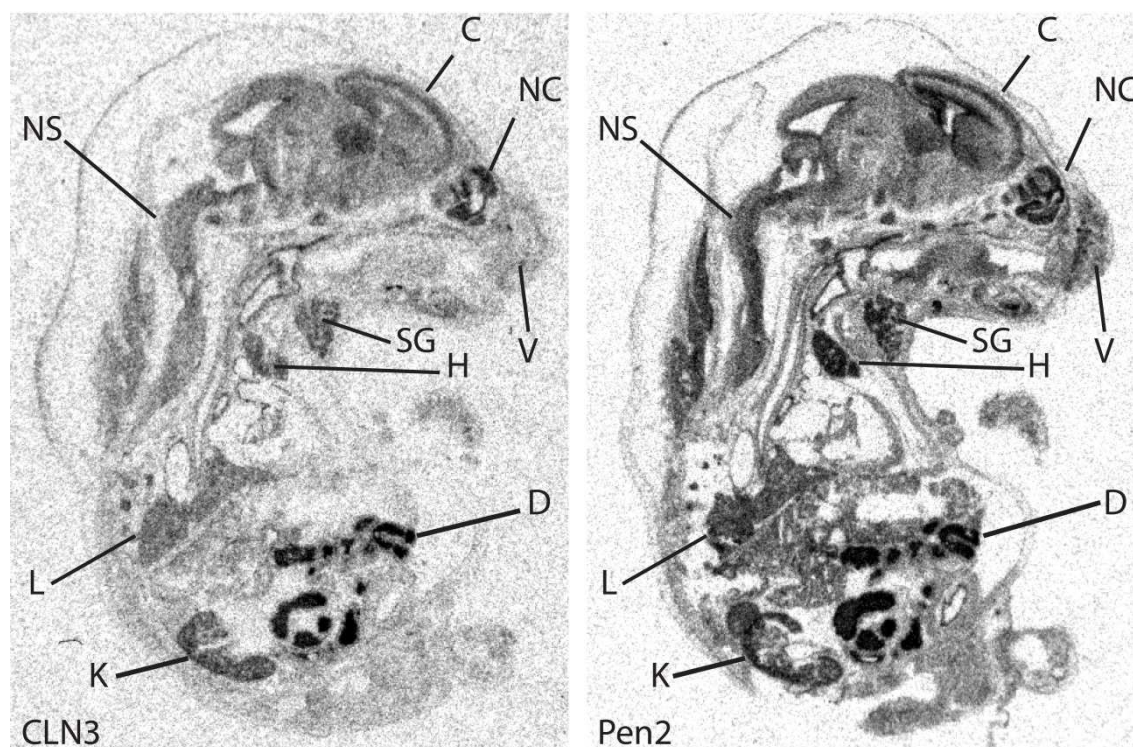


**Figure 28.** The expression patterns of CLN3 and Pen2 mRNA in radioactive in situ hybridizations on E16 embryonic mice are very similar.

Sagittal sections of embryonic mice were probed for CLN3 and Pen2 mRNA with radioactively labelled mRNA-probes. The labelling was visualized on x-ray films which were exposed for 14 days for CLN3 and 2 days for Pen2. Both expression patterns show maxima in the embryonic gastrointestinal tract, the kidney, liver, heart and thymus and a moderate expression in the nervous system. C: Cortex; D: Duodenum; K: Kidney; L: Liver; NC: Nasal cavity; SC: Spinal cord; SG: Submandibular gland; T: Thymus; V: Vibrissae.

In adult mouse brains the expression patterns are again very similar and show the highest expression for both mRNAs in the hippocampal area (Figure 29). The expression pattern for Pen2 mRNA is both in the embryonic as well as in the adult brain slice on a much higher total level than the CLN3 mRNA.

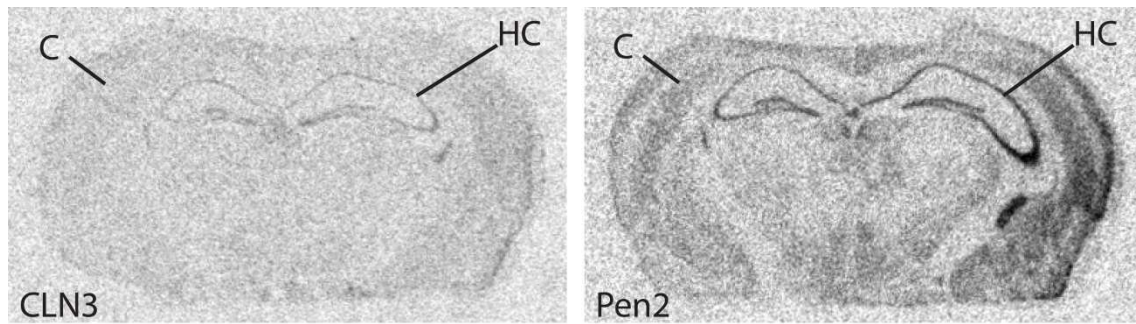


**Figure 29.** The expression patterns of CLN3 and Pen2 mRNA in radioactive in situ hybridizations on adult mouse brains are very similar.

Coronal sections of embryonic mouse brains were probed for CLN3 and Pen2 mRNA with radioactively labelled mRNA-probes. The labelling was visualized on x-ray films which were exposed for 14 days for CLN3 and 2 days for Pen2. Both expression patterns show maxima in the hippocampal formation. (C: Cerebral Cortex; H: Hippocampus)

#### 4.6.2 Co-localization of CLN3 and Pen2

Co-localization studies of CLN3 and the  $\gamma$ -secretase subunit Pen2 were performed in co-transfected HeLa cells and primary hippocampal mouse embryo neurons. Both cell types showed a vesicular localization pattern for CLN3 and a vesicular and ER pattern for Pen2 (Figure 30). In the vesicular structures both proteins showed significant co-localization as can also be seen in the line plots (Figure 30).

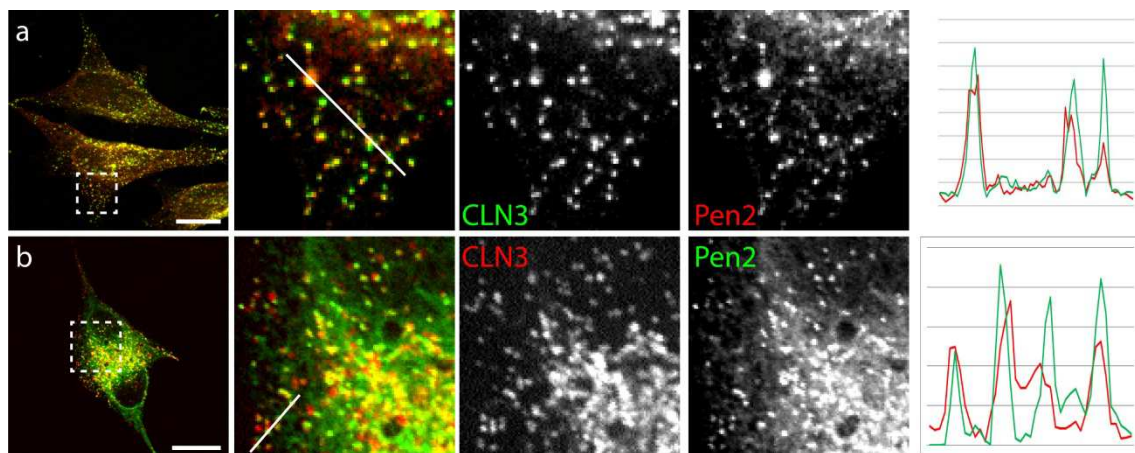


**Figure 30.** CLN3 and Pen2 show co-localization on the subcellular level in transfected HeLa-cells. HeLa-cells were co-transfected with GFP-CLN3 (green) and tdTomato-Pen2 (red) (a) or mCherry-CLN3 (red) and GFP-Pen2 (green) (b). After methanol- (a) or PFA- (b) fixation the proteins were either visualized through a Zeiss Axiovert microscope with ApoTome (a) or by confocal laser scanning microscopy (b). For each co-expression experiment a merged image, a zoom-in of the dotted box and the respective single images for both proteins are displayed. The zoom-in shows a line through several labelled vesicles that is analysed by line plot at the right side for the expression profile of the two proteins. CLN3 and Pen2 show co-localization to the same endosomal structures in both experiments (a, b). Scale bar overview in a and b: 20  $\mu$ m.

In neurons both proteins were found in the soma as well as in neurites (Figure 31). They localize to large endosomal structures distributed all over the soma and in the neurite mostly localizing to the edges and not to the middle region. Arrows point to regions of co-localization (Figure 31a, b). The partial co-localization of Pen2 with CLN is indicative of a putative interaction of the two proteins.

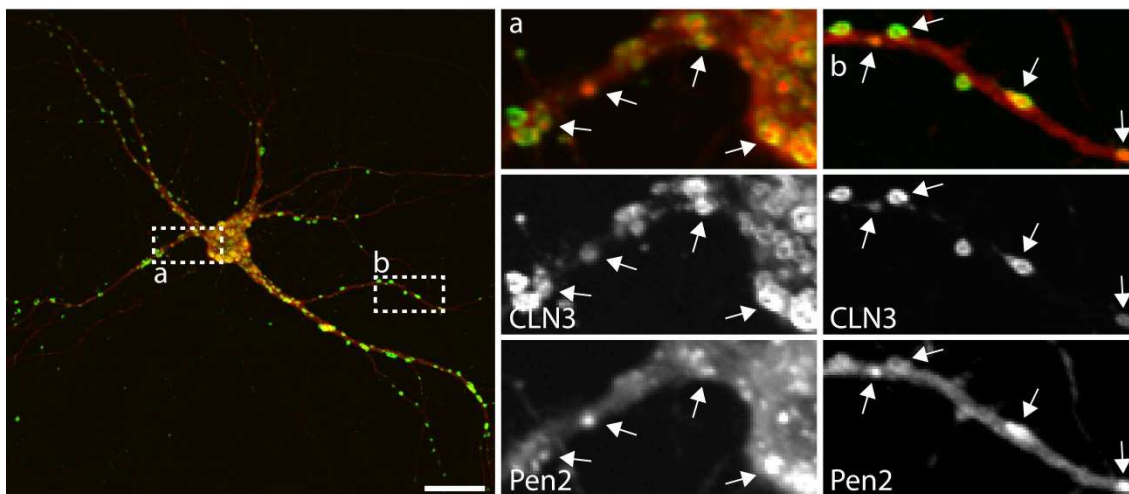


**Figure 31. CLN3 and Pen2 show co-localization on the subcellular level in transfected primary hippocampal mouse neurons.**

Primary hippocampal mouse embryo neurons were co-transfected with GFP-CLN3 (green) and tdTomato-Pen2 (red). After PFA-fixation the proteins were labelled by anti-GFP and anti-dsRed antibodies and fluorescently labelled secondary antibodies. A merged image and a somatic (a) and a neuritic (b) zoom-in with the respective single images for both proteins are displayed. The arrows point to regions of interest. CLN3 and Pen2 show strong co-localization in somatic and neuritic regions. Zoom-in size: 22,56 x 11,39  $\mu\text{m}$ . Confocal laser scanning microscope. Scale bar in overview: 20  $\mu\text{m}$ . Confocal laser scanning microscope.

#### 4.6.2.1 Co-localization of CLN3 and Pen2 in specific endosomal structures

The co-localization of CLN3 and Pen2 was shown in HeLa-cells and in primary hippocampal neurons. I showed that CLN3 localizes primarily to late endosomal and lysosomal structures (see results section 4.3). In addition there was also an overlap of CLN3 with some other marker proteins, but to a lower degree. In order to analyse the nature of the endosomes that harbour CLN3 co-localization with Pen2 the two proteins were co-expressed in HeLa-cells together with different marker proteins of subcellular structures.

Like for CLN3 alone, CLN3 and Pen2 showed most co-localization with the marker for late endosomes and lysosomes Rab7 (Figure 32d). With Rab1 only small spots of overlap can be found for co-localization-areas of CLN3 and Pen2. In rare spots co-localization of Rab1 with Pen2 was observed. Rab4 also shows little co-localization with the two other proteins (Figure 32a, b). There are some endosomal structures on which CLN3 and Pen2 seem to be localized adjacent of Rab4 (Figure 32b). CLN3 and Pen2 both show little overlap with early endosomes that are positive for Rab5 (Figure 32c). Even less co-localization can be observed between CLN3 and Pen2 and overexpressed Rab11 (Figure 32e).

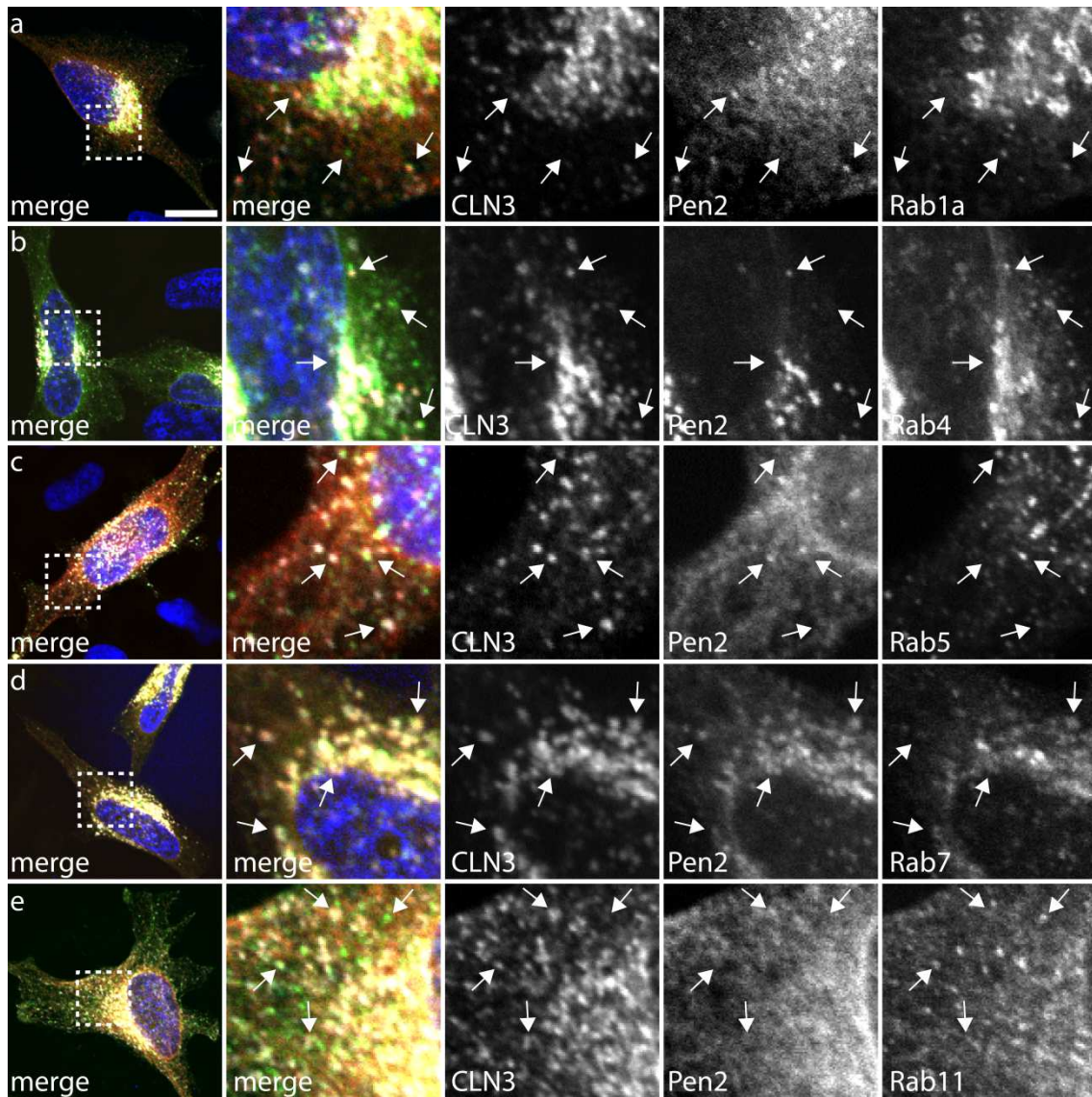


**Figure 32. Subcellular localization of CLN3 and Pen2 in comparison to subcellular marker proteins in transfected HeLa-cells.**

HeLa-cells were co-transfected with HA-CLN3 (grey), tdTomato-Pen2 (red) and GFP-Rab1 (a), GFP-Rab4 (b), GFP-Rab5 (c), GFP-Rab7 (d) or GFP-Rab11 (e) (green). After methanol-fixation the cells were labelled by anti-HA antibody and a fluorescently labelled secondary antibody and mounted with Dapi (blue). For each co-expression experiment a merged image, a zoom-in of the dotted box and the respective single images for all three proteins are displayed. The arrows point to regions of interest. a: CLN3 and Pen2 show only small spots of overlap with Rab1 in areas of their co-localization. b: CLN3 and Pen2 show adjacent localization with Rab4 next to areas of co-localization and also some overlap. c: CLN3 and especially Pen2 show little overlap with Rab5 localization. d: There are large areas of co-localization between CLN3, Pen2 and Rab7. e: CLN3 and Pen2 show almost no overlap with Rab11 localization. Scale bar in a (applies to all panels): 15  $\mu$ m. Confocal laser scanning microscope.

#### 4.6.3 CLN3 and other $\gamma$ -secretase-associated proteins

In addition to the interaction of CLN3 directly with the  $\gamma$ -secretase subunit Pen2, an analysis of interconnection of CLN3 with other  $\gamma$ -secretase associated proteins was performed. Presenilin1 (PS1), the largest subunit of the  $\gamma$ -secretase complex, was found to be transported in the same vesicles as CLN3 (Figure 33). I observed as well the partial co-localization of CLN3 with the  $\gamma$ -secretase substrate APP on the same cellular endosomal

structures (Figure 34). These findings underline the putative functional association of CLN3 with the  $\gamma$ -secretase complex.

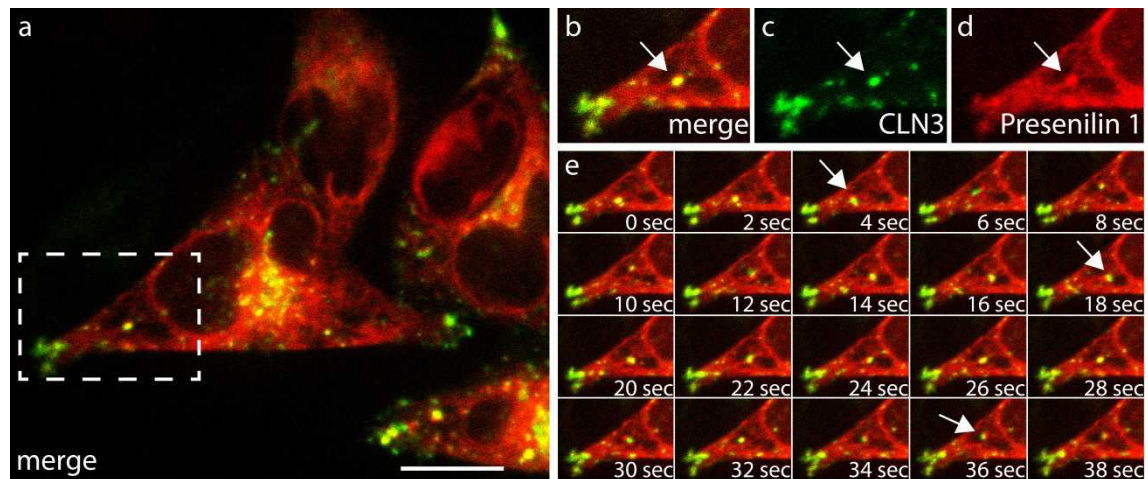


**Figure 33. CLN3 and Presenilin 1 show partial co-localization on moving endosomal structures in live-cell video microscopy of transfected HeLa-cells.**

HeLa-cells were co-transfected with GFP-CLN3 (green) and Presenilin 1 with an internal mCherry-tag (red) and imaged 48 hours after transfection. a: Overview of the first image from the live-cell-imaging-sequence of transfected HeLa-cells. b: Zoom-in on a region with CLN3- and Presenilin-1-positive structures. The arrows (b-e) point to the moving CLN3- and Presenilin 1-positive vesicular-like structure. c, d: single channel images of b. e: Image sequence of live-cell video over 38 seconds. CLN3- and Presenilin 1 show joint movement. Scale bar 15  $\mu$ m. VisiTron Systems Spinning Live Cell Confocal; 37  $^{\circ}$ C and 5 % CO<sub>2</sub>.

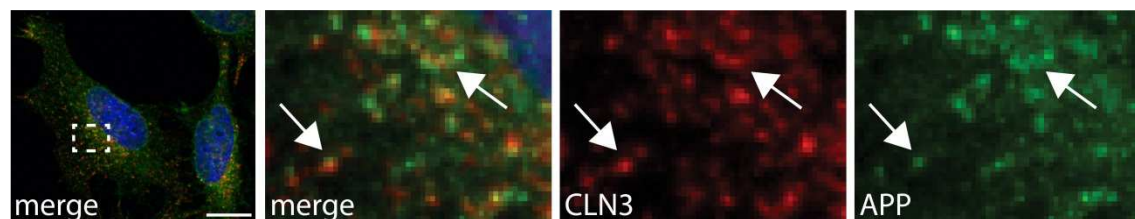


**Figure 34. CLN3 and APP show partial co-localization on the subcellular level in transfected HeLa-cells.**

HeLa-cells were co-transfected with mCherry-CLN3 (red) and GFP-APP (green). For the dotted box in the overview the zoom-in and the respective single images for both proteins are displayed. CLN3 and APP show partial co-localization to the same endosomal structures (arrows). Methanol-fixation. Scale bar in overview: 15  $\mu$ m. Zeiss Axiovert microscope with ApoTome.

#### 4.6.4 Co-immunoprecipitation of CLN3 and Pen2

In order to confirm the interaction of the two proteins on a biochemical level co-immunoprecipitations were performed. For the co-immunoprecipitations anti-GFP-nanobody-coated magnetic beads were used. The proteins were precipitated from lysates of double-transfected HeLa-cells expressing HA-CLN3- and GFP-Pen2. The input fraction on the western blots of the IPs shows strong bands for the tested proteins (Figure 35). In the specific IP with anti-GFP coupled beads there is a strong precipitation of GFP-Pen2 and HA-CLN3 is co-precipitated (Figure 35). In the control-IP with non-antigenic beads none of the two proteins is precipitated (Figure 35).

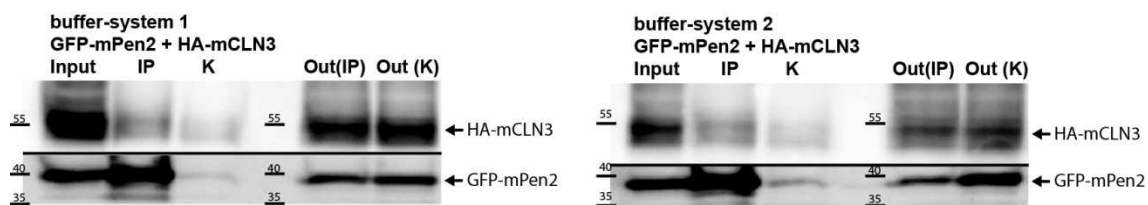


**Figure 35. CLN3 co-immunoprecipitates with Pen2 under different conditions from HeLa-cell lysates.**

HA-tagged human CLN3 was co-expressed with GFP-tagged Pen2 in HeLa-cells and cell lysates were collected after 24 hours. The co-immunoprecipitation was conducted with anti-GFP-nanobody-coupled magnetic beads binding the GFP-tag of CLN3. Immunoprecipitations were conducted with different buffer systems (1 and 2). The protein-fractions were separated by SDS-PAGE and transferred to PVDF-membranes by western blotting. The proteins were visualized on the blots through antibodies and chemiluminescence. The input presents the used cell lysates and shows the strong expression of HA-CLN3 and GFP-Pen2 in both experiments. The IP-fraction represents the precipitated protein and the control precipitation. The specific IP shows a strong band for GFP-Pen2 and a weaker but clearly visible band for HA-CLN3. The control-IP shows very little to no signal for both proteins. In the “Output”-fraction the supernatants of the co-immunoprecipitations are plotted. The marker-bands for 55, 40 and 35 kDa are indicated.

The interaction seemed to be weak but could be confirmed with a stronger co-immunoprecipitation result after protein-crosslinking in the cell lysates before the purification of complexes (Figure 36). In these experiments the transfected cells were treated with the chemical crosslinker DSP (Dithiobis[succinimidyl propionate]) that has a spacer arm length of 12 Å. In the crosslinking experiments in the control EGFP instead of GFP-Pen2 was co-expressed with HA-CLN3. The same magnetic beads were used in the specific as well as in the control immunoprecipitation. GFP-Pen2 and EGFP were both precipitated with the beads but there is no co-precipitation of CLN3 in the control with EGFP (Figure 36). The experiment was conducted under five different buffer conditions to test the most suited conditions for the precipitation of two membrane proteins. Two conditions for each IP are depicted in Figure 35 and Figure 36.

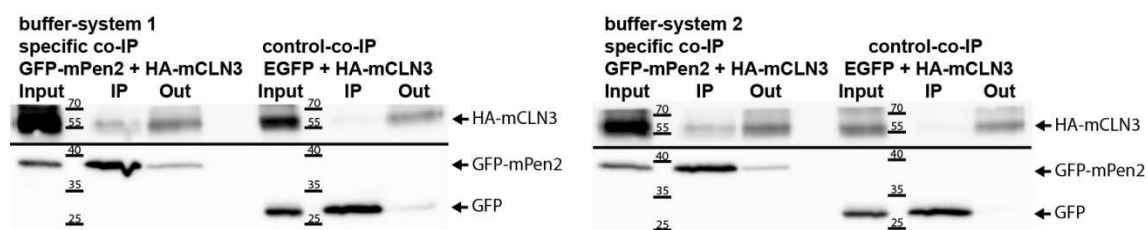


**Figure 36. CLN3 co-immunoprecipitates with Pen2 after crosslinking under different conditions from HeLa-cell lysates.**

HA-tagged human CLN3 was co-expressed with GFP-tagged Pen2 in HeLa-cells and cell lysates were collected after 24 hours. For the control-IP HA-CLN3 was co-expressed with GFP. The co-immunoprecipitation was conducted with anti-GFP-nanobody-coupled magnetic beads binding the GFP-tag of CLN3. The protein-fractions were separated by SDS-PAGE and transferred to PVDF-membranes by western blotting. The proteins were visualized on the blots through antibodies and chemiluminescence. Immunoprecipitations were conducted with different buffer systems (1 and 2) after crosslinking of adjacent proteins through DSP before the precipitation. The Input shows the used cell lysates and demonstrates the strong expression of CLN3 and Pen2 or GFP in both experiments. The IP-fraction represents the precipitated protein. The specific IP shows a strong band for GFP-Pen2 and a weaker but clearly visible band for HA-CLN3. In the control-IP GFP precipitates with the beads but there is no co-precipitation of HA-CLN3. In the “Output”-fraction the supernatants of the co-immunoprecipitations are plotted. The marker-bands for 70, 55, 40, 35 and 25 kDa are indicated.

In conclusion the co-precipitations of HA-CLN3 with GFP-Pen2 confirm the interaction of CLN3 and Pen2 identified in a Tap-tag screen. Both proteins co-localize and are therefore good candidates for a joint function in subcellular processes.

#### 4.6.5 Co-trafficking of CLN3 and Pen2

To analyse the functional role of the interaction of CLN3 with Pen2 on the subcellular level life-cell video microscopy studies were conducted. Like shown in the studies of co-trafficking of CLN3 with different organelle markers fluorescently tagged CLN3 and Pen2 were co-expressed in HeLa-cells and in primary hippocampal mouse embryo neurons. The living cells were analysed with spinning disc microscopy.

##### 4.6.5.1 Co-trafficking of CLN3 and Pen2 in HeLa cells

The trafficking studies of CLN3 revealed a constant movement of a large part of the cellular pool of CLN3 positive vesicles. The motile vesicles of various sizes move with different velocity supposedly along cytoskeletal structures and show fusion and fission events. Life-cell video imaging of GFP-CLN3 and tdTomato-Pen2 positive cells revealed as well as the co-localization studies an overlap of the protein-pools in the same vesicular structures (Figure 37). In Figure 37a, the path taken by a CLN3- and Pen2-positive endosome is drawn. The vesicle was tracked in the single channels with the ImageJ manual tracking tool. Automatic tracking with Trackmate gave no comparable results due to the different background-signal of CLN3 and Pen2. The tracks that trace the movement of a GFP-CLN3 and tdTomato-Pen2 positive structure are overlapping showing a joint movement of the two proteins in total and a co-localization at specific time points (figure a). In the zoom-in frame at 32 seconds the localization of the GFP-CLN3- and tdTomato-Pen2-positive endosome is slightly next to each other. This is due to the fact that the colours are imaged not simultaneously but after one another for each time point.

The spatial behaviour of fluorescently labelled CLN3 and Pen2-positive endosomal structures can be followed over time in a 3D reconstruction. From a z-stack of a live cell imaging sequence a 3D-reconstruction of a GFP-CLN3- and tdTomato-Pen2-positive HeLa-cell was built (Figure 37b). The fusion and fission events between endosomes positive for one or for both of the proteins can be observed. The arrows point to structures that are positive for both CLN3 and Pen2 and show such docking-events (Figure 37b). Similar fusion-events can also observed in high resolution videos of the co-trafficking of mCherry-CLN3 and GFP-Pen2 in HeLa-cells (Figure 37c).

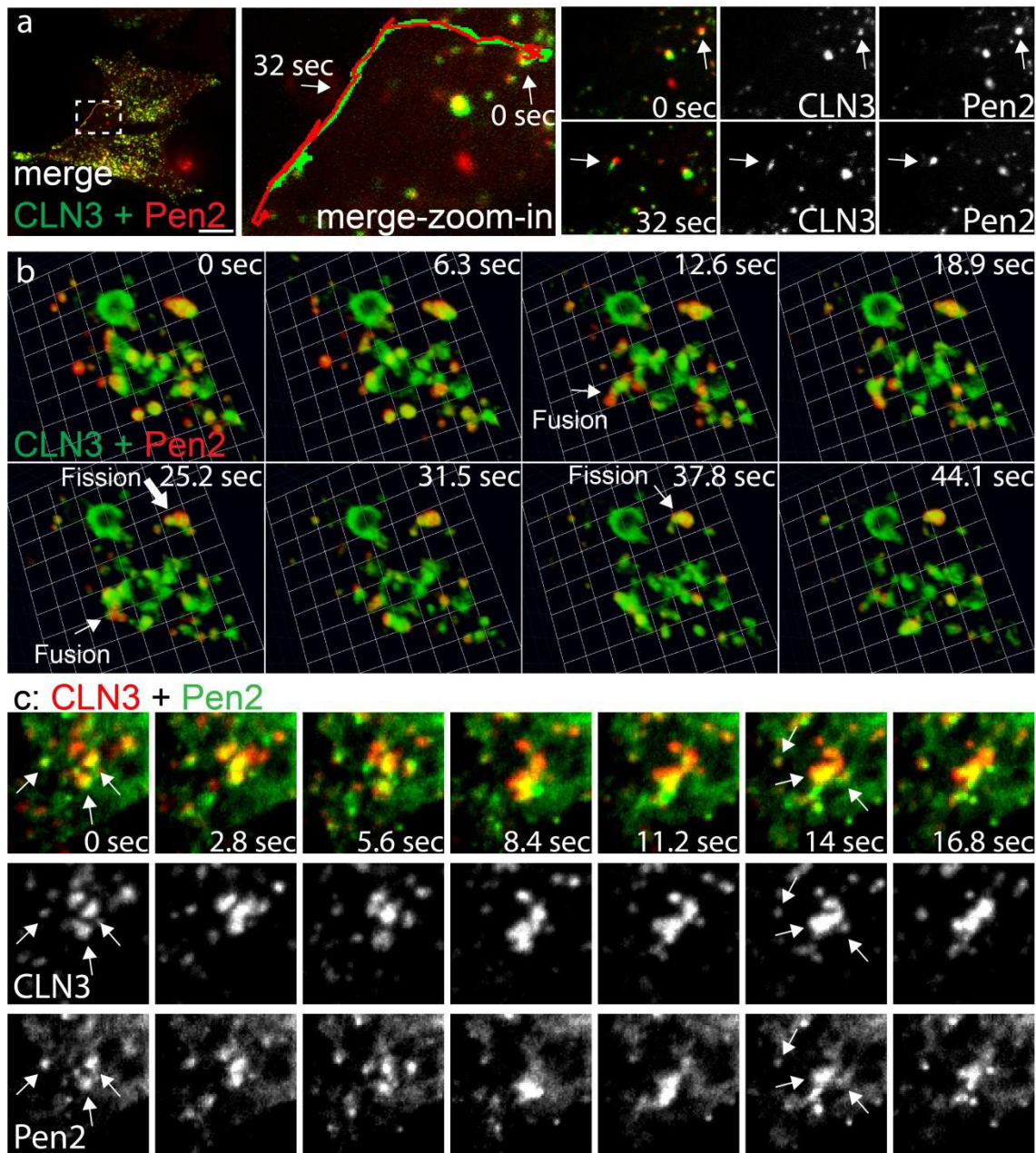


**Figure 37. CLN3 and Pen2 show co-localization on moving endosomal structures in live-cell video microscopy of transfected HeLa-cells.**

HeLa-cells were co-transfected with GFP-CLN3 (green) and tdTomato-Pen2 (red) (a, b) or mCherry-CLN3 (red) and GFP-Pen2 (green) (c). 48 hours after transfection the cells were imaged with spinning disc microscopy at 37 °C and 5 % CO<sub>2</sub>. a: Tracking of a CLN3- (green) and Pen2- (red) positive vesicle with ImageJ manual tracking over 1 minute. The proteins and the resulting tracks show a high overlap in their trafficking. An overview and zoom-ins of the merged-image are provided with the single-channel images for 2 different time-points (0 seconds, 32 seconds). Scale bar: 10 μm b: 3D projection of a 1 minute live-cell video microscopy sequence of a CLN3- (green) and Pen2 (red)-positive HeLa-cell. GFP-CLN3 and tdTomato-Pen2 positive vesicles show fusion and fission events. 1 Unit = 1,72 μm. c: 17 seconds zoom-in of an imaging sequence of a mCherry-CLN3- (red) and GFP-Pen2- (green) positive HeLa-cell. The fluorescent labelling for both proteins overlaps in defined endosomal structures that show fusion-events. Size of zoom-in: 8.5 x 8.5 μm. a, c: Visitron Systems Spinning Live Cell Confocal; b: Perkin Elmer Spinning Disk Confocal microscope.

#### 4.6.5.2 Co-trafficking of CLN3 and Pen2 in primary hippocampal neurons

To get further information on the endosomal structures harbouring CLN3 and Pen2 the trafficking of the proteins was analysed in live-cell spinning disk microscopy in primary hippocampal mouse embryo neurons. Such an analysis is relevant with regard to the neurodegeneration seen in JNCL patients.

In neurons co-localization of CLN3 and Pen2 to partly the same vesicular structures was observed (Figure 38). This is in agreement with the co-localization in HeLa cells. In HeLa-cells migration of CLN3-and Pen2-positive endosomes was observed along defined tracks and seemed to be directed (Figure 37). In the neurites of immature neurons (DIV6) the majority of the CLN3- and Pen2-positive vesicular structures show a retrograde movement to the soma of the neurons (Figure 38). Only a fraction of the total CLN3-positive endosomes is also positive for Pen2. Also, Pen2 only is present in retrogradely moving CLN3-positive endosomes but not in the ones that are moving anterogradely. There are no Pen2-positive vesicular structures that are not positive for CLN3 (Figure 38).

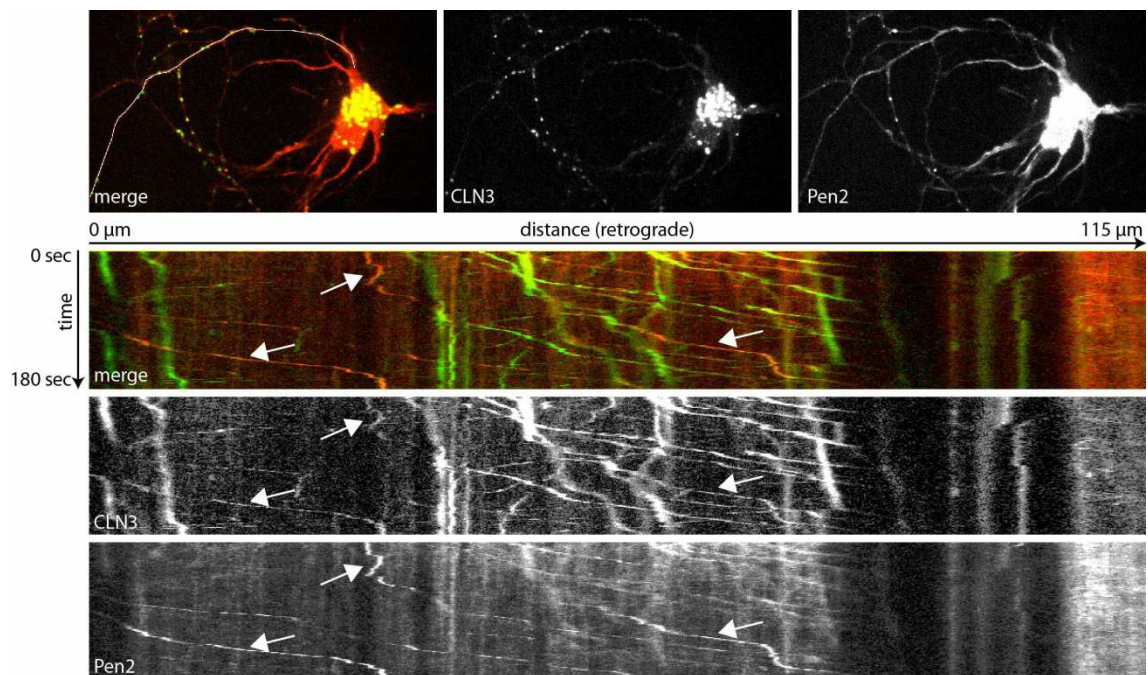


**Figure 38. Subcellular trafficking of CLN3 and Pen2 in a young transfected primary hippocampal neuron.**

Living neurons overexpressing GFP-CLN3 and tdTomato-Pen2 were imaged for 3 min. GFP-CLN3 (green) and tdTomato-Pen2 (red) are localized to overlapping endosomal structures moving more or less fast in the cell soma and processes. A merge and single channels of the first image of the sequence are displayed with a line in the merged image marking the neurite where vesicles were tracked in. Along the line a kymograph was generated with the ImageJ plugin MultipleKymograph. The kymograph shows the movement of vesicles in retrograde and anterograde direction in the neurite along a distance of 115  $\mu\text{m}$ . A merge and single channel kymographs are displayed showing co-localization in retrograde trafficking of a fraction of GFP-CLN3 and tdTomato-Pen2. Timeframe of imaging sequence: 180 sec. Perkin Elmer Spinning Disk Confocal microscope, 37  $^{\circ}\text{C}$  and 5 %  $\text{CO}_2$ .

In the neurites of immature neurons (DIV6) the endosomal structures show a higher motility than in more differentiated cells (DIV12). CLN3 and Pen2 also show a high degree

of co-localization in mature neurons but most of the protein in the dendrite (Figure 39) is residing in large vesicular, mainly stationary structures. In the axon, fluorescently labelled endosomes are still showing a similar movement as in young neurons and in the dendrite there are some smaller punctae that still show fast movement (Figure 39).

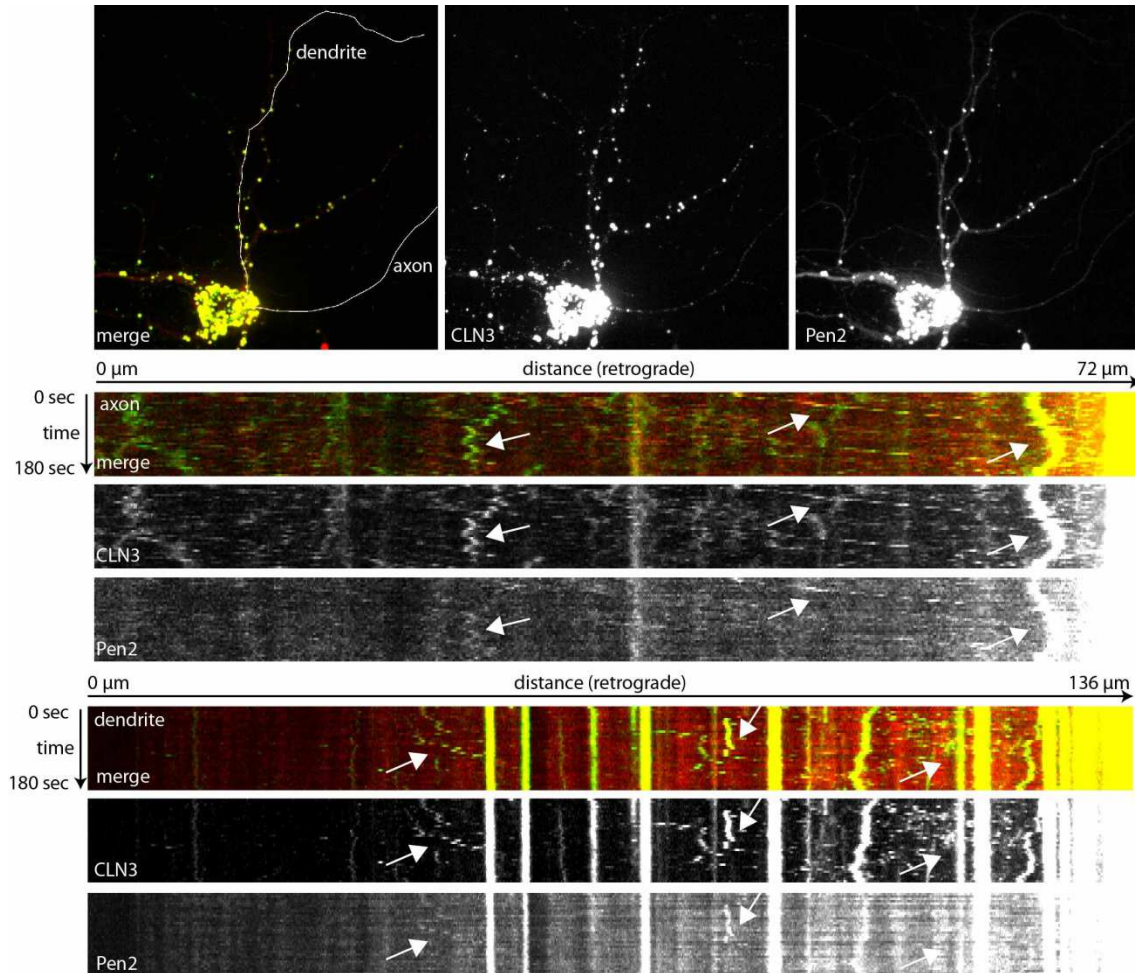


**Figure 39. Subcellular trafficking of CLN3 and Pen2 in a mature transfected primary hippocampal neuron.**

Living neurons overexpressing GFP-CLN3 and tdTomato-Pen2 were imaged for 3 min. GFP-CLN3 (green) and tdTomato-Pen2 (red) are localized to overlapping endosomal structures that are stationary or moving more or less fast in the cell soma and processes. A merge and single channels of the first image of the sequence are displayed with a lines in the merged image marking the dendrite and axon where vesicles were tracked in. Along the lines kymographs were generated with the ImageJ plugin MultipleKymograph. The kymographs show the movement of vesicles in retrograde and anterograde direction in the neurite along a distance of 136  $\mu\text{m}$ . A merge and single channel kymographs are displayed. The kymograph of the axon shows the movement of small vesicular structures that are positive for CLN3- and Pen2. The movement of the vesicles positive for both proteins is mainly directed retrogradely. Two big endosomes remain stationary over the whole sequence. The dendritic kymograph shows a large fraction of big stationary CLN3- and Pen2-positive endosomes. Only a small fraction of vesicles shows movement. CLN3 and Pen2 show almost total overlap. Timeframe of imaging sequence: 180 sec. Perkin Elmer Spinning Disk Confocal microscope, 37  $^{\circ}\text{C}$  and 5 %  $\text{CO}_2$ .

#### 4.6.6 CLN3 and $\gamma$ -secretase-activity

In my studies, I was able to confirm the interaction of CLN3 with the  $\gamma$ -secretase subunit Pen2. In addition, in experiments with other  $\gamma$ -secretase-associated proteins there was a

partial co-localization between CLN3 and APP and co-trafficking of CLN3 and Presenilin 1 (Figure 33, Figure 34).

In order to analyse a putative functional implication of the interaction between CLN3 and Pen2, I established an assay that measured the cleavage of  $\gamma$ -secretase substrates. Since Pen2 is a subunit of the  $\gamma$ -secretase complex, CLN3 could influence the  $\gamma$ -secretase via binding to Pen2. The metabolism of the  $\gamma$ -secretase substrate APP has been previously described to be affected in environments with altered CLN3-activity (Wisniewski, Maslinska, et al. 1990; Wisniewski, Kida, et al. 1990; Golabek et al. 2000). The best-studied substrates of the  $\gamma$ -secretase are the transmembrane receptors APP and Notch. APP can be cleaved by the  $\gamma$ -secretase after previous cleavage by the  $\beta$ -secretase. Different cleavage sites exist that all generate a soluble intracellular C-terminal fragment. Cleavage near residue 713 leads to generation of the toxic A- $\beta_{42}$  that is associated with Alzheimer's disease. Notch is cleaved by the  $\gamma$ -secretase after ligand-binding and processing by ADAM10 (Sisodia & St George-Hyslop 2002; Dries & Yu 2008).

#### 4.6.6.1 Development of the $\gamma$ -secretase-activity-assay

In order to measure the activity of the  $\gamma$ -secretase I constructed tagged versions of the  $\gamma$ -secretase substrates APP and Notch that contained a nuclear localization sequence (NLS), a Gal-4-promoter-binding domain and a VP16 transcriptional activation domain at their C-termini. After cleavage of the transmembrane substrate by the  $\gamma$ -secretase, the C-terminus of the substrate is released into the cytosol and can enter the nucleus where a luciferase-gene under the control of the Gal-4-promoter on a co-transfected reporter-plasmid can be transcribed. The read out of the assay is the luciferase activity which is detected by a luminometer. For APP it was assumed that there is  $\beta$ -secretase-activity in the used cell-system (N2A-cells) and  $\gamma$ -secretase cleavage could follow and be analysed. Notch normally needs ligand-binding and processing by ADAM10 before the cleavage by the  $\gamma$ -secretase. I used a construct that lacks the ligand-binding-domain and can be cleaved independently of ligands (Schroeter et al. 1998; Kopan 2012). Constructs are displayed in Figure 40 As controls for luciferase-induction, the intracellular domains (ICDs) of APP and Notch were used. As negative control, CLN3, tagged C-terminally with the NLS, Gal-4-promoter-binding domain and transcriptional activation domain was used, since for this protein no cleavage of the C-terminus is described but the C-terminus is directed to the cytosol.

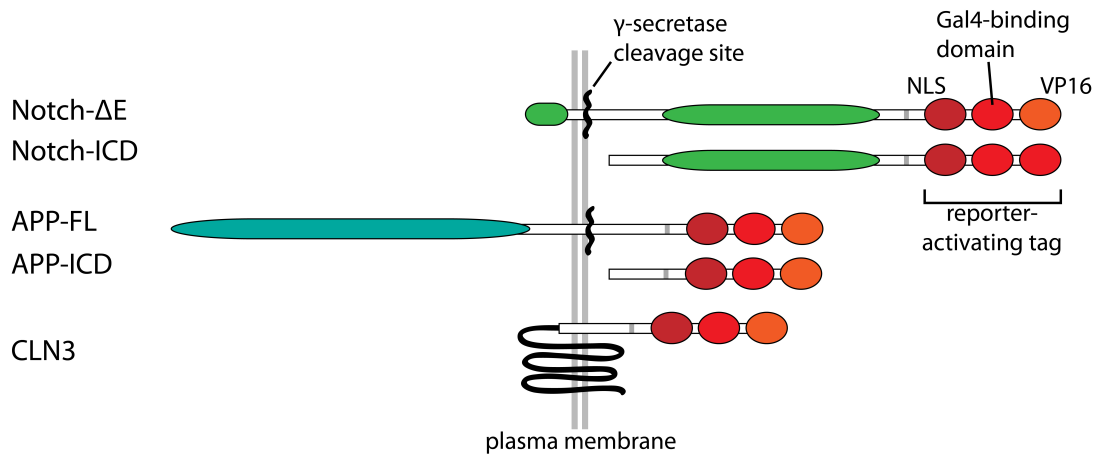


**Figure 40. APP and Notch-1 constructs used in this study**

All construct contain a NLS (nuclear localization sequence), a Gal-4-promoter-binding domain and a VP16 transcriptional activation domain at their C-termini. Notch-ΔE and APP-FL (APP-full length) have a single transmembrane-domain and a  $\gamma$ -secretase-cleavage site at the intracellular side of the plasma membrane. Notch-ICD and APP-ICD do not contain a transmembrane-domain. CLN3 lacks the  $\gamma$ -secretase-cleavage site. (Partly modified after Schroeter et al. 1998)

The developed constructs were expressed in N2A-cells in a 96-well format together with EGFP as transfection control and the luciferase-reporter-plasmid. 29 hours after transfection, the luciferase-activity was measured and normalized to the EGFP-expression in the cells. As expected, for the positive controls Notch-ICD and APP-ICD consistently high luciferase-activity-induction was observed (Figure 41).

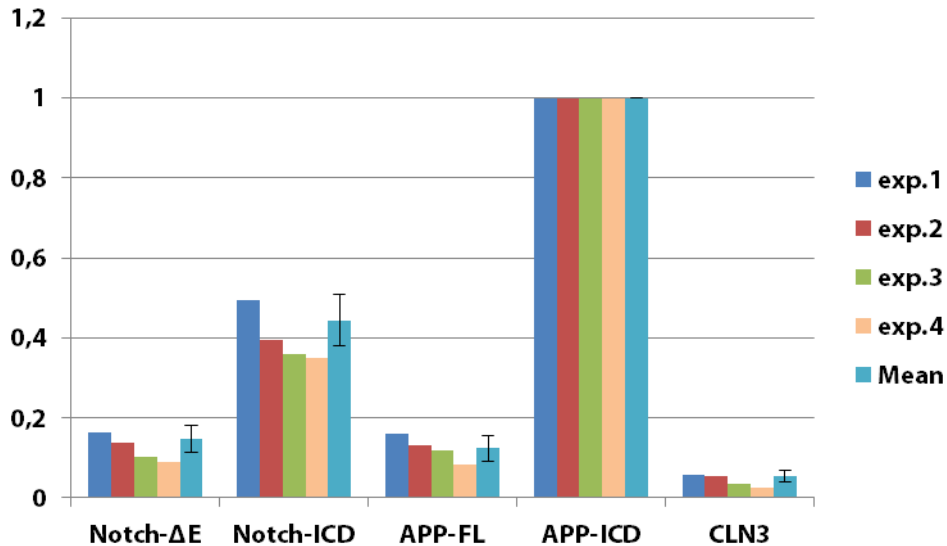


**Figure 41. Normalized Luciferase-activity-induction by  $\gamma$ -secretase substrate-constructs.**

The positive controls APP-ICD and Notch-ICD showed a significantly higher induction of the luciferase activity, compared to their respective cleavable transmembrane relatives Notch-ΔE and APP-FL. The negative control shows a significantly lower value for luciferase activity than Notch-ΔE and APP-FL. (exp. = experiment; the mean value was generated from all experiments and shows the standard deviation of the mean values).

CLN3 proved to be a reliable negative-control, with the smallest luciferase-activity-induction. The cleavable-constructs Notch-ΔE and APP-FL (APP-full length) resulted in almost identical luciferase activity. This was lower than in the measurements for the

positive controls, but considerably higher as compared to the negative control. The results of each individual assay were normalized to the mean of the highest positive control which was APP-ICD.

Since the observed values for Notch-ICD and Notch- $\Delta E$  were in a smaller range to each other than the values for APP-FL, the Notch constructs were used to assess  $\gamma$ -secretase cleavage activity in the following assay format.

#### 4.6.6.2 CLN3 and Pen2 specific shRNAs for the $\gamma$ -secretase-activity-assay

To assess the impact of CLN3 on the activity of the  $\gamma$ -secretase complex shRNAs were constructed to knock-down CLN3 in cells. With the help of different online-tools three different shRNAs were selected. Pen2-knockdown should serve as a control. Therefore shRNAs were selected also for Pen2.

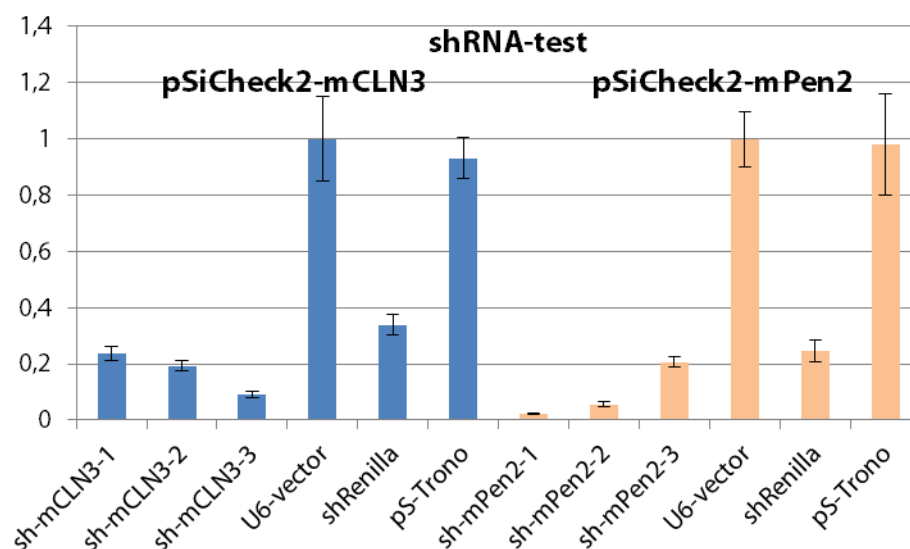


**Figure 42. Test of shRNAs for murine CLN3 and Pen2.**

The shRNAs for murine CLN3 and murine Pen2 were tested with the psiCheck2-system in combination with a Dual-Glo<sup>®</sup> Luciferase Assay System. The shRNAs for CLN3 as well as the shRNAs for Pen2 all show a comparable knock-down capacity to the positive control shRNA against Renilla-mRNA. The negative controls were the empty U6-vector (used for expression of shRNAs) and a scrambled shRNA against Renilla (pS-Trono). These showed no knockdown effect. For all samples the mean value is displayed with the standard deviation. The data was normalized to the U6-negative control.

The constructed shRNAs were tested with a Dual-Glo<sup>®</sup> Luciferase Assay System in combination with the Promega psiCHECK<sup>™</sup> vector system. The psiCHECK vector encodes two independent luciferase genes, the Renilla luciferase and the Firefly luciferase. To apply this assay system, a cDNA corresponding to the target-gene is cloned into the psiCHECK<sup>™</sup> vector in frame with the Renilla luciferase, which results in a fused mRNA, encoding the gene to be targeted and the Renilla luciferase. The modified psiCHECK vector is transfected into cells and these are subjected to knock down experiments. If a knock-down of the gene of interest is successful, the fused Renilla luciferase mRNA is

targeted by this knock-down as well. The Renilla luciferase activity is normalized to Firefly luciferase activity which is assessed in a second luciferase reaction. In the assay, knockdown-capacity of the constructed shRNAs was compared to the specific knockdown of the Renilla luciferase with a Renilla-specific shRNA. As negative controls the empty shRNA-vector and a scrambled luciferase-shRNA were used. All selected shRNAs for CLN3 and Pen2 proved to have a knockdown effect 29 hours after transfection (Figure 42).

#### 4.6.6.3 Assessment of CLN3-influence on $\gamma$ -secretase-cleavage activity on Notch

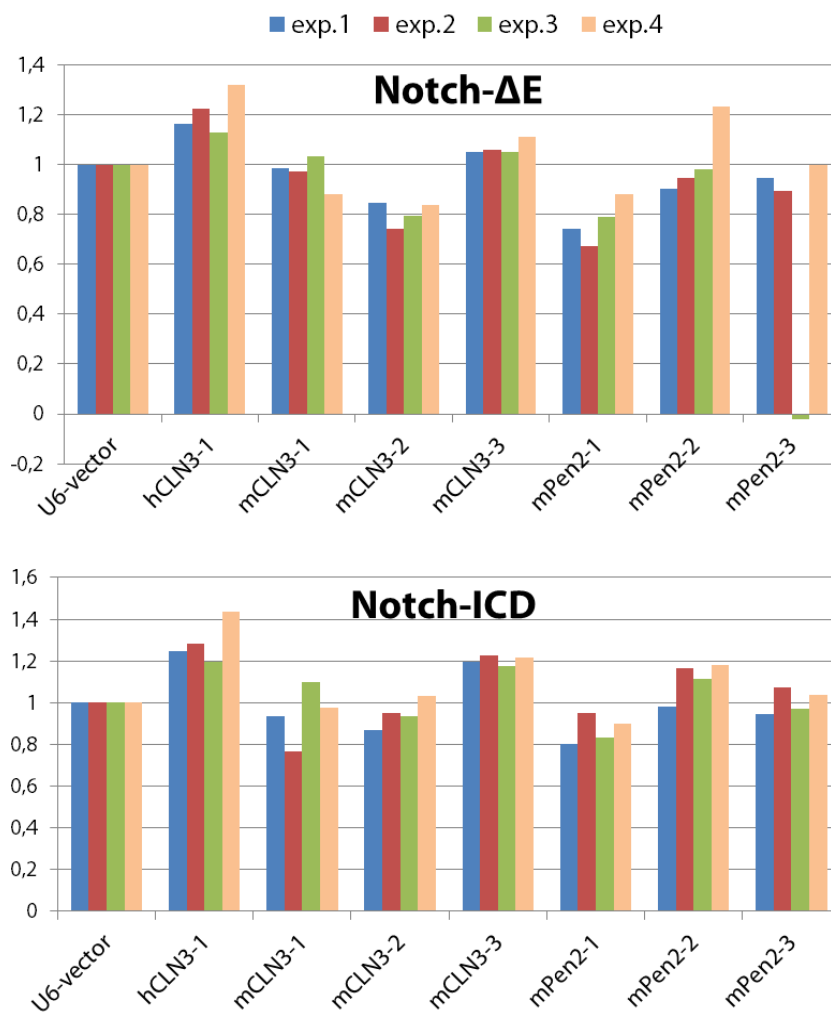


**Figure 43. Overview of the data from all experiments for luciferase-activity-induction by  $\gamma$ -secretase substrate-constructs under influence of shRNA-knockdown.**

The mean values of luciferase induction in all four experiments for the  $\gamma$ -secretase activity assay are displayed for Notch- $\Delta E$  and Notch-ICD. At the y-axis the shRNAs used in the experiments are listed. The values for each experiment were normalized to the mean value of the empty-U6-vector negative control. For the following analysis the value from experiment (exp.) 3 for mPen2-shRNA in the Notch- $\Delta E$ -assays was excluded since this showed no luciferase activity.

The influence of CLN3 on  $\gamma$ -secretase-cleavage activity was assessed by knockdown of mouse CLN3. Notch- $\Delta E$  was used as reporter substrate for  $\gamma$ -secretase activity and

knockdown of mouse Pen2 as a positive-control. As negative-controls the empty shRNA vector and an shRNA for human CLN3 was used. Notch-ICD served as negative-control for the influence of CLN3 on the cleavage activity.

In the case that CLN3 is influencing  $\gamma$ -secretase activity, a knock-down of CLN3 should alter the activity. Pen2-shRNAs should reduce  $\gamma$ -secretase activity due to the necessity of Pen2 for active  $\gamma$ -secretase complexes (Dries & Yu 2008). The luciferase-reporter-signal in the assay with Notch-ICD as substrate should not show any changes in luciferase-reporter-signal since the solubility of Notch-ICD is independent of  $\gamma$ -secretase-mediated cleavage.

The  $\gamma$ -secretase-activity assay was performed using Notch- $\Delta$ E as a substrate. CLN3 knock-down should lead either to a reduction in the luciferase-activity – which would mean that the  $\gamma$ -secretase has less cleavage activity – or to an increase in luciferase activity – which would mean that the  $\gamma$ -secretase has higher cleavage activity.

In Figure 43 the mean values of all experiments are displayed for Notch- $\Delta$ E and Notch-ICD. For the analysis and comparison of the different parameters the value from experiment 3 for mPen2-shRNA in the Notch- $\Delta$ E-assays was excluded since this showed no luciferase activity at all (Figure 43).

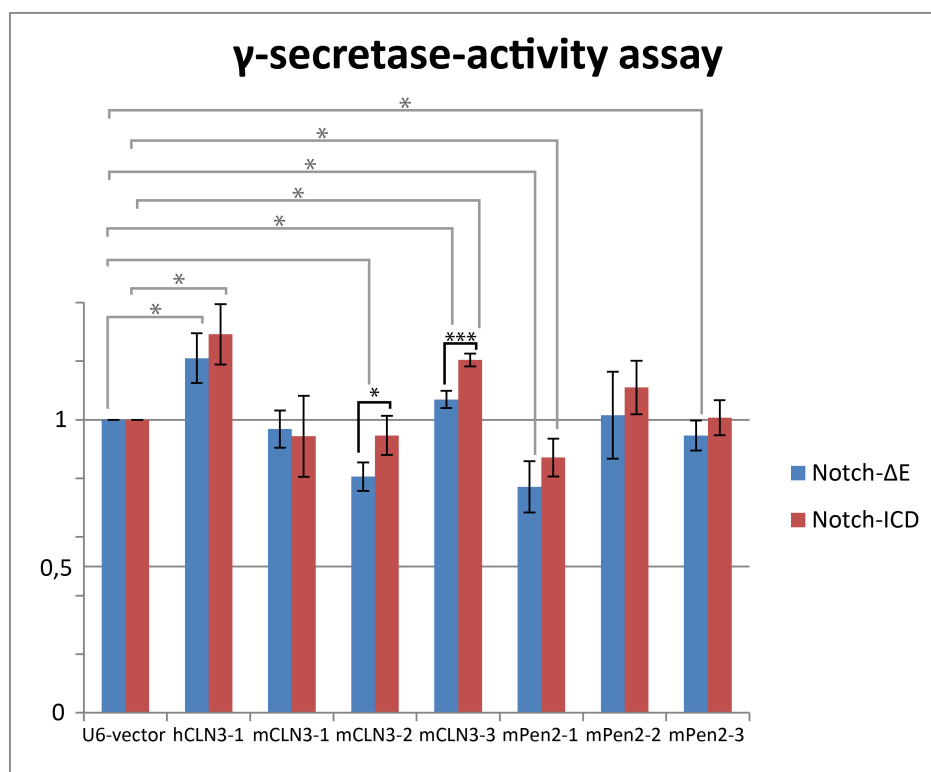


**Figure 44. Comparison of luciferase-activity-induction by the  $\gamma$ -secretase substrate-construct Notch-  $\Delta$ E and its control Notch-ICD under influence of shRNA-knockdown.**

The averaged mean values of the luciferase induction in all experiments and the standard deviation of the means are displayed for the controls U6-vector and hCLN3-shRNA, and for the specific shRNAs mCLN3-1, 2, 3 and mPen2-1, 2, 3. The values from the assays assessing luciferase-induction by the Notch- $\Delta$ E-construct and the Notch-ICD construct are compared to each other and to the U6-vector negative control. Comparison of Notch-  $\Delta$ E to Notch-ICD was conducted by t-test (significant differences are labelled by black bars). Comparison of all values to the U6-negative control was conducted by rank sum test (significant differences are labelled by grey bars). Display of significance levels: \*:  $p \leq 0.05$ ; \*\*\*:  $p \leq 0.001$ .

---

For comparison of all experiments, all values in each experiment were normalized to the particular U6-vector-negative control mean value of the experiment. From these data the mean values were generated for each single experiment. These mean values were averaged and the standard deviation of the mean values was calculated (Figure 44). Values for Notch- $\Delta$ E and Notch-ICD are displayed adjacent to each other for comparison. The statistical analysis was conducted using SigmaPlot. The mean values for the single shRNAs were compared to the U6-vector by rank sum test (Mann–Whitney U test), due to the lacking normality in the values for the U6-vector. The comparison of the shRNA values to the human CLN3-shRNA (hCLN3-shRNA) negative control was conducted by t-test (significance levels for this comparison are not displayed in figure). The comparison of the Notch- $\Delta$ E to the Notch-ICD values was also conducted by t-test (Figure 44).

Apart from the U6-vector as another negative control a shRNA against the human version of CLN3 which is not specific for the murine CLN3 was used (Figure 44). This shRNA induced a higher luciferase transcription than any other shRNA. This could be due to an influence of the shRNA treatment on the cells in general. Application of the shRNAs against mCLN3-1, mCLN3-2 and mCLN3-3 (only in the Notch- $\Delta$ E-assay) resulted in significantly lower luciferase activity as compared to the unspecific hCLN3-shRNA.

Compared to the U6-vector the shRNAs mCLN3-2 and mCLN3-3 gave significant deviations in the Notch- $\Delta$ E-assay. shRNA mCLN3-2 induced a significant reduction in luciferase activity compared to U6-negative control. The mCLN3-3-shRNA induced an increase in luciferase activity. In the Notch-ICD-assay only shRNA-mCLN3-3 gave a significantly higher result in luciferase-induction compared to U6 (Figure 44).

For Pen2 the shRNA-2 did not show an effect in the Notch- $\Delta$ E-assay. shRNA-mPen2-1 and mPen2-3 induced significant reductions from the U6-control value in the Notch- $\Delta$ E-assay. In the Notch-ICD-assay, only shRNA mPen2-1 induced a reduction (Figure 44). Compared to the hCLN3-shRNA all Pen2-shRNAs, but not shRNA-mPen2-2, induced a reduction. As shown, the shRNAs partially gave a reduction not only in the Notch- $\Delta$ E-assay but also in the Notch-ICD-assay (Figure 44). This could be due to general metabolic responses of the cell to the shRNAs.

The aim of this experiment was the comparison of shRNA influence on  $\gamma$ -secretase with Notch- $\Delta$ E as the substrate and Notch-ICD as control. While most values do not differ between Notch- $\Delta$ E- and Notch-ICD-assays the values for the knockdown of CLN3 by shRNA-mCLN3-2 and shRNA-CLN3-3 did give significant differences in luciferase activity between the Notch- $\Delta$ E and the Notch-ICD value. Notch- $\Delta$ E-luciferase-activity was significantly reduced after treatment of the cells with these shRNAs (Figure 44).

In conclusion, there is a reduction of Notch- $\Delta$ E-luciferase-activity in the  $\gamma$ -secretase-activity assays after treatment with two different shRNAs against murine CLN3 compared to the negative control Notch-ICD. However, the assay needs further improvement and controls to rule out unspecific effects of some of the shRNAs. So far the current results only hint at an influence of CLN3 on the  $\gamma$ -secretase-activity.



## 5 Discussion

This thesis aimed to get more insights into the cellular function of the protein CLN3 which is defective in the childhood neurodegenerative disease JNCL. So far the function is still elusive and the molecular mechanisms causing the disease are not clarified. In the course of the disease lysosomal storage material accumulates in several cell types in the body but only neuronal cells seem to be affected dramatically (Anderson et al. 2013). The protein has been most often observed to localize to the late endosomal and lysosomal system but has also been found in other subcellular compartments (Phillips et al. 2005). Several interaction partners for CLN3 have been identified so far but none of them helped to provide a clear answer to unravel the disease mechanisms (Kollmann et al. 2013). In this study two new putative interaction partners for CLN3 were analysed in order to get more information on the cellular role of CLN3.

### 5.1 Global and subcellular localization of CLN3

#### 5.1.1 CLN3 mRNA shows highest expression in the gastrointestinal tract

A first step in this study was the analysis of mRNA expression of CLN3 in mice because primary hippocampal mouse embryo neurons were an experimental tool to be used.

In mouse embryos CLN3 mRNA shows highest expression in the gastrointestinal tract and kidney and moderate expression in the central nervous system. In the adult mouse brain the highest expression can be found in the hippocampus. In previous experiments CLN3 mRNA expression has been tested in reporter mice with  $\beta$ -galactosidase (Eliason et al. 2007; Stein et al. 2010; Ding et al. 2011), in adult brain and human tissue (Pane et al. 1999; Chattopadhyay & Pearce 2000; Luiro et al. 2001; Cotman et al. 2002; Ding et al. 2011). The expression pattern found in my experiments is concurrent with the literature.

Seizures are a described feature of JNCL and the activity-regulation of CLN3 promoter-driven  $\beta$ -galactosidase expression in reporter CLN3 knock-in mouse hippocampus after pentylenetetrazole induced seizures was described. Therefore, I analysed the seizure-dependent induction of endogenous mRNA expression. In CLN3 knock-in mice the expression of  $\beta$ -galactosidase was increased 24 hours after seizure (Eliason et al. 2007). In my experiments, I did not observe an induction of endogenous mRNA expression of CLN3 by in situ hybridizations within the first 24h after seizure onset. The difference might be due to the animal model since Eliason et al. used a CLN3 knock-in mouse that lacks CLN3 expression and I analysed wild type animals. Another difference is the seizure-

---

inducing agent. In my experiments kainic acid was used for seizure-induction while Eliason et al. used pentylenetetrazole (Eliason et al. 2007). However, the kainic acid induced seizure paradigm has been already used in the context of NCL and expression of the two NCL genes cathepsin D (CLN10) and PPT1 (CLN1) has been demonstrated to be induced after kainic acid provokes seizures (Hetman et al. 1995; Suopanki et al. 2002).

### **5.1.2 CLN3 localizes to late endosomes and lysosomes**

For the validation of potential new interaction partners of CLN3 it is crucial to analyse their localization on the subcellular level. The best method is the labelling of the protein of interest with specific antibodies in fixed cells. For CLN3 a specific antibody is so far not available for immunocytochemistry. Several different attempts have been made to generate specific antibodies but most of them were either not verified sufficiently or gave conflicting results in the analysis of subcellular localization of CLN3. Published experiments described CLN3 localization for example in the nucleus (Margraf et al. 1999) but most studies found CLN3 to be localized in late endosomes or lysosomes (Kollmann et al. 2013). Due to the lack of specific antibodies, I generated and used tagged versions of CLN3. Either HA or fluorescent protein tags were added to the termini of CLN3. The addition of the protein tag to the N-terminus of CLN3 gave the most consistent results and presumably interferes little with identified targeting sequences and posttranslational modifications of the protein. A C-terminal tag may interfere with the described functional unconventional lysosomal targeting motif and C-terminal prenylation (Kyttälä et al. 2004; Storch et al. 2004; Storch et al. 2007).

The localization of the N-terminally tagged CLN3 expression constructs was analysed in HeLa-cells and in primary hippocampal mouse neurons. CLN3 was co-expressed with different subcellular marker proteins and endogenous proteins were labelled via antibodies in CLN3-expressing cells. Subcellular marker proteins are localized to specific subcellular compartments where they exert their particular cellular function and can therefore be used to determine the localization of other proteins (Pfeffer 2003; Ali & Seabra 2005). In overexpression experiments in HeLa-cells and in primary hippocampal neurons I observed N-terminally HA-tagged CLN3-localization in the late endosomal and lysosomal system. CLN3 shows an almost complete overlap with Limp1 / CD63 which is a lysosomal membrane protein that was also found in late endosomes (Kobayashi et al. 2000). Another late endosomal protein – Rab7 – also co-localized with CLN3 which is in agreement with published data on CLN3. In a previous study Rab7 and the Rab7-interacting lysosomal protein (RILP) were described as interaction partners for CLN3 (Uusi-Rauva et al. 2012).

In my experiments N-terminally tagged CLN3 localized only to a minor degree to the Golgi in HeLa cells. In primary hippocampal mouse neurons there is no co-localization of CLN3 with the Golgi-markers TGN46 and GM130. The small GTPase Rab1 is localized adjacent to the Golgi at Golgi-to-ER transition sites. The co-localization of CLN3 with Rab1 was also analysed and little overlap was found in HeLa cells. Both proteins localize to the perinuclear region and do localize to the same structures in some occasions but are rather localized next to each other. The observed localization of CLN3 and Rab1 on identical structures may be due to the passing of CLN3 from the ER through the Golgi where posttranslational modification occurs (Storch et al. 2007). It was also suggested that CLN3 may function in transitional processes between organelles (Rusyn et al. 2008). Btn1 - the yeast homologue of CLN3 - was found to control SNARE (soluble N-ethylmaleimide sensitive protein attachment protein receptor) phosphorylation and to regulate late endosome to Golgi and intra-Golgi protein sorting (Kama et al. 2011). In addition, Btn1 was found in the yeast-Golgi (Codlin & Mole 2009; Kama et al. 2011). The organelle system is not completely identical in yeast and mammalian cells and CLN3 might also execute additional functions in the Golgi in yeast, although deficiency of Btn1 influences vacuolar (the yeast lysosome-like structure) homeostasis (Gachet et al. 2005).

There is little to no co-localization of CLN3 with early or recycling endosomes in my experiments. The small GTPase Rab4 – a marker for early and recycling endosomes – shows only minor overlap with CLN3 localization. Moreover, the early endosomal marker Rab5 and the marker for recycling endosomes Rab11 show almost no co-localization with CLN3. The small portion of CLN3 that co-localizes with early or recycling endosomes can be associated to a small fraction of CLN3 that was observed to be localized to the plasma membrane (Storch et al. 2007). It is conceivable that such a small fraction of CLN3 represents a population of miss-sorted protein that escaped directed subcellular targeting. One research group found CLN3 localized to Rab4 and Rab11 positive recycling endosomes and the Golgi and excluded from late endosomes and lysosomes (Persaud-Sawin et al. 2004; Rusyn et al. 2008). CLN3 was tagged with YFP in the second luminal loop in these studies and this intraprotein-tagging might have led to targeting-defects. In total, the current data suggest that N-terminal tagging of CLN3 results in subcellular targeting which is likely to be identical with the distribution of the endogenous protein.

### **5.1.3 CLN3 localizes primarily to the somatodendritic region of neurons**

In a previous study CLN3 was found in neurites of cultured neurons but the nature of the neurites was not classified (Kyttälä et al. 2004). Here, I analysed the localization of CLN3

---

in neurons in more detail. In primary hippocampal mouse embryo neurons, N-terminally tagged CLN3 shows a strong localization to the somatic region. This was expected, as lysosomal organelles predominantly localize to this region in neurons (Lasiacka & Winckler 2011). In dendrites CLN3 also localizes to relatively large endosomal structures that have a comparable size to those in the soma. CLN3 can also be found in the axon but in contrast to dendrites to a lesser degree and the CLN3 positive vesicular structures are smaller than the labelled vesicles in the soma and in the dendrites. In agreement with the axonal localization, CLN3 was previously found to co-localize with the presynaptic marker SV2 and the growth associated protein GAP-43 in mouse retinal cells (Luiro et al. 2001). However, since SV2 has also been found in multi-vesicular bodies this co-localization does not necessarily indicate a localization to presynapses (Wittich et al. 1994).

In subcellular fractionations of neurons CLN3 was detected in the synaptosomal fraction but not in the synaptic vesicle fraction (Luiro et al. 2001). My data confirmed the presence of CLN3 in the axonal presynaptic compartment but showed a stronger localization of CLN3 to somatic and postsynaptic compartments. CLN3 might be involved in trafficking and degradation of synaptic content. It is likely that it is localized to multi-vesicular bodies that have been found in dendrites adjacent to spines and in axons at presynaptic sites (Von Bartheld & Altick 2011; Harris & Weinberg 2012). At higher magnification, I observed CLN3 in single dendritic spines. In these experiments dendrites were marked by Map2 labelling and GFP-GluR1 or GFP was overexpressed to label spines. CLN3 is only present in a limited population of analysed spines. In the positive spines the CLN3 level is very low. This was compared to the presence of the chimeric sorting receptor IL2-SorCS3 in spines. SorCS3 shows an abundant localization to dendritic spines (Oetjen et al. 2014) and was detected in the postsynaptic density in subcellular fractionations of neurons before (Breiderhoff et al. 2013). The presence of CLN3 in some spines can be a link to putative functional roles. Since CLN3 localizes mainly to degradative subcellular compartments I assume that this would be the case in or near dendritic spines as well. The CLN3-positive spines may represent a population of spines under plasticity-regulated transition and CLN3 could play an important role in trafficking or degradation of postsynaptic proteins (Bingol & Sheng 2011).

The co-localization of CLN3 with organelle-markers was also analysed in primary hippocampal mouse neurons. In neurons, the localization of CLN3 in comparison to subcellular marker proteins is very similar to that in HeLa-cells. CLN3 localizes to late endosomal and lysosomal structures in the soma and in neurites. With Rab1 at Golgi-to-ER transition sites there is little co-localization in the soma but in neurites CLN3 and Rab1 seem to co-localize. These locations may be sites that contain ER-to-Golgi-transition zones

at Golgi-outposts and mediate release of CLN3 to late endosomes (Gardiol et al. 1999; Horton & Ehlers 2003; Cui-Wang et al. 2012). The marker proteins for early or recycling endosomes, Rab4, 5 and 11 again show little co-localization with CLN3. In contrast to my data, in a previously published study in rat hippocampal neurons CLN3 co-localized with the early endosome marker EEA1 (Kyttälä et al. 2004). This conflicting data may be due to the usage of another marker protein.

In the localization studies in HeLa cells and primary hippocampal mouse neurons, I detected CLN3 primarily in late endosomal and lysosomal structures. In neurons CLN3 localizes to the somatic, dendritic and in a limited number to very small vesicular structures in axons. In dendrites it can also be found in a small fraction of spines. These observations are in agreement with the notion that CLN3 is a part of the proteolytic and degradative system of neurons and putatively involved in remodelling processes and degradation of toxic protein content (Bingol & Sheng 2011).

#### **5.1.4 Trafficking of CLN3-positive endosomes**

In order to determine the nature and physiology of the CLN3-positive structures that are presumably of late endosomal or lysosomal nature in HeLa-cells and primary hippocampal neurons I analysed their trafficking behaviour in living cells. In HeLa-cells the CLN3-positive endosomes show all kinds of behaviour ranging from stagnation to fast movement of a mean speed of 1.27  $\mu\text{m}/\text{sec}$ . The endosome-movement seems to be directed in retrograde or anterograde direction with regard to the nucleus, but also goes along the cell edges. CLN3 has been reported to interact with various cytoskeletal components and motor proteins. Thus the movement of CLN3-positive vesicles may be conveyed by non-muscle Myosin IIB along actin filaments of the submembranous actin network (Getty et al. 2011) or the movement can be directed along microtubules in retrograde and anterograde direction via Dynein intermediate chain or the kinesin subunit Kif3A (Uusi-Rauva et al. 2012). A speed of up to about 1.25  $\mu\text{m}/\text{sec}$  in microtubule-dependent transport was shown before (Wacker et al. 1997) and it would be interesting to test whether CLN3-transport is microtubule-dependent by application of the nocodazole which induces the depolymerization of microtubules. One indication for a microtubule-dependent transport is the speed of CLN3-positive endosomes that is similar to Kif3A-dependent transport of N-Cadherin-positive endosomes (Phang et al. 2014).

In neurons CLN3 shows fast transport of a mean speed of 0.776  $\mu\text{m}/\text{sec}$  in neuritic processes in both retrograde and anterograde direction. This transport behaviour is again in agreement with the interaction of CLN3 with molecules of microtubule-dependent-

---

transport in retrograde (Dynein intermediate chain) and anterograde (Kif3A) direction (Uusi-Rauva et al. 2012). The CLN3-positive endosomes in living neurons show not much overlap with Rab5-positive endosomes which is in agreement with my studies on fixed cells. Retrogradely trafficking endosomes show a large ratio of overlap between CLN3 and Rab7. Anterogradely trafficking endosomes are mainly only CLN3 positive. The movement of Rab5- and Rab7-positive endosomes in retrograde direction along neuronal processes is in accordance with previous observations. Thus, Rab5 localizes to rather stationary vesicles and Rab7 to retrogradely moving vesicles (Deinhardt et al. 2006).

## **5.2 Identification of new interaction partners for CLN3**

In order to get more insights into the cellular function of CLN3 I looked for new interaction partners. In TAP-tag screens two putative new interaction partners for CLN3 were identified – SorCS1 and Pen2. In my thesis, I aimed to verify and analyse their interaction with CLN3.

### **5.2.1 CLN3 does co-localize with members of the Vps10p protein family but SorCS1 was not confirmed as an interaction partner**

SorCS1 is a member of the Vps10p-Domain family of receptor proteins. Members have been implicated in internalization and trafficking of proteins to the lysosome (Ni & Morales 2006; Nielsen et al. 2008). Another link to JNCL is the genetic association of SorCS1 to the neurodegenerative diseases Morbus Alzheimer (Lane et al. 2010; Reitz et al. 2011) and Prion disease (Brown et al. 2014). SorCS1 was also found to be a regulating factor in APP metabolism (Lane et al. 2010). A link between CLN3 and the Vps10p-Domain receptor family has previously been established in yeast. The yeast homologue of CLN3, Btn1, was shown to affect trafficking of the yeast receptor Vps10p (Codlin & Mole 2009).

I compared the mRNA expression patterns of CLN3 and SorCS1 in embryonic mice and adult mouse brains. SorCS1 mRNA is highly expressed in the nervous system and shows only minor expression in the rest of the mouse embryo. In the brain, SorCS1 mRNA shows maxima in the CA1 region of the hippocampus and in the cerebral cortex. The expression patterns for both mRNAs are not very similar but the overlapping expression in the nervous system is in agreement with a linked functional role that is restricted to this tissue. Proteins can have a variable role in different tissues that is adapted to their

environment and relies on other proteins that are expressed in a tissue-specific fashion. This was for example shown for members of the LDL receptor family (Lillis et al. 2008).

On the subcellular level, I identified regions of co-localization of CLN3 with SorCS1a and SorCS1c. This co-localization was not total but was restricted to some endosomal structures. SorCS1b did not show co-localization with CLN3. This was not expected as SorCS1b is primarily localized to the cell surface (Hervey et al. 2003). SorCS1a and SorCS1c were previously found in intracellular endosomal structures and are able to internalize cargo to the lysosome (Nielsen et al. 2008). The interaction of CLN3 and SorCS1-splice-variants was not verified by co-immunoprecipitations. There might still be an interaction between endogenous CLN3 and SorCS1 in the nervous system that was missed due to the tagging of CLN3 or the cell or buffer systems used for the co-immunoprecipitations but in my study the negative results were consistent.

Since other members of the Vps10p-Domain receptor family like Sortilin and SorLA were also connected to neurodegeneration and Alzheimer's disease (Lane et al. 2012) and SorCS3 was genetically associated to the neuropsychiatric attention deficit hyperactivity disorder (Lionel et al. 2011) – psychiatric disturbances were also shown in JNCL patients (Schulz et al. 2013) - their subcellular co-localization with CLN3 was also tested. SorLA and Sortilin showed some areas of co-localization with CLN3. However, this may be due to their functional role in the late endosomal-lysosomal pathway (Nielsen et al. 2001; Lefrancois et al. 2003; Ni & Morales 2006; Mari et al. 2008; Canuel et al. 2008). SorCS3 did not show co-localization with CLN3. This is consistent with our previous results which located SorCS3 to the TGN, plasma membrane and early endosomes (Oetjen et al. 2014). For future projects the analysis of an interaction between CLN3 and SorLA or Sortilin is an interesting aim due to their similar localization, a putative function of them in lysosomal targeting and their roles in neurodegenerative diseases.

### **5.2.2 Pen2 is a new interaction partner for CLN3**

In a TAP-tag screen in which Pen2 was used as the bait protein CLN3 was found as a putative interaction partner. Pen2 is one of the four subunits of the  $\gamma$ -secretase complex. The other subunits are Presenilin 1 or 2, Aph-1a or b and Nicastrin (St George-Hyslop & Fraser 2012). The  $\gamma$ -secretase is the protease responsible for the cleavage event that generates amyloid-beta (A- $\beta$ ) from amyloid-precursor protein (APP). The optimal environment for  $\gamma$ -secretase activity is at a low pH of 4.5 (Pasternak et al. 2003; Pasternak et al. 2004). The final cleavage of APP can take place at different sites but mostly the final cleavage site is at amino acid 40 or 42 generating A- $\beta_{40}$  or A- $\beta_{42}$ . When a large proportion

---

of A- $\beta_{42}$  is generated, the risk for Alzheimer's disease is increased. The cleavage site and therefore the risk to develop Alzheimer's disease can for example be influenced by mutations in APP or Presenilin 1 (Haass et al. 2012). Alterations in the APP metabolism have also been found in JNCL patients and patients of other lysosomal storage disorders in comparison to healthy subjects (Wisniewski, Maslinska, et al. 1990; Wisniewski, Kida, et al. 1990; Herva et al. 2000). In a study that analysed the impact of CLN3 on APP processing and lysosomal pH on the cellular level, Golabek and colleagues found increased levels of a 10 kDa APP-C-terminal fragment in CLN3 overexpressing cells. They also observed an increased lysosomal pH of 4.83 after CLN3 overexpression compared to pH 4.48 in control cells (Golabek et al. 2000). Since the  $\gamma$ -secretase activity on APP cleavage does not change significantly in a pH range of 4 to 5 (Pasternak et al. 2003) the influence of CLN3 on APP-C-terminal-fragment concentration might result from an interaction of CLN3 with one of the subunits of the  $\gamma$ -secretase complex. The signalling of another substrate of the  $\gamma$ -secretase - Notch - has been found to be altered in *Drosophila* after overexpression of CLN3 (Tuxworth et al. 2009). These facts suggest a connection between the  $\gamma$ -secretase complex and its activity and CLN3. An interaction of CLN3 with Pen2 would support such evidence and may contribute to the understanding of the underlying mechanisms.

Radioactive in situ hybridizations revealed that the mRNA expression patterns of CLN3 and Pen2 are very similar. Both mRNAs are expressed ubiquitously in the mouse embryo with the highest expression in the gastrointestinal tract. The kidney, liver, thymus, nasal cavity and submandibular gland also show high expression of the two mRNAs compared to other tissues. The nervous system shows a moderate expression. For Pen2 this is in agreement with published data from tissue extract analysis from adult mice on Northern and Western blots (Hébert et al. 2004). In the brain, both proteins show a balanced expression with a maximum in the hippocampal formation. The high similarity of the mRNA expression patterns may indicate a linked functional role. The mRNAs of all four members of the  $\gamma$ -secretase, which are functionally very closely linked to each other also show similar expression patterns (Hébert et al. 2004).

On the subcellular level, CLN3 and Pen2 localized to the same endosomal structures in HeLa-cells and in primary hippocampal mouse neurons. Both proteins label mostly the same endosomal structures. The subcellular localizations are not completely overlapping, with Pen2 showing also ER-localization and CLN3 being localized almost exclusively to endosomal structures. In addition, some endosomal structures are either positive for CLN3 or Pen2 in HeLa-cells. In neurons, the overlap is similar and structures positive for both proteins can also be found in neuritic processes. The localization of Pen2 and other members of the  $\gamma$ -secretase in neuronal extrusions has been described before. One study

found all members of the  $\gamma$ -secretase and APP in synaptic fractions and synaptic vesicles fractionated from rat brain homogenates (Frykman et al. 2010). Others found Presenilin 1 N- and C-terminal fragment in synaptosomal fractions and synaptic vesicles from rat brain (Efthimiopoulos et al. 1998; Beher et al. 1999). Efthimiopoulos et al. did find Presenilin 1 only in large dense core vesicles but not in small clear core synaptic vesicles (Efthimiopoulos et al. 1998). This group also did not find Presenilin 1 in nerve terminal clathrin-coated vesicles whereas Beher et al. described its localization to growth cone membrane fractions (Beher et al. 1999).

For the analysis of subcellular Pen2 localization, tagged variants of the protein were used due to the lack of a specific antibody for immunocytochemistry. Different tagging variants were used. Since C-terminal tagging of Pen2 was described to interfere with functionality of the  $\gamma$ -secretase N-terminally tagged constructs for Pen2 were generated (Dries & Yu 2008). I tested different N-terminally tagged versions of Pen2. The tdTomato-tagged variant gave results that showed a stronger localization of Pen2 to endosomal structures than the GFP-tagged variant. This might be due to two reasons. Firstly, the tdTomato-tag consists of a tandem of two tomato-fluorescent proteins that give a higher total fluorescence signal. Secondly, GFP has been found to be sensitive to low pH-environment. The pH in the structures that are CLN3- and Pen2-positive is presumably around 5 since they are of late endosomal or lysosomal nature (Saftig & Klumperman 2009). In this pH some of the GFP-signal might be lost (Day & Davidson 2009). For this reason in most optical-experiments tdTomato-tagged Pen2 was used but GFP-tagged Pen2 showed the same localization and was used in the co-immunoprecipitations. Since I was able to show strong co-localization between CLN3 and Pen2, I aimed at identifying the nature of the endosomal structures positive for both proteins. I had already confirmed the localization of CLN3 to late endosomal and lysosomal structures in HeLa-cells and primary hippocampal neurons. Since the overexpression of three proteins together proved to be rather difficult, the analysis of the nature of CLN3- and Pen2-positive endosomes was conducted in HeLa-cells. Pen2 – as a member of the  $\gamma$ -secretase complex - has its described functional role in an acidic environment that can also be found in late endosomal and lysosomal structures (Pasternak et al. 2003) but a fraction of the  $\gamma$ -secretase was found to localize to the plasma membrane (Chyung et al. 2005). The endosomes positive for CLN3 and Pen2 show most overlap with the late endosomal marker Rab7 in my expression studies. This is consistent with the previously described localization of the proteins. Very little overlap exists with Rab1, Rab5 and Rab11. Rab4 also shows little overlap with the two proteins but can be often observed to be localized next to them. This small overlap might be due to the connection of the  $\gamma$ -secretase with the plasma membrane.

---

Since CLN3 and Pen2 showed consistent subcellular co-localization I analysed their interaction in co-immunoprecipitations. The overexpressed proteins were precipitated from HeLa-cell lysates. In conventional co-immunoprecipitations and co-immunoprecipitations after crosslinking of closely together localized proteins, I could verify the interaction of Pen2 and CLN3 on the biochemical level. These data suggest an *in vivo* interaction between the two proteins.

The interaction and co-localization was further analysed in trafficking studies in HeLa-cells and primary hippocampal mouse neurons of different age. In HeLa-cells I observed fusion and fission events between endosomal structures positive for CLN3 and Pen2 and of endosomes positive for one of them. There seems to be an exchange of material or the transition into a different subcellular compartment during the imaging process for example a fusion of late endosomes and lysosomes (Bright et al. 2005).

In living mouse hippocampal neurons as well as in fixed neuronal cells the two proteins were observed in the same vesicular-like structures but not all were positive for both. In young neurons, high trafficking rates of vesicles occur in neuritic processes. In single-transfections, I showed that the trafficking of CLN3 has a retrograde as well as an anterograde direction. For CLN3 this is also true in neurons expressing both CLN3 and Pen2. Pen2 in contrast can only be observed to travel retrogradely towards the soma. For this trafficking Pen2 localizes to the same vesicular-like structures as CLN3. All endosomes positive for Pen2 are also positive for CLN3 as indicated in the kymographs. Inversely this is not true. Not all CLN3-positive structures harbour Pen2. CLN3 might be involved in more general trafficking functions that are necessary for neuronal function (Lasiecka & Winckler 2011). In older neurons less trafficking can be observed as was already shown for CLN3 but there is almost a complete overlap between CLN3 and Pen2 with exception of anterogradely trafficking CLN3-positive structures. CLN3 is putatively involved in the retrograde transport of Pen2 and its retrieval from synaptic sites of A- $\beta$  generation by the  $\gamma$ -secretase. If Pen2 would be removed from these sites, the number of active  $\gamma$ -secretase complexes would be reduced and less amyloidogenic A- $\beta$  could be generated at the synapse. This would in turn protect the synapse from degeneration caused by toxic A- $\beta_{42}$ .

A first indication that CLN3 is not only linked to Pen2 but also to other  $\gamma$ -secretase-associated proteins is provided by data from co-expression experiments of CLN3 with Presenilin 1 or APP. Presenilin 1 is mostly localized to the ER in overexpressing cells but seems to show co-trafficking with CLN3-positive structures in life-cell-imaging. I also found a partial co-localization between APP and CLN3.

In order to gain insights into the functional connection of the interaction between CLN3 and Pen2 I aimed to analyse the influence of CLN3 on the  $\gamma$ -secretase cleavage activity. I established an assay that displays the  $\gamma$ -secretase-cleavage activity under CLN3-shRNA-knockdown. In the first steps I tested the different  $\gamma$ -secretase substrates APP and Notch for their cleavage by the  $\gamma$ -secretase. The results showed expected differences between positive and negative controls and the actual substrates. APP- and Notch-ICD expression resulted in high luciferase-activity while the CLN3 construct induced only very low luciferase-activity-levels. The transmembrane substrates APP-FL and Notch- $\Delta$ E gave results that lay in between the results of the negative control and the respective positive control. For the actual assessment of CLN3-knockdown-influence on  $\gamma$ -secretase-cleavage activity only Notch-constructs were used because the range of the achieved values was smaller and therefore less prone to outliers in the luciferase activity. The knockdown by shRNAs, which was established for CLN3 and Pen2 shRNAs in a separate assay before, resulted in similar tendencies for Notch-  $\Delta$ E and Notch-ICD in the samples. This might be due to a general effect of the shRNAs on the cell system, for example an immune reaction could have been caused (Marques & Williams 2005; Reynolds et al. 2006). For Pen2 the knockdown was expected to have a stronger effect on  $\gamma$ -secretase and therefore luciferase activity than CLN3-knockdown. This could not be observed in my experiments. One reason might be the short incubation time of 29 hours that might not be long enough to target already assembled Pen2 in the  $\gamma$ -secretase efficiently. The efficiencies of shRNA mediated knock down were tested with a plasmid-based-system and not on endogenous mRNA – the knock-down capacity might be different on those. Another reason might be off-target effects of the shRNAs (Fedorov et al. 2006). Notch signalling is also involved in various cellular processes and therefore expression of the Notch constructs might have an effect by itself (Kopan 2012). Nevertheless, a difference between Notch- $\Delta$ E and Notch-ICD in the luciferase-activity after knock-down of CLN3 with two different shRNAs was observed. This indicates that CLN3 may have an influence on  $\gamma$ -secretase-cleavage activity. For future experiments in order to verify the findings, rescue experiments with CLN3 need to be done, the knock-down capacity of the shRNAs needs to be tested with endogenous mRNA and  $\gamma$ -secretase inhibitors could be used as a negative control (Barten et al. 2006).

In my experiments, I was able to verify the interaction between CLN3 and Pen2. The two proteins show extensive co-localization and can be co-immunoprecipitated. This interaction provides either evidence for a connection between CLN3 and the  $\gamma$ -secretase or for a new undiscovered intracellular role of Pen2 independent of the  $\gamma$ -secretase. Pen2 has so far only been described in association with the  $\gamma$ -secretase complex. Three other

---

interaction partners have previously been described apart from the other members of the  $\gamma$ -secretase. The ER retrieval protein Retention in endoplasmic reticulum 1 (Rer1) was found to bind to Nicastrin and Pen2 (Spasic et al. 2007; Kaether et al. 2007). This protein has a function in the retrieval of unassembled Nicastrin from the Golgi to the ER and it can bind to Pen2 to withhold it in the ER for assembly of the  $\gamma$ -secretase (Spasic et al. 2007; Kaether et al. 2007). It was also found that depletion of Rer1 resulted in a higher  $\gamma$ -secretase activity. CLN3 might have an opposite function to Rer1 since it was described that overexpression of CLN3 resulted in an increased level of APP-C-terminal fragment (Golabek et al. 2000). Another interaction partner of Pen2 is Transmembrane trafficking protein 21 (Timp21) which was found to interact with all four members of the  $\gamma$ -secretase complex. It was described to have a modulating effect on  $\gamma$ -secretase activity (Chen et al. 2006; Pardossi-Piquard et al. 2009) and also be involved in APP trafficking (Vetrivel et al. 2007). The third recently found interaction partner is Ferritin light chain (Li et al. 2013). The investigators found increased levels of Pen2 and Presenilin 1 N-terminal fragment and an increase in  $\gamma$ -secretase activity after overexpression of Ferritin light chain.

Now, CLN3 is another candidate protein that is putatively involved in regulation of membrane and protein trafficking and can have an influence on  $\gamma$ -secretase assembly or function.

#### **5.2.2.1 CLN3 – a new link between defects in NCL and Alzheimer’s disease?**

The newly identified interaction of CLN3 with Pen2 can have different functional implications:

- CLN3 could have a direct influence on the activity of the  $\gamma$ -secretase complex substrate cleavage through the interaction with Pen2.
- There could be an influence of CLN3 through Pen2 on a function of Presenilin that is  $\gamma$ -secretase-independent.
- Pen2 and CLN3 could be important for intracellular trafficking of one-another and this could regulate CLN3 function.

In the case the interaction between Pen2 and CLN3 is functionally linked to the  $\gamma$ -secretase complex activity, this provides a direct link between JNCL and Alzheimer’s disease. As described above there is evidence for altered processing of  $\gamma$ -secretase substrates in environments with altered CLN3-expression (Wisniewski, Maslinska, et al. 1990; Wisniewski, Kida, et al. 1990; Golabek et al. 2000). In CLN8-deficiency which also belongs to the NCLs, A- $\beta$ -storage content has also been found (Herva et al. 2000). The

transmembrane-protein CLN8 was observed to be able to complement the growth and apoptosis phenotype in CLN3-deficient patient cells and they seem to belong to a common functional pathway (Persaud-Sawin et al. 2007). Another link between CLN3, the  $\gamma$ -secretase complex and presumably apoptosis is the interaction of CLN3 with Calsenilin. This calcium-binding protein was found to interact with the C-terminus of CLN3 and to play a role in calcium induced cell death in CLN3 knock-down cells. After CLN3 overexpression Calsenilin levels were down-regulated (Chang et al. 2007). Calsenilin was also described to interact with Presenilin 1 (Buxbaum et al. 1998). This interaction was found to influence calcium stores and to contribute to apoptosis (Buxbaum 2004). A connection to APP and  $\gamma$ -secretase activity was found in Alzheimer's disease patient brains where Calsenilin levels were up-regulated. In vitro cultured neurons exposure to A- $\beta_{42}$  led to increased Calsenilin mRNA- and protein-levels and cell death (Jo et al. 2004). Overexpression of Calsenilin was in turn observed to enhance  $\gamma$ -secretase activity on APP (Jo et al. 2005). An additional link between the lysosomal protein CLN3 and  $\gamma$ -secretase function is given by clinical data of Alzheimer's disease patients showing alterations of the endosomal and lysosomal system (Nixon 2000). Moreover, an Alzheimer's disease mouse model with mutations in Presenilin1 and APP - PS1<sub>M146V</sub>/APP<sub>K670N,M671L</sub> – was more prone to neurodegeneration caused by lysosomal inhibition than wildtype animals (Nixon et al. 2002). The connection between CLN3 and  $\gamma$ -secretase provides a new link to the Vps10p-Domain receptor family. The level of Sortilin was shown to be increased in human AD brains (Saadipour et al. 2013) and SorCS1, Sortilin and SorLA were found to be cleaved by the  $\gamma$ -secretase (Hermeijer et al. 2006; Beel & Sanders 2008).

In conclusion there is evidence from JNCL patients, NCL patient cells and experimental data for a link between CLN3 and  $\gamma$ -secretase activity.

Only few publications address the role of Pen2 outside the  $\gamma$ -secretase complex since it is a small and hard to study protein. Most publications analyse putative new functions of Presenilin. Since Pen2 and Presenilin can presumably also interact outside a  $\gamma$ -secretase-associated function, findings on Presenilin with a putative link to CLN3 function are discussed here.

There was a recent discussion in the literature about the functional role of the biggest member of the  $\gamma$ -secretase, Presenilin. Observations point to a role independent of its function in the  $\gamma$ -secretase complex in lysosomal proteolysis and autophagy. It is under debate whether Presenilin 1 defects impair lysosomal acidification (Lee et al. 2010) or if it has no impact on lysosomal pH (Zhang et al. 2012; Coen et al. 2012). All groups agree on the occurrence of lysosomal defects in Presenilin deficient cells. Lysosomal or yeast

---

vacuolar pH was also observed to be altered in CLN3 or Btn1 defective cells. In yeast, Btn1 defects lead to an increased vacuolar pH that can be rescued by overexpression of Btn1 (Pearce & Sherman 1998; Chattopadhyay et al. 2000; Gachet et al. 2005) and in CLN3-defective fibroblasts, a higher pH than in control cells was observed (Holopainen et al. 2001; Vidal-Donet et al. 2013). Interestingly, in transcriptome studies of frontal cortex homogenates from conditional Presenilin 1-knock-out mice Zhang and colleagues found an increase in CLN3 and CLN5 levels together with an increase in expression of many other genes of the lysosomal biogenesis CLEAR network (Zhang et al. 2012). There was less increase in the NCL genes Ppt1, Ppt2 and Tpp1. CLN3 and CLN5 were found to interact (Vesa et al. 2002). Therefore, CLN3 association with Pen2 and Presenilin might also influence CLN5.

Vidal-Donet et al. also analysed in their studies the levels of the autophagosome marker LC3-II (Mizushima 2004) and found a decrease in the LC3-II to LC3-I ratio under normal growth conditions but an increase in the ratio after starvation of CLN3-deficient fibroblasts. This is an indication for defective autophagosome maturation (Vidal-Donet et al. 2013). In Presenilin 1 and Presenilin 2 knock-down and knock-out cells an increase in the levels of the LC3-II was found (Lee et al. 2010; Neely et al. 2011). In CLN3-defective as well as in Presenilin 1-defective cells treated with lysosomal inhibitors the increase of LC-II levels is absent, suggesting a failure in autophagosome maturation (Neely et al. 2011; Vidal-Donet et al. 2013). A defective autophagic vacuolar fusion was suggested by Cao et al. who found increased levels of LC3-II in CLN3<sup>Δex7/8</sup>-knock-in mice (Cao et al. 2006). This defect might be due to an impaired autophagosome-lysosome fusion where CLN3 and Presenilin may function together and are linked by the new CLN3 interaction partner Pen2. Presenilin was described to act independently of  $\gamma$ -secretase function in these processes but it may still interact with Pen2. Accumulation of enlarged degradative vacuoles which seem to lack the ability to fuse with lysosomes was observed in Presenilin 1 defective cells before (Wilson et al. 2004; Esselens et al. 2004). In an interaction study of the autophagy-system CLN3 was also found to be associated with this process (Behrends et al. 2010). Another link between CLN3 and Presenilin are increased levels of  $\alpha$ -synuclein in Batten disease lymphoblasts as well as in Presenilin-knock-out-neurons (Wilson et al. 2004; Kang et al. 2014).

There is a broad range of data from analysis of molecular relationships underlining a connection between CLN3 and  $\gamma$ -secretase-independent Presenilin function that may be mediated through the interaction of both proteins with Pen2. It remains to be proven if this evidence leads to a real functional role. In future experiments the role of autophagosome-maturation in CLN3, Presenilin and Pen2 deficient cells can for example

be tested with a specially designed LC3-II construct indicating the nature of autophagosomal compartments in living cells (Lee et al. 2011). One more strategy to test a direct effect of CLN3 on Presenilin 1 is a Presenilin 1 FRET construct that contains two different fluorophore tags on the cytosolic N-termini of the two parts of Presenilin. Differences in their position to each other that is putatively influenced by CLN3 through the interaction with Pen2 would be visible in the FRET ratio of the fluorophores (Uemura et al. 2009).

Another option for a putative functional role of the interaction between CLN3 and Pen2 is a  $\gamma$ -secretase-independent and Presenilin-independent new function of Pen2. It is possible that correct subcellular targeting of CLN3 depends on Pen2 or vice versa and both proteins are needed for proper formation of functional endosomes of the lysosomal-autophagosome system. This needs to be tested in future-experiments by knock-downs of the two proteins and analysis of trafficking processes and targeting of the respective interaction partner.

In conclusion I assume the functional role of the interaction of CLN3 and Pen2 lies probably outside the  $\gamma$ -secretase function in cleavage of transmembrane proteins. There is some data providing evidence for a connection between CLN3 and APP procession but this can also be a secondary effect. In total there are more indications for a role of CLN3 – presumably in concert with Pen2 and Presenilin – in membrane-trafficking and the maturation of autophagosomes. A new role of Pen2 that is completely independent of the so far described function has also several interesting and challenging aspects, but there is no data supporting such a role so far.



## 6 Appendix

### 6.1 References

- Ali B, Seabra M. 2005. Targeting of Rab GTPases to cellular membranes.
- Allavena P, Chieppa M, Monti P, Piemonti L. 2004. From pattern recognition receptor to regulator of homeostasis: the double-faced macrophage mannose receptor. *Critical reviews in immunology*. 24:179–92.
- Anderson GW, Goebel HH, Simonati A. 2013. Human pathology in NCL. *Biochimica et biophysica acta*. 1832:1807–26.
- Ascaño M, Richmond A, Borden P, Kuruvilla R. 2009. Axonal targeting of Trk receptors via transcytosis regulates sensitivity to neurotrophin responses. *The Journal of neuroscience : the official journal of the Society for Neuroscience*. 29:11674–85.
- Barten DM, Meredith JE, Zaczek R, Houston JG, Albright CF. 2006. Gamma-secretase inhibitors for Alzheimer's disease: balancing efficacy and toxicity. *Drugs in R&D*. 7:87–97.
- Von Bartheld CS, Altick AL. 2011. Multivesicular bodies in neurons: distribution, protein content, and trafficking functions. *Progress in neurobiology*. 93:313–40.
- Beel AJ, Sanders CR. 2008. Substrate specificity of gamma-secretase and other intramembrane proteases. *Cellular and molecular life sciences : CMLS*. 65:1311–34.
- Behr D, Elle C, Underwood J, Davis JB, Ward R, Karran E, Masters CL, Beyreuther K, Multhaup G. 1999. Proteolytic Fragments of Alzheimer's Disease-Associated Presenilin 1 Are Present in Synaptic Organelles and Growth Cone Membranes of Rat Brain. *Journal of Neurochemistry*. 72:1564–1573.
- Behrends C, Sowa ME, Gygi SP, Harper JW. 2010. Network organization of the human autophagy system. *Nature*. 466:68–76.
- Beugnet A, Tee AR, Taylor PM, Proud CG. 2003. Regulation of targets of mTOR (mammalian target of rapamycin) signalling by intracellular amino acid availability. *The Biochemical journal*. 372:555–66.
- Bingol B, Sheng M. 2011. Deconstruction for reconstruction: the role of proteolysis in neural plasticity and disease. *Neuron*. 69:22–32.
- Boland B, Nixon RA. 2006. Neuronal macroautophagy: from development to degeneration. *Molecular aspects of medicine*. 27:503–19.
- Bond M, Holthaus S-MK, Tammen I, Tear G, Russell C. 2013. Use of model organisms for the study of neuronal ceroid lipofuscinosis. *Biochimica et biophysica acta*. 1832:1842–65.
- Bonifacino JS, Traub LM. 2003. Signals for sorting of transmembrane proteins to endosomes and lysosomes. *Annual review of biochemistry*. 72:395–447.

---

Boya P, Reggiori F, Codogno P. 2013. Emerging regulation and functions of autophagy. *Nature cell biology*. 15:713–20.

Breiderhoff T, Christiansen GB, Pallesen LT, Vaegter C, Nykjaer A, Holm MM, Glerup S, Willnow TE. 2013. Sortilin-related receptor SORCS3 is a postsynaptic modulator of synaptic depression and fear extinction. *PLoS one*. 8:e75006.

Bright NA, Gratian MJ, Luzio JP. 2005. Endocytic delivery to lysosomes mediated by concurrent fusion and kissing events in living cells. *Current biology : CB*. 15:360–5.

Brown C a, Schmidt C, Poulter M, Hummerich H, Klöhn P-C, Jat P, Mead S, Collinge J, Lloyd SE. 2014. In vitro screen of prion disease susceptibility genes using the scrapie cell assay. *Human molecular genetics*.1–7.

Brown TC, Tran IC, Backos DS, Esteban JA. 2005. NMDA receptor-dependent activation of the small GTPase Rab5 drives the removal of synaptic AMPA receptors during hippocampal LTD. *Neuron*. 45:81–94.

Burkovetskaya M, Karpuk N, Xiong J, Bosch M, Boska MD, Takeuchi H, Suzumura A, Kielian T. 2014. Evidence for Aberrant Astrocyte Hemichannel Activity in Juvenile Neuronal Ceroid Lipofuscinosis (JNCL). *PLoS one*. 9:e95023.

Burman C, Ktistakis NT. 2010. Autophagosome formation in mammalian cells. *Seminars in immunopathology*. 32:397–413.

Buxbaum JD, Choi EK, Luo Y, Lilliehook C, Crowley AC, Merriam DE, Wasco W. 1998. Calsenilin: a calcium-binding protein that interacts with the presenilins and regulates the levels of a presenilin fragment. *Nature medicine*. 4:1177–81.

Buxbaum JD. 2004. A role for calsenilin and related proteins in multiple aspects of neuronal function. *Biochemical and biophysical research communications*. 322:1140–4.

Canuel M, Korkidakis A, Konnyu K, Morales CR. 2008. Sortilin mediates the lysosomal targeting of cathepsins D and H. *Biochemical and biophysical research communications*. 373:292–7.

Cao Y, Espinola JA, Fossale E, Massey AC, Cuervo AM, MacDonald ME, Cotman SL. 2006. Autophagy is disrupted in a knock-in mouse model of juvenile neuronal ceroid lipofuscinosis. *The Journal of biological chemistry*. 281:20483–93.

Chang J-W, Choi H, Kim H-J, Jo D-G, Jeon Y-J, Noh J-Y, Park WJ, Jung Y-K. 2007. Neuronal vulnerability of CLN3 deletion to calcium-induced cytotoxicity is mediated by calsenilin. *Human molecular genetics*. 16:317–26.

Chattopadhyay S, Muzaffar NE, Sherman F, Pearce DA. 2000. The yeast model for batten disease: mutations in BTN1, BTN2, and HSP30 alter pH homeostasis. *Journal of bacteriology*. 182:6418–23.

Chattopadhyay S, Pearce DA. 2000. Neural and extraneural expression of the neuronal ceroid lipofuscinoses genes CLN1, CLN2, and CLN3: functional implications for CLN3. *Molecular genetics and metabolism*. 71:207–11.

- Chen F, Hasegawa H, Schmitt-Ulms G, Kawarai T, Bohm C, Katayama T, Gu Y, Sanjo N, Glista M, Rogaeva E, et al. 2006. TMP21 is a presenilin complex component that modulates gamma-secretase but not epsilon-secretase activity. *Nature*. 440:1208–12.
- Chyung JH, Raper DM, Selkoe DJ. 2005. Gamma-secretase exists on the plasma membrane as an intact complex that accepts substrates and effects intramembrane cleavage. *The Journal of biological chemistry*. 280:4383–92.
- Codlin S, Haines RL, Burden JJE, Mole SE. 2008. Btn1 affects cytokinesis and cell-wall deposition by independent mechanisms, one of which is linked to dysregulation of vacuole pH. *Journal of cell science*. 121:2860–70.
- Codlin S, Mole SE. 2009. *S. pombe* btn1, the orthologue of the Batten disease gene CLN3, is required for vacuole protein sorting of Cpy1p and Golgi exit of Vps10p. *Journal of cell science*. 122:1163–73.
- Coen K, Flannagan RS, Baron S, Carraro-Lacroix LR, Wang D, Vermeire W, Michiels C, Munck S, Baert V, Sugita S, et al. 2012. Lysosomal calcium homeostasis defects, not proton pump defects, cause endo-lysosomal dysfunction in PSEN-deficient cells. *J Cell Biol*. 198:23–35.
- Cotman SL, Staropoli JF. 2012. The juvenile Batten disease protein, CLN3, and its role in regulating anterograde and retrograde post-Golgi trafficking. *Clin Lipidol*. 7:79–91.
- Cotman SL, Vrbanac V, Lebel L-A, Lee RL, Johnson KA, Donahue L-R, Teed AM, Antonellis K, Bronson RT, Lerner TJ, MacDonald ME. 2002. Cln3(Deltaex7/8) knock-in mice with the common JNCL mutation exhibit progressive neurologic disease that begins before birth. *Human molecular genetics*. 11:2709–21.
- Cui-Wang T, Hanus C, Cui T, Helton T, Bourne J, Watson D, Harris KM, Ehlers MD. 2012. Local zones of endoplasmic reticulum complexity confine cargo in neuronal dendrites. *Cell*. 148:309–21.
- Day RN, Davidson MW. 2009. The fluorescent protein palette: tools for cellular imaging. *Chemical Society reviews*. 38:2887–921.
- Deinhardt K, Salinas S, Verastegui C, Watson R, Worth D, Hanrahan S, Bucci C, Schiavo G. 2006. Rab5 and Rab7 control endocytic sorting along the axonal retrograde transport pathway. *Neuron*. 52:293–305.
- Díaz E, Schimmöller F, Pfeffer SR. 1997. A novel Rab9 effector required for endosome-to-TGN transport. *The Journal of cell biology*. 138:283–90.
- Ding S-L, Tecedor L, Stein CS, Davidson BL. 2011. A knock-in reporter mouse model for Batten disease reveals predominant expression of Cln3 in visual, limbic and subcortical motor structures. *Neurobiology of disease*. 41:237–48.
- Drack A V, Miller JN, Pearce DA. 2013. A novel c.1135\_1138delCTGT mutation in CLN3 leads to juvenile neuronal ceroid lipofuscinosis. *Journal of child neurology*. 28:1112–6.
- Dries D, Yu G. 2008. Assembly, maturation, and trafficking of the  $\gamma$ -secretase complex in Alzheimer's disease. *Current Alzheimer Research*.

- 
- Efthimiopoulos S, Floor E, Georgakopoulos A, Shioi J, Cui W, Yasothornsrikul S, Hook VYH, Wisniewski T, Buee L, Robakis NK. 1998. Enrichment of presenilin 1 peptides in neuronal large dense-core and somatodendritic clathrin-coated vesicles. *Journal of neurochemistry*. 71:2365–72.
- Eliason SL, Stein CS, Mao Q, Tecedor L, Ding S-L, Gaines DM, Davidson BL. 2007. A knock-in reporter model of Batten disease. *The Journal of neuroscience : the official journal of the Society for Neuroscience*. 27:9826–34.
- Elvevold K, Simon-Santamaria J, Hasvold H, McCourt P, Smedsrød B, Sørensen KK. 2008. Liver sinusoidal endothelial cells depend on mannose receptor-mediated recruitment of lysosomal enzymes for normal degradation capacity. *Hepatology (Baltimore, Md)*. 48:2007–15.
- Esselens C, Oorschot V, Baert V, Raemaekers T, Spittaels K, Serneels L, Zheng H, Saftig P, De Strooper B, Klumperman J, Annaert W. 2004. Presenilin 1 mediates the turnover of telencephalin in hippocampal neurons via an autophagic degradative pathway. *The Journal of cell biology*. 166:1041–54.
- Eva R, Dassie E, Caswell PT, Dick G, French-Constant C, Norman JC, Fawcett JW. 2010. Rab11 and its effector Rab coupling protein contribute to the trafficking of beta 1 integrins during axon growth in adult dorsal root ganglion neurons and PC12 cells. *The Journal of neuroscience : the official journal of the Society for Neuroscience*. 30:11654–69.
- Ezaki J, Takeda-Ezaki M, Koike M, Ohsawa Y, Taka H, Mineki R, Murayama K, Uchiyama Y, Ueno T, Kominami E. 2003. Characterization of Cln3p, the gene product responsible for juvenile neuronal ceroid lipofuscinosis, as a lysosomal integral membrane glycoprotein. *Journal of neurochemistry*. 87:1296–308.
- Fariás GG, Cuitino L, Guo X, Ren X, Jarnik M, Mattera R, Bonifacino JS. 2012. Signal-mediated, AP-1/clathrin-dependent sorting of transmembrane receptors to the somatodendritic domain of hippocampal neurons. *Neuron*. 75:810–23.
- Fedorov Y, Anderson EM, Birmingham A, Reynolds A, Karpilow J, Robinson K, Leake D, Marshall WS, Khvorova A. 2006. Off-target effects by siRNA can induce toxic phenotype. *RNA (New York, NY)*. 12:1188–96.
- De Filippis L. 2011. Neural stem cell-mediated therapy for rare brain diseases: perspectives in the near future for LSDs and MNDs. *Histology and histopathology*. 26:1093–109.
- Finn R, Kovács AD, Pearce DA. 2011. Altered sensitivity of cerebellar granule cells to glutamate receptor overactivation in the Cln3( $\Delta$ ex7/8)-knock-in mouse model of juvenile neuronal ceroid lipofuscinosis. *Neurochemistry international*. 58:648–55.
- Fossale E, Wolf P, Espinola JA, Lubicz-Nawrocka T, Teed AM, Gao H, Rigamonti D, Cattaneo E, MacDonald ME, Cotman SL. 2004. Membrane trafficking and mitochondrial abnormalities precede subunit c deposition in a cerebellar cell model of juvenile neuronal ceroid lipofuscinosis. *BMC neuroscience*. 5:57.
- Frykman S, Hur J-Y, Frånberg J, Aoki M, Winblad B, Nahalkova J, Behbahani H, Tjernberg LO. 2010. Synaptic and endosomal localization of active gamma-secretase in rat brain. Linden R, editor. *PloS one*. 5:e8948.

- Fuller M, Meikle PPJ, Hopwood JJ. 2006. Epidemiology of lysosomal storage diseases: an overview. *Fabry Disease: Perspectives from 5 Years of FOS*.
- Gachet Y, Codlin S, Hyams JS, Mole SE. 2005. *btn1*, the *Schizosaccharomyces pombe* homologue of the human Batten disease gene *CLN3*, regulates vacuole homeostasis. *Journal of cell science*. 118:5525–36.
- Gardiol A, Racca C, Triller A. 1999. Dendritic and postsynaptic protein synthetic machinery. *The Journal of neuroscience : the official journal of the Society for Neuroscience*. 19:168–79.
- Getty AL, Benedict JW, Pearce DA. 2011. A novel interaction of *CLN3* with nonmuscle myosin-IIb and defects in cell motility of *Cln3(-/-)* cells. *Experimental cell research*. 317:51–69.
- Getty AL, Pearce DA. 2011. Interactions of the proteins of neuronal ceroid lipofuscinosis: clues to function. *Cellular and molecular life sciences : CMLS*. 68:453–74.
- Gey GO, Coffmann W, Kubicek MT. 1952. Tissue culture studies of the proliferative capacity of cervical carcinoma and normal epithelium. *Cancer Research*. 12:264–265.
- Golabek AA, Kida E, Walus M, Kaczmarek W, Michalewski M, Wisniewski KE. 2000. *CLN3* protein regulates lysosomal pH and alters intracellular processing of Alzheimer's amyloid-beta protein precursor and cathepsin D in human cells. *Molecular genetics and metabolism*. 70:203–13.
- Grubman A, Pollari E, Duncan C, Caragounis A, Blom T, Volitakis I, Wong A, Cooper J, Crouch PJ, Koistinaho J, et al. 2014. Deregulation of biometal homeostasis: the missing link for neuronal ceroid lipofuscinoses? *Metallomics : integrated biometal science*. 6:932–43.
- Haass C, Kaether C, Thinakaran G, Sisodia S. 2012. Trafficking and proteolytic processing of APP. *Cold Spring Harbor perspectives in medicine*. 2:a006270.
- Hailey DW, Rambold AS, Satpute-Krishnan P, Mitra K, Sougrat R, Kim PK, Lippincott-Schwartz J. 2010. Mitochondria supply membranes for autophagosome biogenesis during starvation. *Cell*. 141:656–67.
- Harris KM, Weinberg RJ. 2012. Ultrastructure of synapses in the mammalian brain. *Cold Spring Harbor perspectives in biology*. 4.
- Hartmann B. 2012. p70S6 kinase phosphorylation for pharmacodynamic monitoring. *Clinica chimica acta; international journal of clinical chemistry*. 413:1387–90.
- Hébert SS, Serneels L, Dejaegere T, Horr  K, Dabrowski M, Baert V, Annaert W, Hartmann D, De Strooper B. 2004. Coordinated and widespread expression of gamma-secretase in vivo: evidence for size and molecular heterogeneity. *Neurobiology of disease*. 17:260–72.
- Hermey G, Keat SJ, Madsen P, Jacobsen C, Petersen CM, Gliemann J. 2003. Characterization of sorCS1, an alternatively spliced receptor with completely different

---

cytoplasmic domains that mediate different trafficking in cells. *The Journal of biological chemistry*. 278:7390–6.

Hermey G, Plath N, Hubner CA, Kuhl D, Schaller HC, Hermans-Borgmeyer I. 2004. The three sorCS genes are differentially expressed and regulated by synaptic activity. *J Neurochem*. 88:1470–1476.

Hermey G, Sjøgaard SS, Petersen CM, Nykjaer A, Gliemann J. 2006. Tumour necrosis factor alpha-converting enzyme mediates ectodomain shedding of Vps10p-domain receptor family members. *The Biochemical journal*. 395:285–93.

Hermey G. 2009. The Vps10p-domain receptor family. *Cellular and molecular life sciences : CMLS*. 66:2677–89.

Herrmann P, Druckrey-Fiskaen C, Kouznetsova E, Heinitz K, Bigl M, Cotman SL, Schliebs R. 2008. Developmental impairments of select neurotransmitter systems in brains of Cln3(Deltaex7/8) knock-in mice, an animal model of juvenile neuronal ceroid lipofuscinosis. *Journal of neuroscience research*. 86:1857–70.

Herva R, Tyynelä J, Hirvasniemi A, Syrjäkallio-Ylitalo M, Haltia M. 2000. Northern epilepsy: a novel form of neuronal ceroid-lipofuscinosis. *Brain pathology (Zurich, Switzerland)*. 10:215–22.

Hetman M, Filipkowski RK, Domagala W, Kaczmarek L. 1995. Elevated cathepsin D expression in kainate-evoked rat brain neurodegeneration. *Experimental neurology*. 136:53–63.

Hollenbeck PJ. 1993. Products of endocytosis and autophagy are retrieved from axons by regulated retrograde organelle transport. *The Journal of cell biology*. 121:305–15.

Holopainen JM, Saarikoski J, Kinnunen PK, Järvelä I. 2001. Elevated lysosomal pH in neuronal ceroid lipofuscinoses (NCLs). *European journal of biochemistry / FEBS*. 268:5851–6.

Horton A, Ehlers M. 2003. Neuronal polarity and trafficking. *Neuron*. 40:277–295.

Huber LA. 2003. Is proteomics heading in the wrong direction? *Nature reviews Molecular cell biology*. 4:74–80.

Int. Batten Disease Consortium. 1995. Isolation of a novel gene underlying Batten disease, CLN3. *The International Batten Disease Consortium. Cell*. 82:949–57.

Jalanko A, Braulke T. 2009. Neuronal ceroid lipofuscinoses. *Biochimica et biophysica acta*. 1793:697–709.

Janvier K, Bonifacino JS. 2005. Role of the endocytic machinery in the sorting of lysosome-associated membrane proteins. *Molecular biology of the cell*. 16:4231–42.

Järvelä I, Lehtovirta M, Tikkanen R, Kyttälä A, Jalanko A. 1999. Defective intracellular transport of CLN3 is the molecular basis of Batten disease (JNCL). *Human molecular genetics*. 8:1091–8.

- Jean S, Kiger AA. 2012. Coordination between RAB GTPase and phosphoinositide regulation and functions. *Nature reviews Molecular cell biology*. 13:463–70.
- Jo D-G, Jang J, Kim B-J, Lundkvist J, Jung Y-K. 2005. Overexpression of calsenilin enhances gamma-secretase activity. *Neuroscience letters*. 378:59–64.
- Jo D-G, Lee J-Y, Hong Y-M, Song S, Mook-Jung I, Koh J-Y, Jung Y-K. 2004. Induction of pro-apoptotic calsenilin/DREAM/KChIP3 in Alzheimer's disease and cultured neurons after amyloid-beta exposure. *Journal of neurochemistry*. 88:604–11.
- Jutras I, Laplante A, Boulais J, Brunet S, Thinakaran G, Desjardins M. 2005. Gamma-secretase is a functional component of phagosomes. *J Biol Chem*. 280:36310–36317.
- Kaether C, Scheuermann J, Fassler M, Zilow S, Shirotani K, Valkova C, Novak B, Kacmar S, Steiner H, Haass C. 2007. Endoplasmic reticulum retention of the gamma-secretase complex component Pen2 by Rer1. *EMBO reports*. 8:743–8.
- Kama R, Kanneganti V, Ungermann C, Gerst JE. 2011. The yeast Batten disease orthologue Btn1 controls endosome-Golgi retrograde transport via SNARE assembly. *The Journal of cell biology*. 195:203–15.
- Kang S, Heo T-H, Kim S-J. 2014. Altered levels of  $\alpha$ -synuclein and sphingolipids in Batten disease lymphoblast cells. *Gene*. 539:181–5.
- Katz ML, Shibuya H, Liu PC, Kaur S, Gao CL, Johnson GS. 1999. A mouse gene knockout model for juvenile ceroid-lipofuscinosis (Batten disease). *Journal of neuroscience research*. 57:551–6.
- Kawauchi T, Sekine K, Shikanai M, Chihama K, Tomita K, Kubo K, Nakajima K, Nabeshima Y-I, Hoshino M. 2010. Rab GTPases-dependent endocytic pathways regulate neuronal migration and maturation through N-cadherin trafficking. *Neuron*. 67:588–602.
- Kim Y, Ramirez-Montealegre D, Pearce DA. 2003. A role in vacuolar arginine transport for yeast Btn1p and for human CLN3, the protein defective in Batten disease. *Proceedings of the National Academy of Sciences of the United States of America*. 100:15458–62.
- Kitzmüller C, Haines RL, Codlin S, Cutler DF, Mole SE. 2008. A function retained by the common mutant CLN3 protein is responsible for the late onset of juvenile neuronal ceroid lipofuscinosis. *Human molecular genetics*. 17:303–12.
- Klebe RJ, Ruddle FH. 1969. Neuroblastoma: Cell culture analysis of a differentiating stem cell system. *J Cell Biol*. 43.
- Klionsky DJ. 2007. Autophagy: from phenomenology to molecular understanding in less than a decade. *Nature reviews Molecular cell biology*. 8:931–7.
- Kobayashi T, Vischer UM, Rosnoblet C, Lebrand C, Lindsay M, Parton RG, Kruithof EK, Gruenberg J. 2000. The tetraspanin CD63/lamp3 cycles between endocytic and secretory compartments in human endothelial cells. *Molecular biology of the cell*. 11:1829–43.
- Kohlschütter A, Schulz A. 2009. Towards understanding the neuronal ceroid lipofuscinoses. *Brain & development*. 31:499–502.

- 
- Kollmann K, Uusi-Rauva K, Scifo E, Tyynela J, Jalanko A, Braulke T. 2013. Cell biology and function of neuronal ceroid lipofuscinosis-related proteins. *Biochim Biophys Acta*. 1832:1866–1881.
- Kopan R. 2012. Notch signaling. *Cold Spring Harbor perspectives in biology*. 4:a011213–.
- Kousi M, Lehesjoki A-E, Mole SE. 2012. Update of the mutation spectrum and clinical correlations of over 360 mutations in eight genes that underlie the neuronal ceroid lipofuscinoses. *Human mutation*. 33:42–63.
- Kovács AD, Weimer JM, Pearce DA. 2006. Selectively increased sensitivity of cerebellar granule cells to AMPA receptor-mediated excitotoxicity in a mouse model of Batten disease. *Neurobiology of disease*. 22:575–85.
- Kyttälä A, Ihrke G, Vesa J, Schell MJ, Luzio JP. 2004. Two motifs target Batten disease protein CLN3 to lysosomes in transfected nonneuronal and neuronal cells. *Molecular biology of the cell*. 15:1313–23.
- Kyttälä A, Yliannala K, Schu P, Jalanko A, Luzio JP. 2005. AP-1 and AP-3 facilitate lysosomal targeting of Batten disease protein CLN3 via its dileucine motif. *The Journal of biological chemistry*. 280:10277–83.
- Lalli G, Schiavo G. 2002. Analysis of retrograde transport in motor neurons reveals common endocytic carriers for tetanus toxin and neurotrophin receptor p75<sup>NTR</sup>. *The Journal of cell biology*. 156:233–9.
- Lane RF, Raines SM, Steele JW, Ehrlich ME, Lah JA, Small SA, Tanzi RE, Attie AD, Gandy S. 2010. Diabetes-associated SorCS1 regulates Alzheimer's amyloid-beta metabolism: evidence for involvement of SorL1 and the retromer complex. *The Journal of neuroscience : the official journal of the Society for Neuroscience*. 30:13110–5.
- Lane RF, St George-Hyslop P, Hempstead BL, Small S a, Strittmatter SM, Gandy S. 2012. Vps10 family proteins and the retromer complex in aging-related neurodegeneration and diabetes. *The Journal of neuroscience : the official journal of the Society for Neuroscience*. 32:14080–6.
- Lasiecka ZM, Winckler B. 2011. Mechanisms of polarized membrane trafficking in neurons -- focusing in on endosomes. *Molecular and cellular neurosciences*. 48:278–87.
- Lee J-HH, Yu WH, Kumar A, Lee S, Mohan PS, Peterhoff CM, Wolfe DM, Martinez-Vicente M, Massey AC, Sovak G, et al. 2010. Lysosomal proteolysis and autophagy require presenilin 1 and are disrupted by Alzheimer-related PS1 mutations. *Cell*. 141:1146–1158.
- Lee S, Sato Y, Nixon RA. 2011. Lysosomal proteolysis inhibition selectively disrupts axonal transport of degradative organelles and causes an Alzheimer's-like axonal dystrophy. *The Journal of neuroscience : the official journal of the Society for Neuroscience*. 31:7817–30.
- Lefrancois S, Zeng J, Hassan AJ, Canuel M, Morales CR. 2003. The lysosomal trafficking of sphingolipid activator proteins (SAPs) is mediated by sortilin. *The EMBO journal*. 22:6430–7.

- Li X, Liu Y, Zheng Q, Yao G, Cheng P, Bu G, Xu H, Zhang Y. 2013. Ferritin light chain interacts with PEN-2 and affects  $\gamma$ -secretase activity. *Neuroscience letters*. 548:90–4.
- Lillis AP, Van Duyn LB, Murphy-Ullrich JE, Strickland DK. 2008. LDL receptor-related protein 1: unique tissue-specific functions revealed by selective gene knockout studies. *Physiological reviews*. 88:887–918.
- Lionel AC, Crosbie J, Barbosa N, Goodale T, Thiruvahindrapuram B, Rickaby J, Gazzellone M, Carson AR, Howe JL, Wang Z, et al. 2011. Rare copy number variation discovery and cross-disorder comparisons identify risk genes for ADHD. *Science translational medicine*. 3:95ra75.
- Little L, Alcouloumre M, Drotar AM, Herman S, Robertson R, Yeh RY, Miller AL. 1987. Properties of N-acetylglucosamine 1-phosphotransferase from human lymphoblasts. *The Biochemical journal*. 248:151–9.
- Lojewski X, Staropoli JF, Biswas-Legrand S, Simas AM, Haliw L, Selig MK, Coppel SH, Goss KA, Petcherski A, Chandrachud U, et al. 2014. Human iPSC models of neuronal ceroid lipofuscinosis capture distinct effects of TPP1 and CLN3 mutations on the endocytic pathway. *Human molecular genetics*. 23:2005–22.
- Luiro K, Kopra O, Lehtovirta M, Jalanko A. 2001. CLN3 protein is targeted to neuronal synapses but excluded from synaptic vesicles: new clues to Batten disease. *Human molecular genetics*. 10:2123–31.
- Luiro K, Yliannala K, Ahtiainen L, Maunu H, Jarvela I, Kyttala A, Jalanko A. 2004. Interconnections of CLN3, Hook1 and Rab proteins link Batten disease to defects in the endocytic pathway. *Hum Mol Genet*. 13:3017–3027.
- Lund TC. 2013. Hematopoietic stem cell transplant for lysosomal storage diseases. *Pediatric endocrinology reviews : PER*. 11 Suppl 1:91–8.
- Lyly A, Von Schantz C, Heine C, Schmiedt M-L, Sipilä T, Jalanko A, Kyttälä A. 2009. Novel interactions of CLN5 support molecular networking between Neuronal Ceroid Lipofuscinosis proteins. *BMC cell biology*. 10:83.
- Mao Q, Foster BJ, Xia H, Davidson BL. 2003. Membrane topology of CLN3, the protein underlying Batten disease. *FEBS letters*. 541:40–6.
- Margraf LR, Boriack RL, Routheut AA, Cuppen I, Alhilali L, Bennett CJ, Bennett MJ. 1999. Tissue expression and subcellular localization of CLN3, the Batten disease protein. *Molecular genetics and metabolism*. 66:283–9.
- Mari M, Bujny M V, Zeuschner D, Geerts WJC, Griffith J, Petersen CM, Cullen PJ, Klumperman J, Geuze HJ. 2008. SNX1 defines an early endosomal recycling exit for sortilin and mannose 6-phosphate receptors. *Traffic (Copenhagen, Denmark)*. 9:380–93.
- Marques JT, Williams BRG. 2005. Activation of the mammalian immune system by siRNAs. *Nature biotechnology*. 23:1399–405.

- 
- Metcalf DJ, Calvi AA, Seaman MN, Mitchison HM, Cutler DF. 2008. Loss of the Batten disease gene CLN3 prevents exit from the TGN of the mannose 6-phosphate receptor. *Traffic (Copenhagen, Denmark)*. 9:1905–14.
- Meyer C, Zizioli D, Lausmann S, Eskelinen EL, Hamann J, Saftig P, Von Figura K, Schu P. 2000. mu1A-adaptin-deficient mice: lethality, loss of AP-1 binding and rerouting of mannose 6-phosphate receptors. *The EMBO journal*. 19:2193–203.
- Mindell JA. 2012. Lysosomal acidification mechanisms. *Annual review of physiology*. 74:69–86.
- Mitchison HM, Bernard DJ, Greene ND, Cooper JD, Junaid MA, Pullarkat RK, De Vos N, Breuning MH, Owens JW, Mobley WC, et al. 1999. Targeted disruption of the Cln3 gene provides a mouse model for Batten disease. *The Batten Mouse Model Consortium [corrected]*. *Neurobiology of disease*. 6:321–34.
- Mitchison HM, Munroe PB, O’Rawe AM, Taschner PE, De Vos N, Kremmidiotis G, Lensink I, Munk AC, D’Arigo KL, Anderson JW, et al. 1997. Genomic structure and complete nucleotide sequence of the Batten disease gene, CLN3. *Genomics*. 40:346–50.
- Mizushima N. 2004. Methods for monitoring autophagy. *The international journal of biochemistry & cell biology*. 36:2491–502.
- Mu FT, Callaghan JM, Steele-Mortimer O, Stenmark H, Parton RG, Campbell PL, McCluskey J, Yeo JP, Tock EP, Toh BH. 1995. EEA1, an early endosome-associated protein. EEA1 is a conserved alpha-helical peripheral membrane protein flanked by cysteine “fingers” and contains a calmodulin-binding IQ motif. *The Journal of biological chemistry*. 270:13503–11.
- Narayan SB, Rakheja D, Tan L, Pastor J V, Bennett MJ. 2006. CLN3P, the Batten’s disease protein, is a novel palmitoyl-protein Delta-9 desaturase. *Annals of neurology*. 60:570–7.
- Neely KM, Green KN, LaFerla FM. 2011. Presenilin is necessary for efficient proteolysis through the autophagy-lysosome system in a  $\gamma$ -secretase-independent manner. *The Journal of neuroscience : the official journal of the Society for Neuroscience*. 31:2781–91.
- Ni X, Morales CR. 2006. The lysosomal trafficking of acid sphingomyelinase is mediated by sortilin and mannose 6-phosphate receptor. *Traffic (Copenhagen, Denmark)*. 7:889–902.
- Nielsen MS, Keat SJ, Hamati JW, Madsen P, Gutzmann JJ, Engelsberg A, Pedersen KM, Gustafsen C, Nykjaer A, Gliemann J, et al. 2008. Different motifs regulate trafficking of SorCS1 isoforms. *Traffic (Copenhagen, Denmark)*. 9:980–94.
- Nielsen MS, Madsen P, Christensen EI, Nykjaer A, Gliemann J, Kasper D, Pohlmann R, Petersen CM. 2001. The sortilin cytoplasmic tail conveys Golgi-endosome transport and binds the VHS domain of the GGA2 sorting protein. *The EMBO journal*. 20:2180–90.
- Nixon R a. 2013. The role of autophagy in neurodegenerative disease. *Nature medicine*. 19:983–97.

- Nixon RA, Mathews PM, Cataldo AM, Mohan PS, Schmidt SD, Duff K, Berg M, Marks N, Peterhoff C, Sershen H. 2002. In Vivo Perturbation of Lysosomal Function Promotes Neuro-degeneration in the PS1M146V/APPK670N,M671L Mouse Model of Alzheimer's Disease Pathology. in *Alzheimer's Disease: Advances in Etiology, Pathogenesis and Therapeutics* (eds K Iqbal, S S Sisodia and B Winblad), John Wiley & Sons, Ltd, Chichester, UK.687–695.
- Nixon RA, Yang D-S, Lee J-H. 2008. Neurodegenerative lysosomal disorders: a continuum from development to late age. *Autophagy*. 4:590–9.
- Nixon RA. 2000. A “protease activation cascade” in the pathogenesis of Alzheimer's disease. *Annals of the New York Academy of Sciences*. 924:117–31.
- Nugent T, Mole SE, Jones DT. 2008. The transmembrane topology of Batten disease protein CLN3 determined by consensus computational prediction constrained by experimental data. *FEBS letters*. 582:1019–24.
- Oetjen S, Mahlke C, Hermans-Borgmeyer I, Hermey G. 2014. Spatiotemporal expression analysis of the growth factor receptor SorCS3. *The Journal of comparative neurology*.
- Ostergaard JR, Rasmussen TB, Mølgaard H. 2011. Cardiac involvement in juvenile neuronal ceroid lipofuscinosis (Batten disease). *Neurology*. 76:1245–51.
- Owada M, Neufeld EF. 1982. Is there a mechanism for introducing acid hydrolases into liver lysosomes that is independent of mannose 6-phosphate recognition? evidence from I-cell disease. *Biochemical and Biophysical Research Communications*. 105:814–820.
- Pane MA, Puranam KL, Boustany RM. 1999. Expression of cln3 in human NT2 neuronal precursor cells and neonatal rat brain. *Pediatric research*. 46:367–74.
- Di Paolo G, De Camilli P. 2006. Phosphoinositides in cell regulation and membrane dynamics. *Nature*. 443:651–7.
- Pardossi-Piquard R, Böhm C, Chen F, Kanemoto S, Checler F, Schmitt-Ulms G, St George-Hyslop P, Fraser PE. 2009. TMP21 transmembrane domain regulates gamma-secretase cleavage. *The Journal of biological chemistry*. 284:28634–41.
- Park M, Salgado JM, Ostroff L, Helton TD, Robinson CG, Harris KM, Ehlers MD. 2006. Plasticity-induced growth of dendritic spines by exocytic trafficking from recycling endosomes. *Neuron*. 52:817–30.
- Pasternak SH, Bagshaw RD, Guiral M, Zhang S, Ackerley CA, Pak BJ, Callahan JW, Mahuran DJ. 2003. Presenilin-1, nicastrin, amyloid precursor protein, and gamma-secretase activity are co-localized in the lysosomal membrane. *The Journal of biological chemistry*. 278:26687–94.
- Pasternak SH, Callahan JW, Mahuran DJ. 2004. The role of the endosomal/lysosomal system in amyloid-beta production and the pathophysiology of Alzheimer's disease: reexamining the spatial paradox from a lysosomal perspective. *Journal of Alzheimer's disease : JAD*. 6:53–65.

- 
- Pearce DA, Sherman F. 1998. A yeast model for the study of Batten disease. *Proceedings of the National Academy of Sciences of the United States of America*. 95:6915–8.
- Pebrel-Richard C, Debost-LeGrand A, Eymard-Pierre E, Greze V, Kemeny S, Gay-Bellile M, Gouas L, Tchirkov A, Vago P, Goumy C, Francannet C. 2014. An unusual clinical severity of 16p11.2 deletion syndrome caused by unmasked recessive mutation of CLN3. *European journal of human genetics : EJHG*. 22:369–73.
- Persaud-Sawin DA, McNamara 2nd JO, Rylova S, Vandongen A, Boustany RM. 2004. A galactosylceramide binding domain is involved in trafficking of CLN3 from Golgi to rafts via recycling endosomes. *Pediatr Res*. 56:449–463.
- Persaud-Sawin D-A, Mousallem T, Wang C, Zucker A, Kominami E, Boustany R-MN. 2007. Neuronal ceroid lipofuscinosis: a common pathway? *Pediatric research*. 61:146–52.
- Pfeffer S. 2003. Membrane domains in the secretory and endocytic pathways. *Cell*. 112:507–17.
- Pfeffer SR. 2009. Multiple routes of protein transport from endosomes to the trans Golgi network. *FEBS letters*. 583:3811–6.
- Phang H-Q, Hoon J-L, Lai S-K, Zeng Y, Chiam K-H, Li H-Y, Koh C-G. 2014. POPX2 phosphatase regulates the KIF3 kinesin motor complex. *Journal of cell science*. 127:727–39.
- Phillips SN, Benedict JW, Weimer JM, Pearce DA. 2005. CLN3, the protein associated with batten disease: structure, function and localization. *Journal of neuroscience research*. 79:573–83.
- Platt FM, Boland B, Van der Spoel AC. 2012. The cell biology of disease: lysosomal storage disorders: the cellular impact of lysosomal dysfunction. *The Journal of cell biology*. 199:723–34.
- Prekeris R, Foletti DL, Scheller RH. 1999. Dynamics of tubulovesicular recycling endosomes in hippocampal neurons. *The Journal of neuroscience : the official journal of the Society for Neuroscience*. 19:10324–37.
- Puranam KL, Guo WX, Qian WH, Nikbakht K, Boustany RM. 1999. CLN3 defines a novel antiapoptotic pathway operative in neurodegeneration and mediated by ceramide. *Molecular genetics and metabolism*. 66:294–308.
- Rakheja D, Narayan SB, Pastor J V, Bennett MJ. 2004. CLN3P, the Batten disease protein, localizes to membrane lipid rafts (detergent-resistant membranes). *Biochemical and biophysical research communications*. 317:988–91.
- Ratajczak E, Petcherski A, Ramos-Moreno J, Ruonala MO. 2014. FRET-Assisted Determination of CLN3 Membrane Topology. *PloS one*. 9:e102593.
- Reczek D, Schwake M, Schröder J, Hughes H, Blanz J, Jin X, Brondyk W, Van Patten S, Edmunds T, Saftig P. 2007. LIMP-2 is a receptor for lysosomal mannose-6-phosphate-independent targeting of beta-glucocerebrosidase. *Cell*. 131:770–83.

- Reitz C, Lee JH, Rogers RS, Mayeux R. 2011. Impact of genetic variation in SORCS1 on memory retention. *PloS one*. 6:e24588.
- Reitz C, Tosto G, Vardarajan B, Rogaeva E, Ghani M, Rogers RS, Conrad C, Haines JL, Pericak-Vance M a, Fallin MD, et al. 2013. Independent and epistatic effects of variants in VPS10-d receptors on Alzheimer disease risk and processing of the amyloid precursor protein (APP). *Translational psychiatry*. 3:e256.
- Reynolds A, Anderson EM, Vermeulen A, Fedorov Y, Robinson K, Leake D, Karpilow J, Marshall WS, Khvorova A. 2006. Induction of the interferon response by siRNA is cell type- and duplex length-dependent. *RNA (New York, NY)*. 12:988–93.
- Rusyn E, Mousallem T, Persaud-Sawin D-A, Miller S, Boustany R-MN. 2008. CLN3p impacts galactosylceramide transport, raft morphology, and lipid content. *Pediatric research*. 63:625–31.
- Saadipour K, Yang M, Lim Y, Georgiou K, Sun Y, Keating D, Liu J, Wang Y-R, Gai W-P, Zhong J-H, et al. 2013. Amyloid beta<sub>1-42</sub> (A $\beta$ <sub>42</sub>) up-regulates the expression of sortilin via the p75(NTR)/RhoA signaling pathway. *Journal of neurochemistry*. 127:152–62.
- Saftig P, Klumperman J. 2009. Lysosome biogenesis and lysosomal membrane proteins: trafficking meets function. *Nature reviews Molecular cell biology*. 10:623–35.
- Sanger F, Nicklen S, Coulson AR. 1977. DNA sequencing with chain-terminating inhibitors. *Proceedings of the National Academy of Sciences of the United States of America*. 74:5463–7.
- Sardiello M, Palmieri M, Di Ronza A, Medina DL, Valenza M, Gennarino VA, Di Malta C, Donaudy F, Embrione V, Polishchuk RS, et al. 2009. A gene network regulating lysosomal biogenesis and function. *Science (New York, NY)*. 325:473–7.
- Schröder B, Wrocklage C, Pan C, Jäger R, Kösters B, Schäfer H, Elsässer H-P, Mann M, Hasilik A. 2007. Integral and associated lysosomal membrane proteins. *Traffic (Copenhagen, Denmark)*. 8:1676–86.
- Schroeter EH, Kisslinger JA, Kopan R. 1998. Notch-1 signalling requires ligand-induced proteolytic release of intracellular domain. *Nature*. 393:382–6.
- Schultz ML, Tecedor L, Chang M, Davidson BL. 2011. Clarifying lysosomal storage diseases. *Trends in neurosciences*. 34:401–10.
- Schultz ML, Tecedor L, Stein CS, Stamnes MA, Davidson BL. 2014. CLN3 deficient cells display defects in the ARF1-Cdc42 pathway and actin-dependent events. *PloS one*. 9:e96647.
- Schulz A, Kohlschütter A, Mink J, Simonati A, Williams R. 2013. NCL diseases - clinical perspectives. *Biochim Biophys Acta*. 1832:1801–1806.
- Shapiro BE, Logigian EL, Kolodny EH, Pastores GM. 2008. Late-onset Tay-Sachs disease: the spectrum of peripheral neuropathy in 30 affected patients. *Muscle & nerve*. 38:1012–5.

---

Siintola E, Topcu M, Aula N, Lohi H, Minassian BA, Paterson AD, Liu X-Q, Wilson C, Lahtinen U, Anttonen A-K, Lehesjoki A-E. 2007. The novel neuronal ceroid lipofuscinosis gene MFSD8 encodes a putative lysosomal transporter. *American journal of human genetics.* 81:136–46.

Sisodia SS, St George-Hyslop PH. 2002. gamma-Secretase, Notch, Abeta and Alzheimer's disease: where do the presenilins fit in? *Nature reviews Neuroscience.* 3:281–90.

Sondhi D, Scott EC, Chen A, Hackett NR, Wong AMS, Kubiak A, Nelvagal HR, Pearse Y, Cotman SL, Cooper JD, Crystal RG. 2014. Partial correction of the CNS lysosomal storage defect in a mouse model of juvenile neuronal ceroid lipofuscinosis by neonatal CNS administration of an adeno-associated virus serotype rh.10 vector expressing the human CLN3 gene. *Human gene therapy.* 25:223–39.

Spada M, Pagliardini S, Yasuda M, Tukel T, Thiagarajan G, Sakuraba H, Ponzzone A, Desnick RJ. 2006. High incidence of later-onset fabry disease revealed by newborn screening. *American journal of human genetics.* 79:31–40.

Spasic D, Raemaekers T, Dillen K, Declerck I, Baert V, Serneels L, Füllekrug J, Annaert W. 2007. Rer1p competes with APH-1 for binding to nicastrin and regulates gamma-secretase complex assembly in the early secretory pathway. *The Journal of cell biology.* 176:629–40.

St George-Hyslop P, Fraser PE. 2012. Assembly of the presenilin  $\gamma$ -/ $\epsilon$ -secretase complex. *Journal of neurochemistry.* 120 Suppl :84–8.

Stein CS, Yancey PH, Martins I, Sigmund RD, Stokes JB, Davidson BL. 2010. Osmoregulation of ceroid neuronal lipofuscinosis type 3 in the renal medulla. *American journal of physiology Cell physiology.* 298:C1388–400.

Steiner P, Sarria J-CF, Glauser L, Magnin S, Catsicas S, Hirling H. 2002. Modulation of receptor cycling by neuron-enriched endosomal protein of 21 kD. *The Journal of cell biology.* 157:1197–209.

Stengel OC. 1826. Beretning om et mærkeligt Sygdomstilfælde hos fire Sødskende i Nærheden af Røraas. *Eyr Med Tidsskr.* 1:347–352.

Stenmark H. 2009. Rab GTPases as coordinators of vesicle traffic. *Nature reviews Molecular cell biology.* 10:513–25.

Storch S, Pohl S, Braulke T. 2004. A dileucine motif and a cluster of acidic amino acids in the second cytoplasmic domain of the batten disease-related CLN3 protein are required for efficient lysosomal targeting. *The Journal of biological chemistry.* 279:53625–34.

Storch S, Pohl S, Quitsch A, Falley K, Braulke T. 2007. C-terminal prenylation of the CLN3 membrane glycoprotein is required for efficient endosomal sorting to lysosomes. *Traffic (Copenhagen, Denmark).* 8:431–44.

Strulovici Y, Leopold PL, O'Connor TP, Pergolizzi RG, Crystal RG. 2007. Human embryonic stem cells and gene therapy. *Molecular therapy : the journal of the American Society of Gene Therapy.* 15:850–66.

- Su AI, Wiltshire T, Batalov S, Lapp H, Ching KA, Block D, Zhang J, Soden R, Hayakawa M, Kreiman G, et al. 2004. A gene atlas of the mouse and human protein-encoding transcriptomes. *Proceedings of the National Academy of Sciences of the United States of America*. 101:6062–7.
- Suopanki J, Lintunen M, Lahtinen H, Haltia M, Panula P, Baumann M, Tyynelä J. 2002. Status epilepticus induces changes in the expression and localization of endogenous palmitoyl-protein thioesterase 1. *Neurobiology of disease*. 10:247–57.
- Tecedor L, Stein CS, Schultz ML, Farwanah H, Sandhoff K, Davidson BL. 2013. CLN3 loss disturbs membrane microdomain properties and protein transport in brain endothelial cells. *The Journal of neuroscience : the official journal of the Society for Neuroscience*. 33:18065–79.
- Thompson A, Nessler R, Wisco D, Anderson E, Winckler B, Sheff D. 2007. Recycling endosomes of polarized epithelial cells actively sort apical and basolateral cargos into separate subdomains. *Molecular biology of the cell*. 18:2687–97.
- Tokola AM, Salli EK, Åberg LE, Autti TH. 2014. Hippocampal volumes in juvenile neuronal ceroid lipofuscinosis: a longitudinal magnetic resonance imaging study. *Pediatric neurology*. 50:158–63.
- Tuxworth RI, Vivancos V, O'Hare MB, Tear G. 2009. Interactions between the juvenile Batten disease gene, CLN3, and the Notch and JNK signalling pathways. *Human molecular genetics*. 18:667–78.
- Tyynelä J, Cooper JD, Khan MN, Shemilts SJA, Haltia M. 2004. Hippocampal pathology in the human neuronal ceroid-lipofuscinoses: distinct patterns of storage deposition, neurodegeneration and glial activation. *Brain pathology (Zurich, Switzerland)*. 14:349–57.
- Uemura K, Lill CM, Li X, Peters J a, Ivanov A, Fan Z, DeStrooper B, Bacskai BJ, Hyman BT, Berezovska O. 2009. Allosteric modulation of PS1/gamma-secretase conformation correlates with amyloid beta(42/40) ratio. *PloS one*. 4:e7893.
- Uusi-Rauva K, Kyttala A, Van der Kant R, Vesa J, Tanhuanpaa K, Neefjes J, Olkkonen VM, Jalanko A. 2012. Neuronal ceroid lipofuscinosis protein CLN3 interacts with motor proteins and modifies location of late endosomal compartments. *Cell Mol Life Sci*. 69:2075–2089.
- Uusi-Rauva K, Liiro K, Tanhuanpaa K, Kopra O, Martin-Vasallo P, Kyttala A, Jalanko A. 2008. Novel interactions of CLN3 protein link Batten disease to dysregulation of fodrin-Na<sup>+</sup>, K<sup>+</sup> ATPase complex. *Exp Cell Res*. 314:2895–2905.
- Valayannopoulos V. 2013. Enzyme replacement therapy and substrate reduction therapy in lysosomal storage disorders with neurological expression. *Handbook of clinical neurology*. 113:1851–7.
- Vesa J, Chin MH, Oelgeschläger K, Isosomppi J, DellAngelica EC, Jalanko A, Peltonen L. 2002. Neuronal ceroid lipofuscinoses are connected at molecular level: interaction of CLN5 protein with CLN2 and CLN3. *Molecular biology of the cell*. 13:2410–20.
- Vetrivel KS, Gong P, Bowen JW, Cheng H, Chen Y, Carter M, Nguyen PD, Placanica L, Wieland FT, Li Y-M, et al. 2007. Dual roles of the transmembrane protein p23/TMP21 in

---

the modulation of amyloid precursor protein metabolism. *Molecular neurodegeneration*. 2:4.

Vidal-Donet JM, Cárcel-Trullols J, Casanova B, Aguado C, Knecht E. 2013. Alterations in ROS activity and lysosomal pH account for distinct patterns of macroautophagy in LINCL and JNCL fibroblasts. *PloS one*. 8:e55526.

Vitiello SP, Benedict JW, Padilla-Lopez S, Pearce DA. 2010. Interaction between Sdo1p and Btn1p in the *Saccharomyces cerevisiae* model for Batten disease. *Human molecular genetics*. 19:931–42.

Wacker I, Kaether C, Krömer A, Migala A, Almers W, Gerdes HH. 1997. Microtubule-dependent transport of secretory vesicles visualized in real time with a GFP-tagged secretory protein. *Journal of cell science*. 110 ( Pt 1:1453–63.

Waheed A, Pohlmann R, Hasilik A, Von Figura K, Van Elsen A, Leroy JG. 1982. Deficiency of UDP-N-acetylglucosamine: Lysosomal enzyme N-acetylglucosamine-1-phosphotransferase in organs of I-cell patients. *Biochemical and Biophysical Research Communications*. 105:1052–1058.

Warnock A, Tan L, Li C, An Haack K, Narayan SB, Bennett MJ. 2013. Amlodipine prevents apoptotic cell death by correction of elevated intracellular calcium in a primary neuronal model of Batten disease (CLN3 disease). *Biochem Biophys Res Commun*. 436:645–649.

Wilson CA, Murphy DD, Giasson BI, Zhang B, Trojanowski JQ, Lee VM-Y. 2004. Degradative organelles containing mislocalized alpha-and beta-synuclein proliferate in presenilin-1 null neurons. *The Journal of cell biology*. 165:335–46.

Wilson JM, De Hoop M, Zorzi N, Toh BH, Dotti CG, Parton RG. 2000. EEA1, a tethering protein of the early sorting endosome, shows a polarized distribution in hippocampal neurons, epithelial cells, and fibroblasts. *Molecular biology of the cell*. 11:2657–71.

Wisniewski KE, Kida E, Gordon-Majszak W, Saitoh T. 1990. Altered amyloid beta-protein precursor processing in brains of patients with neuronal ceroid lipofuscinosis. *Neurosci Lett*. 120:94–96.

Wisniewski KE, Maslinska D, Kitaguchi T, Kim KS, Goebel HH, Haltia M. 1990. Topographic heterogeneity of amyloid B-protein epitopes in brains with various forms of neuronal ceroid lipofuscinoses suggesting defective processing of amyloid precursor protein. *Acta Neuropathol*. 80:26–34.

Wittich B, Volkandt W, Zimmermann H. 1994. SV2 and o-rab3 remain associated with recycling synaptic vesicles. *Journal of neurochemistry*. 63:927–37.

Wolfe DM, Padilla-Lopez S, Vitiello SP, Pearce DA. 2011. pH-dependent localization of Btn1p in the yeast model for Batten disease. *Disease models & mechanisms*. 4:120–5.

Wolfe MS. 2006. The gamma-secretase complex: membrane-embedded proteolytic ensemble. *Biochemistry*. 45:7931–7939.

- Wraith JE. 2002. Lysosomal disorders. *Seminars in neonatology* : SN. 7:75–83.
- Wu D, Liu J, Wu B, Tu B, Zhu W, Luo J. 2014. The Batten disease gene CLN3 confers resistance to endoplasmic reticulum stress induced by tunicamycin. *Biochemical and biophysical research communications*. 447:115–20.
- Yap CC, Winckler B. 2012. Harnessing the power of the endosome to regulate neural development. *Neuron*. 74:440–51.
- Yap CC, Wisco D, Kujala P, Lasiecka ZM, Cannon JT, Chang MC, Hirling H, Klumperman J, Winckler B. 2008. The somatodendritic endosomal regulator NEEP21 facilitates axonal targeting of L1/NgCAM. *The Journal of cell biology*. 180:827–42.
- Zhang X, Garbett K, Veeraraghavalu K, Wilburn B, Gilmore R, Mirnics K, Sisodia SS. 2012. A role for presenilins in autophagy revisited: normal acidification of lysosomes in cells lacking PSEN1 and PSEN2. *The Journal of neuroscience : the official journal of the Society for Neuroscience*. 32:8633–48.



## 6.2 Publication

Some results generated during this thesis were included in the following original research article. Data analyzed in both, this thesis and the article, is displayed in Figure 14.

Oetjen, S., Mahlke, C., Hermans-Borgmeyer, I. and Hermsy, G. (2014, Oct. 15), Spatiotemporal expression analysis of the growth factor receptor SorCS3. *J. Comp. Neurol.*, 522: 3386–3402.



### 6.3 Acknowledgement

At this point, I would like to thank all the people that made the work on this doctoral thesis possible for me.

First of all, a great thank you goes to PD Dr. Guido Hermeijer who gave me the opportunity to work on this interesting project. I would also like to thank him for the support he gave by supervision of my work and for the discussions about data and for experimental advice. His broad expertise in molecular cell biology and biochemistry were very helpful for my work.

I would like to thank Professor Dr. Dietmar Kuhl who offered the possibility to conduct the research in his institute.

Further, I would like to thank Prof. Dr. Christian Lohr for agreeing to be a reviewer of this thesis.

The work on this project was funded by a stipend from the NCL-Stiftung Hamburg, for which I am very grateful.

In addition, I would like to thank all members of the Institute Kuhl for a good working atmosphere and their helpfulness regarding questions and problems. Barbara Merz, Andrea Zaisser and Ute Süssens are thanked for technical support. Uwe Borgmeyer helped with expertise on assay formats. Special thanks go to the other PhD students Lars, Jerome, Daniel, Jakob, Florian, Sergio, Xiaoyan and Francesca for discussions and for giving me a nice time.

Last but not least I would like to mention my family and friends without whom it would not have been possible for me to undertake this project. A great thank you goes to my parents, Helmut und Elisabeth Oetjen, and to my sister Birthe and to Ulf for always supporting me. Also I want to thank all the other people – the Helscher, my schoolgirls and all the others from Uni and thereafter - who make life more interesting and always give me a great time.

Thank you!



Universitätsklinikum  
Hamburg-Eppendorf

Zentrum für Molekulare Neuro-  
biologie

Falkenried 94  
20251 Hamburg

Research Group:  
Neuronal Translational Control

Dr. Kent Duncan  
Telefon: +49(0)40 7410-56274  
Telefax: +49(0)40 7410-53436

Kent.Duncan@zmn.uni-hamburg.de  
www.zmn.uni-hamburg.de

Universitätsklinikum Hamburg-Eppendorf Martinistraße 52 20246 Hamburg  
Zentrum für Molekulare Neurobiologie - Forschergruppen

To whom it may concern:

**Sandra Kerstin Oetjen**, who was born on 05.08.1984 in Rotenburg (Wümme), is submitting her doctoral dissertation in English. The title of her thesis is: **‘Characterization of interactions and trafficking of the Neuronal Ceroid Lipofuscinosis protein CLN3’**.

I hereby certify as a native speaker and molecular biologist that the English language used in this thesis is sufficiently correct for submission.

Kent Duncan, Ph.D.

Universität Hamburg  
Universitätsklinikum Hamburg-Eppendorf  
Zentrum für Molekulare Neurobiologie  
AG Duncan  
Falkenried 94 · D-20251 Hamburg

Hamburg, 18.08.2014



Zertifikat Nr. QS-6568HH

Universitätsklinikum Hamburg-Eppendorf  
Körperschaft des öffentlichen Rechts  
Gerichtsstand: Hamburg  
UST-ID-Nr.: DE218618948

Vorstandsmitglieder:  
Prof. Dr. Guido Sauter (Vertr. des Vorsitzenden)  
Dr. Alexander Kirstein  
Prof. Dr. Dr. Uwe Koch-Gromus  
Joachim Pröbß

Bankverbindung:  
HSH Nordbank  
Kto.-Nr.: 104 364 000  
BLZ: 210 500 00  
IBAN-Nr.: DE9721050000104364000